Unclassified

SECURITY CLASSIFICATION OF THIS PAGE

REPORT DOCUMENTATION PAGE

Form Approved
OMB No. 0704-0188

1a. REPORT SECURITY CLASSIFICATION Unclassified	1b. RESTRICTIVE MARKINGS n/a
2a. SECURITY CLASSIFICATION AUTHORITY n/a	3. DISTRIBUTION/AVAILABILITY OF REPORT Approved for public release- distribution unlimited
2b. DECLASSIFICATION/DOWNGRADING SCHEDULE n/a	
4. PERFORMING ORGANIZATION REPORT NUMBER(S) N00014-89-J-1443	5. MONITORING ORGANIZATION REPORT NUMBER(S)
6a. NAME OF PERFORMING ORGANIZATION Optical Society of America 6b. OFFICE SYMBOL (If applicable)	7a. NAME OF MONITORING ORGANIZATION Office of Naval Research, Code 1513:EMT
6c. ADDRESS (City, State, and ZIP Code) 1816 Jefferson Place, N.W. Washington, D.C. 20036	7b. ADDRESS (City, State, and ZIP Code) 800 North Quincy Street Arlington, VA 22217-5000
8a. NAME OF FUNDING/SPONSORING ORGANIZATION 8b. OFFICE SYMBOL (If applicable)	9. PROCUREMENT INSTRUMENT IDENTIFICATION NUMBER N00014-89-J-1443
8c. ADDRESS (City, State, and ZIP Code)	10. SOURCE OF FUNDING NUMBERS PROGRAM ELEMENT NO. / PROJECT NO. / TASK NO. / WORK UNIT ACCESSION NO.

11. TITLE (Include Security Classification)

Organization of the 1989 Picosecond Electronics and Optoelectronics Topical Meeting

12. PERSONAL AUTHOR(S)

13a. TYPE OF REPORT	13b. TIME COVERED	14. DATE OF REPORT (Year, Month, Day)	15. PAGE COUNT
Final	FROM 01/01/89 TO 12/31/89	89/12/31	

16. SUPPLEMENTARY NOTATION

17. COSATI CODES			18. SUBJECT TERMS (Continue on reverse if necessary and identify by block number)
FIELD	GROUP	SUB-GROUP	

19. ABSTRACT (Continue on reverse if necessary and identify by block number)

The purpose of this meeting was to bring together workers in the areas of electronics and optoelectronics who share a common interest in the physics and technology of picosecond solid state devices, their multi-gigahertz applications and ultrafast measurement techniques. Technical areas covered included: Optoelectronic Devices: high speed photodiodes and photoconductive devices; multi-gigahertz and mode-locked simiconductor lasers; integrated optical devices; fast optically bistable devices;Semiconductor Device Physics: transient transport phenomena; hot-electron effects; picosecond electronic and optical properties and conventional as well as superlattice and quantum well structures; physics of fast ultra-small structures; Symposia (hf)

20. DISTRIBUTION/AVAILABILITY OF ABSTRACT ☒ UNCLASSIFIED/UNLIMITED ☐ SAME AS RPT ☐ DTIC USERS	21. ABSTRACT SECURITY CLASSIFICATION Unclassified
22a. NAME OF RESPONSIBLE INDIVIDUAL Jarus W. Quinn, Executive Director	22b. TELEPHONE (Include Area Code) 202/223-8130 22c. OFFICE SYMBOL

DD Form 1473, JUN 86 Previous editions are obsolete.

SECURITY CLASSIFICATION OF THIS PAGE

Unclassified

TABLE OF CONTENTS

PICOSECOND ELECTRONICS AND OPTOELECTRONICS

CONFERENCE EDITION

Summaries of papers presented at the Picosecond Electronics and Optoelectronics Topical Meeting

March 8–10, 1989

Salt Lake City, Utah

PRICE-$30.00 per Optical Society of America, 1816 Jefferson Place, NW Washington, DC 20036
TELECON 4/23/90 VG

Cosponsored by the

Air Force Office of Scientific Research
Lasers and Electro-Optics Society of IEEE
National Science Foundation
Office of Naval Research
Optical Society of America

in Cooperation with

Electronic Devices Society of IEEE
Microwave Theory and Techniques Society of IEEE

Optical Society of America
1816 Jefferson Place, N.W.
Washington, D.C. 20036
(202) 223-8130

Articles in this publication may be cited in other publications. In order to facilitate access to the original publication source, the following form for the citation is suggested:

> Name of Author(s), Title of Paper, Topical Meeting on Picosecond Electronics and Optoelectronics, (Optical Society of America, Washington, D.C. 1989) pp. xx-xx.

ISBN Number
Conference Edition 1-55752-085-2 (softcover)

Library of Congress Catalog Card Number
Conference Edition 88-62707

This material is based upon work supported by the National Science Foundation under Grant No. ECS-8822848. The Government has certain rights in this material. Any opinions, findings, and conclusions or recommendations expressed in this material are those of the author(s) and do not necessarily reflect the views of the National Science Foundation.

This work relates to Department of the Navy Task N00014-89-J-1443 issued by the Office of Naval Research. The U.S. Government has a royalty license through the world in all copyrightable material contained herein.

TUESDAY, MARCH 7, 1989

SALON D

6:00 PM-9:00 PM REGISTRATION/RECEPTION

WEDNESDAY, MARCH 8, 1989

SALON D

7:00 AM-8:15 AM BUFFET BREAKFAST

GRAND BALLROOM FOYER

7:30 AM-5:00 PM REGISTRATION/SLIDE PREVIEW

SALON G

8:15 AM OPENING REMARKS

8:30 AM-10:00 AM
WA LASER DIODES
Jerry Woodall, *IBM T. J. Watson Research Center, Presider*

8:30 AM (Invited Paper)
WA1 High-Frequency Laser Modulation, Robert Olshansky, *GTE Laboratories, Inc.* Microwave subcarrier multiplexing (SCM) is an important new technique for high-speed modulation of either lasers or external modulators. Use of SCM for direct and coherent detection, and detection with optical preamplifiers is discussed. (p. 2)

9:00 AM
WA2 Picosecond Spatially Resolved Optical Detection of Charge-Density Modulation in AlGaAs Lasers, Harley Heinrich, *IBM T. J. Watson Research Center.* We present the first, we believe, spatially resolved observation of charge-density modulation in the cavity of an AlGaAs laser using a confocal optical probing system. (p. 4)

9:15 AM
WA3 Spectral Filtering of Relaxation Oscillations in Injection Current Modulated Diode Lasers, S. Basu, P. May, J. M. Halbout, *IBM T. J. Watson Research Center.* The spectral evolution of an injection current modulated diode laser was time resolved using a streak camera. Significant improvement in pulse quality was achieved by spectral filtering. (p. 6)

WEDNESDAY, MARCH 8, 1989—*Continued*

9:30 AM
WA4 Amplification of Picosecond Pulses Using Pulsed Semiconductor Optical Amplifiers, G. Eisenstein, P. B. Hansen, J. M. Wiesenfeld, R. S. Tucker, G. Raybon, *AT&T Bell Laboratories.* We describe amplification of picosecond pulses by a pulsed semiconductor optical amplifier. We measured the temporal shape of the gain and demonstrated an increase in the maximum obtainable gain compared to the case of a dc drive. (p. 8)

9:45 AM
WA5 Ultrafast Nonlinearities in InGaAsP Diode Laser Amplifiers, K. L. Hall, E. P. Ippen, *Massachusetts Institute of Technology;* J. Mark, *Telecommunications Research Laboratory, Denmark;* G. Eisenstein, *AT&T Bell Laboratories.* Using femtosecond pulses at 1.5 μm, we have studied gain and loss dynamics in InGaAsP optical amplifiers. Subpicosecond recovery times are observed. (p. 10)

SALON D

10:00 AM-10:30 AM COFFEE BREAK

SALON G

10:30 AM-12:15 PM
WB SUPERCONDUCTORS AND MODULATORS
L. Cooper, *U.S. Office of Naval Research, Presider*

10:30 AM (Invited Paper)
WB1 Recent Developments in High T_c Superconducting Films and Devices, R. A. Buhrman, *Cornell U.* I review the current status of research on the growth, processing and patterning of high T_c superconducting (HTS) thin films, with emphasis on the high-frequency properties of HTS films and devices. (p. 14)

11:00 AM
WB2 Propagation of 1-ps Electrical Pulses on $YBa_2Cu_3O_{7-\delta}$ Superconducting Transmission Lines Deposited in $LaGaO_3$, Martin C. Nuss, P. M. Mankiewich, R. E. Howard, T. E. Harvey, C. D. Brandle, B. L. Straughn, P. R. Smith, *AT&T Bell Laboratories.* We have propagated 1-ps electrical pulses on $YBa_2Cu_3O_{7-\delta}$ superconducting coplanar strip lines grown on $LaGaO_3$. The temperature dependent dispersion of these 1-THz bandwidth pulses is reported. (p. 16)

11:15 AM (Invited Paper)
WB3 Spread Spectrum Integrated-Optic Modulators, David W. Dolfi, *Hewlett-Packard Laboratories.* Integrated-optic modulators have been developed which incorporate spread spectrum concepts in their design to achieve high bandwidths. We review their operating principles, limitations, and uses. (p. 17)

11:45 AM (Invited Paper)
WB4 Electrooptical Synthesizing of Picosecond Optical Pulses, Tetsuro Kobayashi, Akihiro Morimoto, *Osaka U., Japan.* We describe three new methods to generate arbitrarily shaped optical pulses in the picosecond range from cw lasers using an electrooptic modulator or a deflector. (p. 19)

12:15 PM-1:30 PM LUNCH BREAK

SALON G

1:30 PM-2:45 PM
WC JOINT SESSION ON TUNNELING AND RESONANT TUNNELING: I
James S. Harris, *Stanford University, Presider*

1:30 PM (Invited Paper)
WC1 Ultrafast Optical Studies of Tunneling and Perpendicular Transport in Semiconductor Microstructures, Jagdeep Shah, *AT&T Bell Laboratories.* We have obtained quantitative information on perpendicular transport and tunneling times in semiconductor microstructures using subpicosecond luminescence spectroscopy. We review the field and present recent results. (p. 22)

2:00 PM
WC2 Optical Detection of Resonant Tunneling of Electrons in Quantum Wells, G. Livescu, A. M. Fox, T. Sizer, W. H. Knox, D. A. B. Miller, *AT&T Bell Laboratories.* Evidence for resonant tunneling of electrons in a *p-i-n* quantum well modulator is provided by picosecond pump-and-probe electroabsorption measurements. (p. 24)

2:15 PM
WC3 Optical Evidence of Charge Accumulation in Double Barrier Diodes, N. Vodjdani, E. Costard, F. Chevoir, C. Thomas, P. Bois, S. Delaitre, *Thomson-CSF, France.* Using photoluminescence we have observed charge build-up in double-barrier diodes in operation, both in the quantum well and emitter layers. (p. 28)

2:30 PM
WC4 Fabrication of Resonant Tunneling Diodes for Switching Applications, S. K. Diamond, E. Ozbay, M. J. W. Rodwell, D. M. Bloom, Y. C. Pao, E. Wolak, J. S. Harris, *Stanford U.* Resonant tunneling diodes have been fabricated in a microwave compatible process with current densities of 1.3 × 10^6 A/cm². Monolithic pulse forming structures have produced switching transition times of 10 ps. (p. 32)

SALON D

2:45 PM-3:15 PM COFFEE BREAK

WEDNESDAY, MARCH 8, 1989—*Continued*

SALON G

3:15 PM-4:45 PM
WD JOINT SESSION ON TUNNELING AND RESONANT TUNNELING: II
James S. Harris, *Stanford University, Presider*

3:15 PM (Invited Paper)
WD1 Tunneling Dynamics and Resonant Coupling of Electrons in GaAs/AlAs Coupled Double Quantum Well Structures under Electric Fields, T. Matsusue, M. Tsuchiya, H. Sakaki, *U. Tokyo, Japan.* The tunneling dynamics of electrons in GaAs/AlAs coupled quantum wells were investigated using a picosecond laser. Their dependence on bias voltage, including resonant coupling phenomena, is demonstrated. (p. 36)

3:45 PM
WD2 Time-Resolved Observation of Luminescence from a Charge-Transfer State in Double Quantum Wells, T. B. Norris, *U. Rochester;* N. Vodjdani, B. Vinter, C. Weisbuch, *Thomson-CSF, France;* G. A. Mourou, *U. Michigan.* We have directly observed the buildup of a charge-transfer state in double quantum well structures due to electron and hole tunneling in opposite directions. (p. 40)

4:00 PM
WD3 Electron Tunneling Times in Coupled Quantum Wells, D. Y. Oberli, J. Shah, T. C. Damen, C. W. Tu, D. A. B. Miller, *AT&T Bell Laboratories.* A direct measurement of tunneling in coupled quantum wells shows a sharp reduction of tunneling times when a resonant condition is reached by applying an electric field. (p. 42)

4:15 PM
WD4 Effect of Quasibound-State Lifetime on the Speed of Resonant Tunneling Diodes, E. R. Brown, C. D. Parker, T. C. L. G. Sollner, *MIT Lincoln Laboratory;* C. I. Huang, C. E. Stutz, *U.S. Air Force Wright Aeronautical Laboratory.* New oscillator power measurements indicate that the quasibound-state lifetime can limit the maximum oscillation frequency of resonant tunneling diodes. An analysis of this effect leads to an inductance in the circuit model of the device. (p. 46)

4:30 PM
WD5 Electric Field Dependence of the Tunneling Escape Time of Electrons from a Quantum Well, T. B. Norris, *U. Rochester;* X. J. Song, G. Wicks, W. J. Schaff, L. F. Eastman, *Cornell U.;* G. A. Mourou, *U. Michigan.* We have directly measured the rate at which electrons tunnel from a quantum well through a thin barrier int he presence of an applied electric field. (p. 48)

SALON D

5:30 PM-7:00 PM
WE POSTER SESSION/CONFERENCE RECEPTION

WE1 Intersubband Relaxation of Electrons and Holes in $Al_xGa_{1-x}As$/GaAs Quantum Wells During Photoexcitation, Stephen M. Goodnick, *Oregon State U.;* Paolo Lugli, *U. Rome, Italy.* Results of a Monte Carlo simulation of electron, hole, and nonequilibrium phonon dynamics in quantum wells during photoexcitation are compared with experimental ultrafast optical studies. (p. 52)

WE2 Phonons and Phonon Interactions in Layered Semiconductors, G. Mahler, *U. Stuttgart, F. R. Germany;* A. M. Kriman, D. K. Ferry, *Arizona State U.* Continuum models are developed to study heterostructure confinement effects on phonon modes and their lifetimes. Wave vector and confinement-length dependence of lifetimes are found. (p. 54)

WE3 Observation of Low Power Level Picosecond Pulses Using a Single Photon Counting Technique, M. Hamana, A. Kimura, T. Shioura, T. Umeda, Y. Cho, *Osaka U., Japan;* M. Kanda, *Sumitomo Electric Industries, Ltd., Japan.* Picosecond measurement capability using low power level pulses from semiconductor lasers based on a combination of nonlinear processing and a single photon counting technique was tested, and the preliminary result showed sensitivities in the μV range. (p. 56)

WE4 Picosecond Time-Resolved Photoluminescence in Gallium Arsenide with 3-μm Spatial Resolution, Thomas A. Louis, *Heriot-Watt U., U.K.* Design and use of a novel photoluminescence lifetime spectrometer based on time-correlated single photon counting for microscopic characterization of gallium arsenide materials and devices are presented. (p. 58)

WE5 Photoconductive and Photovoltaic Picosecond Pulse Generation Using Synthetic Diamond Films, S. T. Feng, J. Goldhar, Chi H. Lee, *U. Maryland.* Photovoltaic and photoconductive electrical pulse generation was investigated in a composite switching device using thin diamond film. Fast response under high fields was observed with picosecond laser pulses. (p. 60)

WE6 Beryllium-Bombarded $In_{0.53}Ga_{0.47}As$ and InP Photoconductors with High Responsivity and Picosecond Resolution, R. Leopfe, A. Schaelin, H. Melchior, *Swiss Federal Institute of Technology, Switzerland.* Small size $In_{0.53}Ga_{0.47}As$ and Fe:InP photoconductors with optimized Be^{3+}-ion bombardment reach response speeds of 2 ps to 4 ps, while maintaining responsivities of 0.006 A/W to 0.02 A/W. (p. 62)

WEDNESDAY, MARCH 8, 1989—*Continued*

WE7 Photocurrent-Voltage Characteristics of Ultrafast Photoconductive Switches, Steven C. Moss, John F. Knudsen, Robert C. Bowman, Paul M. Adams, Duane D. Smith, *Aerospace Corp.;* M. H. Herman, *Charles Evans & Associates.* We report measurements of photocurrent-voltage characteristics of ultrafast photoconductive switches fabricated on gallium arsenide, silicon with a buried oxide layer, and silicon-on-sapphire. (p. 64)

WE8 Use of Tandem Photoconductive Switches for Measuring Picosecond Turn-On Delay of Laser Diodes, P. Blixt, *Royal Institute of Technology, Sweden;* E. Adomaitis, A. Krotkus, *Lithuanian Academy of Sciences, U.S.S.R.* Tandem photoconductive switches, producing pulses with 15-ps rise and fall times with amplitude up to 50 V, were used to characterize a laser diode. (p. 66)

WE9 Differential Sampling with Picosecond Resolution Using Bulk Photoconductors, J. Paslaski, A. Yariv, *California Institute of Technology.* A photoconductive sampling technique is demonstrated whose resolution is independent of carrier lifetime and is in principle limited only by the RC charging time of the photoconductor. (p. 69)

WE10 Timing Jitter in Repetitively Pulsed Semiconductor Lasers, Ruixi Yuan, Henry F. Taylor, *Texas A&M U.* Calculations using a quantum amplifier model indicate how timing jitter in picosecond-pulsed semiconductor lasers can be minimized through proper selection of laser and external cavity parameters. (p. 71)

WE11 Timing Jitter of Colliding Pulse Mode-Locked Lasers, G. T. Harvey, M. S. Heutmaker, P. R. Smith, *AT&T Bell Laboratories;* J. A. Valdmanis, *U. Michigan.* We report on absolute (5-ps) and relative (1.8-ps) jitter of a CPM laser used as a reference oscillator for an rf synthesizer. (p. 73)

WE12 Comparison of Electrooptic and Photoconductive Sampling Using a 28-GHz Monolithic Amplifier, E. Chauchard, G. Treacy, K. Webb, Chi H. Lee, *U. Maryland;* H.-L. A. Hung, H. C. Huang, *COMSAT Laboratories;* P. Polak-Dingels, *University Research Foundation.* The performance of a 28-GHz monolithic amplifier is evaluated using electrooptic sampling, photoconductive sampling, and a network analyzer. The advantages and limitations of each technique are discussed. (p. 75)

THURSDAY, MARCH 9, 1989

SALON D

7:00 AM-8:30 AM BUFFET BREAKFAST

GRAND BALLROOM FOYER

7:30 AM-12:00 M REGISTRATION/SLIDE PREVIEW

SALON G

8:30 AM-10:00 AM
ThA TRANSISTORS
J. Murphy, *Defense Advanced Research Projects Agency, Presider*

8:30 AM (Invited Paper)
ThA1 Silicon FETs at 0.1-μm Gate Length, G. A. Sai-Halasz, *IBM T. J. Watson Research Center.* A study of NMOS technology at 77 K in the 0.1-μm gate-length regime has achieved: clear manifestation of velocity overshoot resulting in extrinsic transconductance of over 940 μS/μm at 0.07-μm gate length; 13-ps delay per stage measured in 0.1-μm gate length ring oscillators with simulations showing potential for below 5-ps performance. (p. 80)

9:00 AM (Invited Paper)
ThA2 High-Speed Performance of InGaAs/InAlAs HEMTs, Umesh K. Mishra, *Hughes Research Laboratories.* (p. 83)

9:30 AM (Invited Paper)
ThA3 Permeable Base Transistor: an Update, Carl O. Bozler, *MIT Lincoln Laboratory.* A number of refinements in fabrication procedures and in device and circuit design have resulted in new performance records for EHF small signal gain and high efficiency power. (p. 85)

SALON D

10:00 AM-10:30 AM COFFEE BREAK

THURSDAY, MARCH 9, 1989--*Continued*

SALON G

10:30 AM-12:00 M
ThB LIGHTWAVE TECHNOLOGY
L. A. Coldren, *University of California, Santa Barbara, Presider*

10:30 AM (Invited Paper)
ThB1 High-Speed Lightwave Systems, Alan H. Gnauck, *AT&T Bell Laboratories.* The status of multigigabit direct-detection lightwave systems is reviewed, with an emphasis on the potential and limitations of present system components. (p. 88)

11:00 AM
ThB2 Picosecond Lasing Dynamics in Quantum Well Lasers and Its Dependence on the Number of Quantum Wells, Y. Arakawa, T. Sogawa, M. Tanaka, H. Sakaki, *U. Tokyo, Japan.* Short pulse generation in GaAs/AlGaAs quantum well lasers is investigated. The results demonstrate strong dependence of pulse duration on the number of quantum wells, which is due to the difference in both the differential gain and the quasi-Fermi energy level of excited carriers. (p. 90)

11:15 AM
ThB3 Subpicosecond Multiple Pulse Formation in Actively Mode-Locked Semiconductor Lasers, P. A. Morton, A. Mar, D. J. Derickson, S. W. Corzine, J. E. Bowers, *UC-Santa Barbara.* Experimental and theoretical results with actively mode-locked lasers in linear and ring cavities explain multiple pulse phenomena and lead to new insights on the inherent pulse width limit achievable with a given modulation waveform. (p. 92)

11:30 AM (Invited Paper)
ThB4 Ultrafast All-Optical Multi/Demultiplexing Techniques for Future Optical Communications, Masatoshi Saruwatari, *NTT Transmission Systems Laboratories, Japan.* We review several kinds of all-optical switching technique based on the Kerr effect in optical waveguides that could be used in time-division multi/demultiplexing of high-speed optical signals. (p. 94)

12:00 M-6:00 PM AFTERNOON FREE

SALON D

6:00 PM-7:00 PM SOCIAL HOUR/REFRESHMENTS

GRAND BALLROOM FOYER

7:00 PM-8:30 PM REGISTRATION/SLIDE PREVIEW

SALON G

7:00 PM-8:30 PM
ThC HIGH-SPEED MEASUREMENT TECHNIQUES
G. A. Mourou, *University of Michigan, Presider*

7:00 PM (Invited Paper)
ThC1 Picosecond Pulse Generation and Sampling with GaAs Monolithic Integrated Circuits, R. A. Marsland, C. J. Madden, V. Valdivia, M. J. W. Rodwell, D. M. Bloom, *Stanford U.* We have fabricated a GaAs nonlinear transmission line which generates 1.6-ps voltage shock wave and a monolithic sampling head with a 130-GHz bandwidth. (p. 98)

7:30 PM
ThC2 Ultrahigh Bandwidth Detachable Optoelectronic Probes, M. Scheuermann, R. Sprik, J. M. Halbout, P. A. Moskowitz, M. B. Ketchen, *IBM T. J. Watson Research Center.* Detachable optoelectronic sampling probes have been fabricated, characterized, and used to measure the response of GaAs photodetectors. These probes have a bandwidth in excess of 250 GHz. (p. 100)

7:45 PM
ThC3 Measurement of Gigahertz Waveforms and Propagation Delays in an InGaAs/InAlAs MODFET using Phase-Space Absorption Quenching, J. M. Wiesenfeld, M. S. Heutmaker, I. Bar-Joseph, D. S. Chemla, J. M. Kuo, T. Y. Chang, C. A. Burrus, *AT&T Bell Laboratories.* By combining the optical probing techniques of phase-space absorption quenching and electrooptic sampling, high-speed waveforms and internal propagation delays in a quantum well MODFET have been measured using ~10-ps optical pulses. (p. 102)

8:00 PM
ThC4 120-GHz Active Wafer Probes for Picosecond Device Measurement, R. Majidi-Ahy, D. M. Bloom, *Stanford U.* Frequency multiplier and harmonic mixer active wafer probes for picosecond device measurements to 120 GHz have been developed and test structures have been measured. (p. 104)

8:15 PM
ThC5 Femtosecond Excitonic Electroabsorption Sampling, W. H. Knox, J. E. Henry, B. Tell, K. D. Li, D. A. B. Miller, D. S. Chemla, *AT&T Bell Laboratories.* We present a new approach to femtosecond optoelectronic sampling. Signals are generated, propagated, and detected with 500-fs resolution in 1-μm free-standing AlGaAs films. (p. 106)

SALON D

7:00 AM-8:30 AM BUFFET BREAKFAST

GRAND BALLROOM FOYER

8:00 AM-3:00 PM REGISTRATION/SLIDE PREVIEW

SALON G

8:30 AM-10:00 AM
FA TRANSISTORS AND TRANSPORT
P. Asbeck, *Rockwell International Science Center, Presider*

8:30 AM (Invited Paper)
FA1 GaAs MESFET and HBT Technology in Picosecond Electronics, Kazuyoshi Asai, Tadao Ishibashi, *NTT LSI Laboratories, Japan.* Recent progress in the high-speed performance of GaAs MESFET and HBT integrated circuits is reviewed. Ultrahigh-speed signal processing should soon be available. (p. 110)

9:00 AM (Invited Paper)
FA2 High-Frequency Heterostructure Bipolar Transistors, Richard Nottenburg, *AT&T Bell Laboratories.* (p. 112)

9:30 AM
FA3 Electron-Hole Effects on the Velocity Overshoot in Photoconductive Switches, R. Joshi, S. Chamoun, R. O. Grondin, *Arizona State U.* We investigate the effects of the electron-hole interaction on the velocity transients. At sufficiently high excitation intensities, this interaction strongly enhances the velocity overshoot. (p. 114)

9:45 AM
FA4 Role of Electron-Electron Scattering on the Ultrafast Relaxation of Hot Photoexcited Carriers in GaAs, M. J. Kann, D. K. Ferry, *Arizona State U.* The femtosecond behavior of laser-generated plasmas is studied by a coupled MD/EMC simulation. Decay from the excitation volume is dominated by electron-electron scattering. (p. 116)

SALON D

10:00 AM-10:30 AM COFFEE BREAK

SALON G

10:30 AM–12:00 M
FB PHOTOCONDUCTIVE SWITCHES AND APPLICATIONS
D. H. Auston, *Columbia University, Presider*

10:30 AM (Invited Paper)
FB1 Picosecond GaAs Based Photoconductive Optoelectronic Detectors, F. W. Smith, H. Q. Le, V. Diadiuk, M. A. Hollis, A. R. Calawa, *MIT Lincoln Laboratory;* S. Gupta, M. Frankel, D. R. Dykaar, G. A. Mourou, T. Y. Hsiang, *U. Rochester.* Picosecond photoconductive-switch performance has been demonstrated with a novel material deposited by molecular beam epitaxy at low substrate temperatures using Ga and As_4 beam fluxes. (p. 120)

11:00 AM
FB2 Mobility and Lifetime Measurements on PECVD and Type IIa Diamonds, D. R. Kania, O. L. Landen, *Lawrence Livermore National Laboratory;* L. Pan, P. Pianetta, *Stanford U.;* K. V. Ravi, *Crystallume, Inc.* Photoconductive devices were tested to measure the mobility and lifetime of plasma enhanced chemical vapor deposition produced diamond films and natural type IIa (insulating) diamonds using picosecond UV laser excitation. (p. 122)

11:15 AM
FB3 Picosecond Optoelectronic Integrated Antennas for Broadband Dielectric Measurements, Y. Pastol, G. Arjavalingam, J. M. Halbout, G. V. Kopcsay, *IBM T. J. Watson Research Center.* The picosecond transient electromagnetic radiation from optoelectronically pulsed integrated antennas is used for broadband coherent microwave spectroscopy experiments in the 10–125-GHz frequency range. (p. 124)

11:30 AM
FB4 Beams of Terahertz Electromagnetic Pulses, C. Fattinger, D. Grischkowsky, *IBM T. J. Watson Research Center.* We have generated freely propagating diffraction-limited beams of single cycle 0.5-THz electromagnetic pulses from a 5-mm diameter coherent source. (p. 126)

11:45 AM
FB5 Photoconductive Characterization of Integrated Optoelectronic Millimeter Wave Antennas, Charles R. Lutz, Alfred P. DeFonzo, *U. Massachusetts.* Photoconductive sampling is used to investigate structural discontinuities and measure far-field radiation patterns of high-speed radiative structures with picosecond resolution. (p. 128)

12:00 M–1:30 PM LUNCH BREAK

FRIDAY, MARCH 10, 1989—*Continued*

SALON G

1:30 PM–3:00 PM
FC OPTICAL DETECTORS AND SWITCHES
C. H. Lee, *University of Maryland, Presider*

1:30 PM (Invited Paper)
FC1 High-Speed Metal-Semiconductor-Metal Detectors, D. L. Rogers, *IBM T. J. Watson Research Center.* Recently, high speed IMSM detectors were demonstrated that are compatible with LSI GaAs MESFET processing. Some theory and recent progress in the field are reviewed. (p. 132)

2:00 PM
FC2 Coplanar Vacuum Photodiode for Measurement of Short-Wavelength Picosecond Pulses, A. M. Johnson, J. Bokor, W. M. Simpson, R. H. Storz, *AT&T Bell Laboratories.* We have fabricated a vacuum photodiode in a coplanar stripline geometry. This device is capable of high quantum efficiency and picosecond response time—useful for diagnostics of picosecond soft x rays from laser produced plasmas. (p. 134)

2:15 PM
FC3 20-ps Resolution Single-Photon Solid-State Detector, M. Ghioni, A. Lacaita, S. Cova, G. Ripamonti, *Milan Polytechnic, Italy.* The highest time resolution so far reported in single-photon timing measurements with solid-state devices is presented. (p. 136)

2:30 PM (Invited Paper)
FC4 Ultrafast Optical Switching Through Virtual Charge Polarization in dc Biased Quantum Well Structures, Masamichi Yamanishi, *Hiroshima U., Japan.* Ultrafast modulation of quantum states, due to virtual charge polarization in asymmetric quantum well structures, is discussed with some comments on its uses. (p. 138)

3:00 PM CLOSING REMARKS

WEDNESDAY, MARCH 8, 1989

SALON G

8:30 AM–10:00 AM

WA1–5

LASER DIODES

Jerry Woodall, IBM T. J. Watson Research Center,
Presider

High Frequency Laser Modulation

by Robert Olshansky

GTE Laboratories Incorporated
40 Sylvan Road
Waltham, MA 02254

Summary

The commercial application of high speed laser diodes and modulators to lightwave systems is restricted by the limited availability of time-division multiplexing (TDM) circuitry at data rates above 2 Gb/s. The multiplexing of modulated microwave subcarriers is a promising new approach for circumventing this TDM bottleneck and for exploiting the full bandwidth capability of lightwave components.

In a subcarrier multiplexed (SCM) lightwave system, a composite microwave signal is formed by power combining signals from a number of modulated microwave subcarriers. The composite signal can then be used to intensity modulate a high speed laser or an external modulator.

Previously published results have shown that SCM techniques can be used to transmit 120 FM video signals in the 2.8-7.6 GHz band [1], 20 subcarriers in the 2-6 GHz band, each frequency-shift-keyed (FSK) at 100 Mb/s [2], and 2 Gb/s on a single PSK subcarrier[3].

This paper will discuss the extension of SCM techniques to the following areas:

(1) Coherent Transmission of SCM Signals

SCM transmitter electronics can be directly used to drive an external phase modulator for coherent phase-modulated (PM) transmission. After coherent heterodyne detection the transmitted signals can be recovered using the same SCM receiver electronics previously reported for direct detection systems [4].

(2) Multigigabit Direct Detection SCM Systems

By using quadrature-phase-shift-keying (QPSK) efficient bandwidth utilization can be achieved, and 3-4 Gb/s can be transmitted on an individual subcarrier. Using multiple subcarriers, QPSK-SCM systems operating above 8 Gb/s can be built.

(3) Direct Detection with Optical Preamplifiers

Since SCM systems rely on conventional low noise microwave amplifiers with input noise currents of 12 pA/√Hz or higher, significant improvement in receiver sensitivity can be achieved using optical preamplifiers. Simple formulae for the improvement in receiver sensitivity will be presented. As an example, the receiver sensitivity of an 8 Gb/s QPSK-SCM system can be improved 8 dB to -30 dBm by using a semiconductor optical preamplifier. A receiver sensitivity of -37 dBm can be achieved with an erbium-doped fiber preamplifier.

This paper will show that subcarrier multiplexing represents an extremely promising alternative to conventional baseband signalling, and provides a versatile approach for exploiting the full bandwidth potential of lightwave technology.

References

[1] R. Olshansky, P. Hill and V. Lanzisera, Eur. Conf. on Opt. Comm., p. 143, Sept. 11-15, 1988.

[2] P. Hill and R. Olshansky, Electron. Letts., 24, p. 892, 1988.

[3] J. Bowers, Electron. Letts., 22, p. 1119, 1986.

[4] R. Gross, R. Olshansky, and P. Hill, Opt. Fiber Commo. Conf., Houston, TX, Feb. 6-9, 1988.

Picosecond, Spatially-Resolved Optical Detection of Charge-Density Modulation in AlGaAs Lasers

Harley Heinrich
IBM
T.J. Watson Research Center
P.O. Box 218
Yorktown Heights, NY 10598

An understanding of charge dynamics within a semiconductor laser cavity is important for determining the performance of the device. Laser carrier dynamics have previously been measured[1] by guiding a subpicosecond laser pulse along the cavity. Spatially resolved carrier dynamics have been measured in both silicon and GaAs IC's by using a modified phase contrast microscope[2,3] with two optical probe spots. This paper describes the first observation of spatially resolved carrier dynamics within the cavity of an AlGaAs laser using a modified picosecond differential phase-contrast confocal microscope[4], which has a single optical probe spot.

Figure 1 shows the optical probing system. The laser source in this optical probing system was a 1.3μm InGaAsP semiconductor laser. The laser was gain switched at 100MHz to produce 40ps optical pulses. Light from the laser passed through an optical isolator and a quarter-wave plate oriented at 22.5° to the horizontal. The light-source and camera systems provide imaging of the AlGaAs laser and the laser probe spot. The objective lens focuses the probe beam to a 3μm spot on the top-surface AlGaAs laser cavity. The optical probe passes through the AlGaAs laser and reflects from the rear surface metalization. The objective lens images the reflected beam onto the two photodetectors in the optical probing system, where one detector is small (60μm diameter), and the other is large (500μm diameter). Index perturbations within the laser cavity, vary the position of the image in the optical probing system. The maximum small-signal sensitivity of this probing system occurs when the small detector is slightly defocused from the AlGaAs laser image, but is still well within the detector lens depth of focus. Since the large detector receives only a constant level, the output of the two detectors may be differenced to cancel the laser amplitude noise. Under these conditions, the shot-noise limited sensitivity of this probing system is $\delta N_e/\sqrt{Hz} = 2.6 \times 10^9 e/(cm^2\sqrt{Hz})$ for a 1mW optical probing system.

The AlGaAs laser that was probed in this experiment, was a Mitsubishi crank transverse junction stripe laser[5]. It was probed near the device center and directly on its cavity. The laser was prebiased below threshold ($I_b = 18mA$, $I_{th} = 22mA$) and pulsed with an HP comb generator to varying levels above threshold. The measurements, shown in figure 2, clearly demonstrate that the internal charge level overshoots and then clamps at threshold, where the amount of overshoot is dependent upon the overdrive conditions. The phase shift between the traces is primarily produced by the RF-power dependent time delay inherent in the HP comb generator. The dip preceding the step in the charge is caused by 100MHz feedthrough from the comb generator. Because the AlGaAs laser was grown on a $< 100 >$ substrate, and the internal electrical fields in the laser cavity were parallel to the surface (transverse junction), theoretically we expect to see no electrooptical effects, which has been experimentally verified.

Since the bandwidth of this measurement is determined by the pulsewidth of the probing laser, future measurements with improved infrared laser sources should be able to reveal spatial carrier dynamics at any point within the laser cavity with subpicosecond temporal resolution.

References

[1] M.P. Kesler, E.P. Ippen, *Appl. Phys. Lett.* **51**, 1765-1767 (1987)

[2] H.K. Heinrich, D.M. Bloom, B.R. Hemenway, *Appl. Phys. Lett.* **48**, 1066-1068 (1986)

[3] U. Keller, S.K. Diamond, B.A. Auld, D.M. Bloom, *Appl. Phys. Lett.* **53**, 388-390 (1988)

[4] T. Wilson, D.K. Hamilton, *Optica Acta* **31**, 453-465 (1984)

[5] K. Isshiki, N. Kaneno, H. Kumabe, H. Namizaki, K. Ikeda, and W. Susaki, *J. Lightwave Tech.* **LT-4**, 1475-1481 (1986)

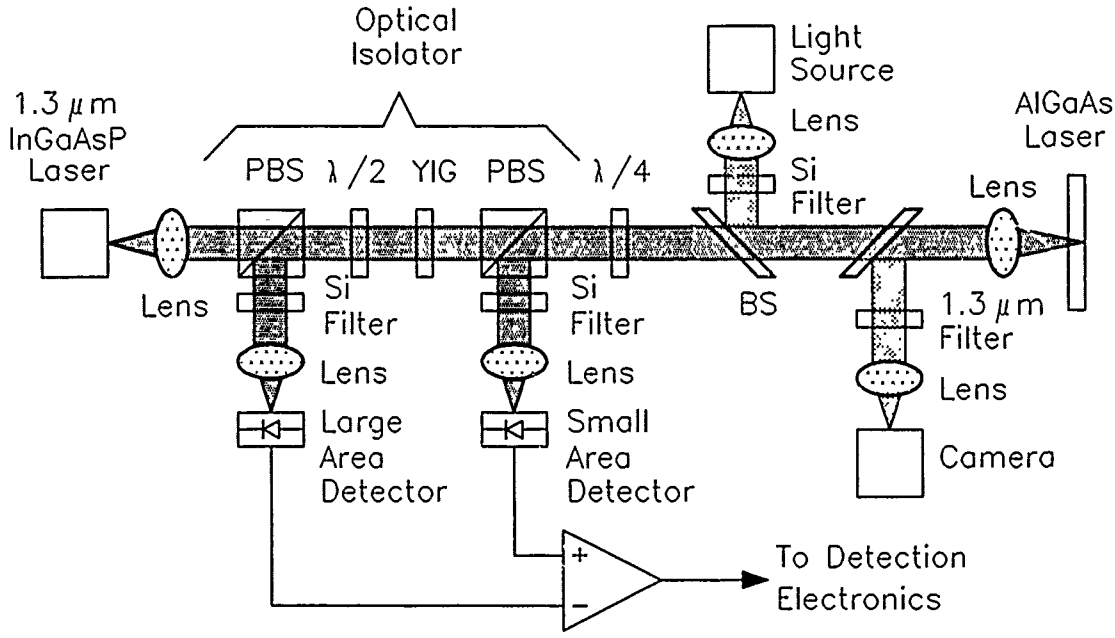

Figure 1: Differential phase contrast confocal microscope. PBS: Polarizing Beam Splitter. $\lambda/2$: Half-wave plate. YIG: Yttrium-Iron-Garnet Faraday rotator. $\lambda/4$: Quarter-wave plate. BS: Beam-Splitter.

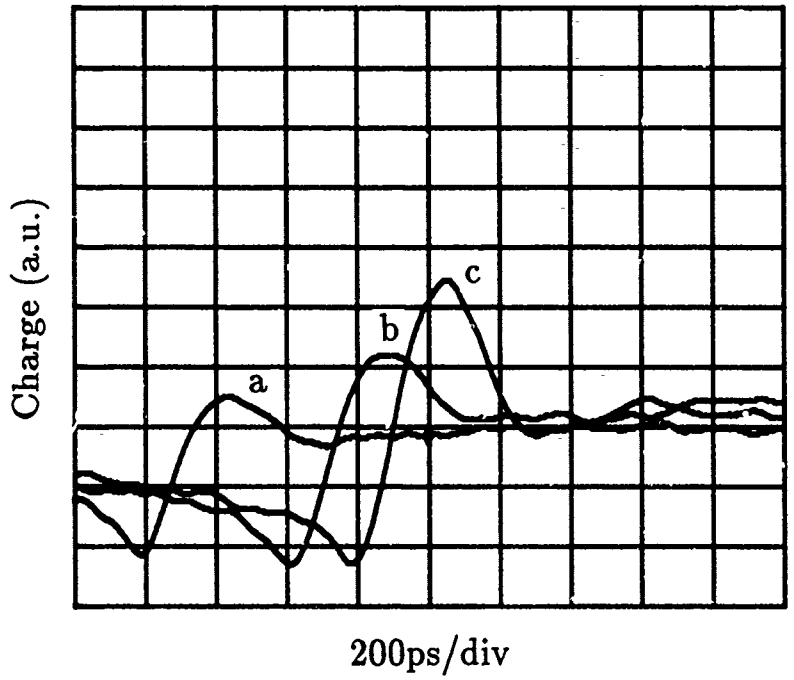

Figure 2: Optical detection of charge-density modulation in an AlGaAs Mitsubishi crank TJS semiconductor laser. a.) 10mA pulse. b.)15mA pulse. c.) 30mA pulse.

Spectral filtering of relaxation oscillations in injection current modulated diode lasers

S. Basu, P. May and J.M. Halbout
IBM Research Division, T.J. Watson Research Center,
Yorktown Heights, NY 10598

The spectral broadening of injection current modulated diode lasers has been reported in the literature(1-2). It was found that the output of a pulse modulated diode laser is chirped by the group velocity dispersion(3). It was also noted that the frequency chirp, which limits the distance bandwidth product in a long distance optical communication system, is dependent on the optical confinement in the semiconductor laser and hence it is possible to optimize the geometry of the laser design to reduce the frequency chirp(4). In this paper, we report our experimental work on time resolved spectral analysis of injection modulated diode lasers. We observed that the relaxation oscillations in a pulse modulated diode laser occur at longer wavelength than the primary pulse and hence simple spectral filtering of the pulse produces a single, clean pulse with a narrower spectral width.

The experimental set up is shown in figure 1. A Mitsubishi crank transverse junction stripe laser (5101A) operating at 830 nm was modulated by the output of a step recovery diode and in presence of different bias currents. The laser output was spectrally filtered by a grating and a slit combination. The wavelength of the beam emitting from the slit was measured by a grating spectrometer. A part of the beam was directed to the input slit of a synchroscan streak camera of 10 ps resolution. By translating the slit across the laser beam, simultaneous measurements of the temporal characteristic and the spectral characteristic of the laser output were made.

In the first experiment, the diode laser with a cw oscillation threshold of 29 mA was biased at 15 mA. A 10.4 V pulse, measured across a 50 ohm load, was delivered from a HP step recovery diode at 100 MHz. The current pulse duration was measured to be 112 ps. The diode laser pulsewidth was dependent on the bias current as expected and the minimum pulsewidth of 24 ps was obtained at 15 mA of bias. The spectrum of the laser output at three different modulation levels are shown in figure 2(a). At 10.4 V modulation voltage, the spectrum extends over 10 nm. The diode laser pulseshape is also shown in figure 2 (b).

Figure 3 shows the temporal shapes of the various spectral components comprising the current pulse modulated laser output. It is seen that the radiation which is emitted during the leading edge of the pulse is at shorter wavelength. The trailing edge of the pulse which contains the relaxation oscillations consists of radiation at longer wavelength. It was found that the shorter wavelength region of the spectrum shown in figure 2(a) with a width of 4 nm was free of any relaxation oscillations. The energy content in this 4 nm wide short wavelength region was 12% of the total energy. For many applications, where a clean pulse free of relaxation oscillations is desired, it thus will be a simple procedure to use a grating to obtain a clean pulse shape. The width of the spectrally filtered pulse in figure 3(a) was 19 ps without adjusting for the time resolution of the streak camera and the jitter of the trigger source.

The output spectrum is determined by various factors. In the transient condition of increasing injection current, a large number of longitudinal modes in the laser cavity reach threshold and hence the spectrum is broadened. The gain spectrum also shifts as a function of the injected current. As the photon density increases, the gain is depleted, and the longitudinal modes at the extreme ends of the lasing spectrum are above threshold for shorter duration than the modes in the center of the gain spectrum. The relaxation oscillations which evolve after the main pulse are at less gain condition and do not contain the extreme short wavelength part of the spectrum which is present in the first optical pulse. As a side effect, the time dependent carrier density inside the resonator also introduces time varying group velocity dispersion inside the resonator, and affects the longitudinal mode-spacing.

In one pulse shaping experiment, the laser beam was coupled into a 200 m long single mode fiber, and the output was spectrally filtered. We observed an asymmetric pulse shape in the short wavelength part of the spectrum. The shortest pulse had an unadjusted halfwidth of 18 ps and a fall time of 11.6 ps. In another experiment, a 21.3 ps diode laser pulse was shortened to a 18.2 ps pulse with 14.6 ps risetime by passing through a grating compressor.

In conclusion, we have investigated temporal and spectral evolution of a gain switched diode laser. The results presented here provide simple means for improving the pulse quality and the possibility of spectral pulse shaping of gain modulated diode lasers.

1. E.O. Gobel, G. Veith et. al., Appl. Phys. Lett, vol. 42(1), p. 25, 1983.
2. K. Petermann, Opt. and Comm. Electron., vol. 10, p. 233, 1978.
3. Y. Silberberg and P.W. Smith, IEEE JQE, vol. QE-22(6), p. 759, 1986.
4. A. Larsson, P. Andersson and A. Yariv, "Picosecond Electronics and Optoelectronics", p. 201, Springer-Verlag, 1987.

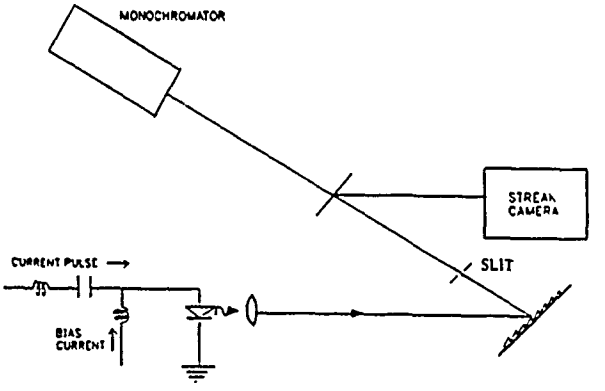

Fig 1. Experimental set up

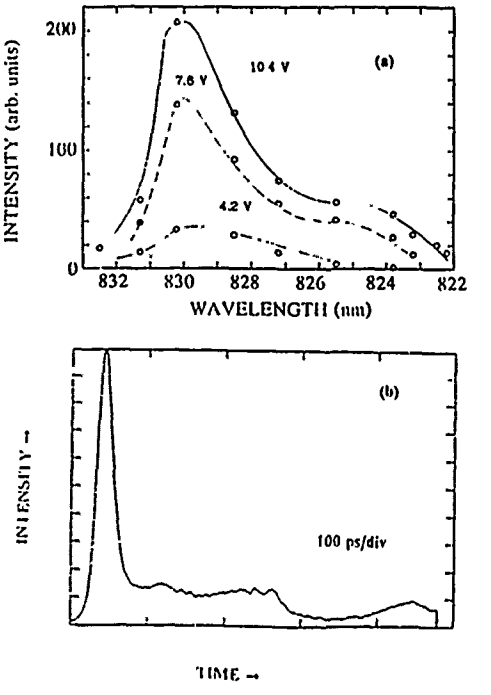

Fig 2. (a) Laser emission spectrum, (b) Laser output at 10.4 V modulation voltage and at 15 mA bias current.

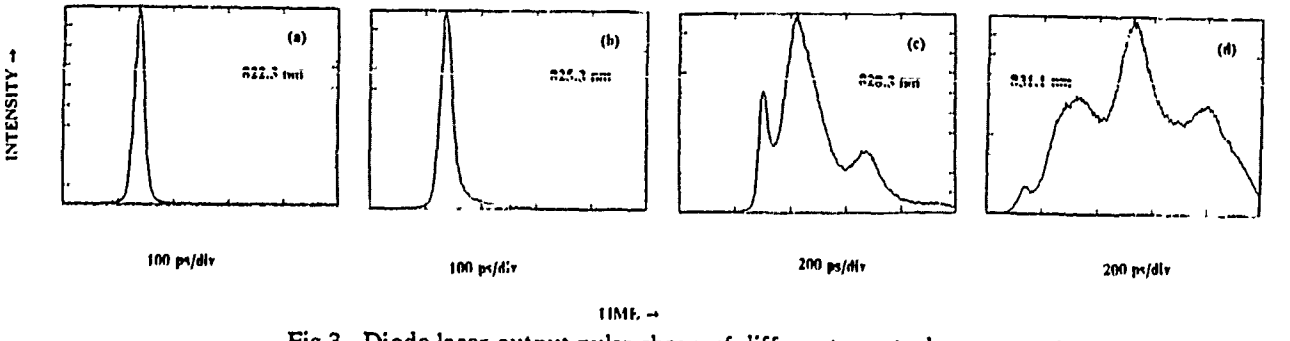

Fig 3. Diode laser output pulse shape of different spectral components. The x-axis represents only the pulse duration but not the delay.

AMPLIFICATION OF PICOSECOND PULSES USING PULSED SEMICONDUCTOR OPTICAL AMPLIFIERS

G. Eisenstein, P. B. Hansen, J. M. Wiesenfeld,
R. S. Tucker, and G. Raybon

AT&T Bell Laboratories
Crawfords Hill Laboratory
Holmdel, NJ 07733
(201) 888-7211

Traveling-wave semiconductor optical amplifiers have recently been used to amplify picosecond pulses [1-3]. Gain compression and the associated gain recovery, as well as pulse shaping have been studied in amplifiers which were driven by a constant bias current. Different gain characteristics are expected when the amplifier dc bias is replaced by short electrical pulses which are synchronized and properly timed relative to the input pulses. Under pulsed drive conditions, the amplifier has several important properties : (a) high gain during the short pumping time, (b) reduced noise, (c) shift of the gain peak toward shorter wavelength (due to band filling) during the electrical pulse. The high gain results from a large rapid increase in the carrier density during the transient and from a reduction in the thermal effects on the gain. A pulsed drive enables an increase in the maximum obtainable gain compared with a dc drive. Amplifiers operating with a pulsed electrical drive are useful in several applications. Examples are : (a) Amplification of picosecond pulses generated in semiconductor mode-locked lasers. (b) Amplifier-Modulators. (c) Studies of amplifier gain dynamics [4]. It is well known that in order to generate the shortest possible pulses, semiconductor mode-locked lasers need to be biased close to threshold. Consequently, their output power is low (typical average powers are less than one mW). A pulsed optical amplifier with high gain and high saturation energy [1] may be used to obtain high power short pulses. Amplifier-modulators have been suggested and demonstrated in both GaAs [5] and InGaAsP [6] devices. This application requires a modulated stream of short electrical pulses.

We report here gain measurements in a 1.3-μm traveling-wave amplifier using 15-ps input pulses and 60-ps electrical drive pulses. The experimental schematic is shown in Fig. 1. A 1-GHz clock signal drives both a semiconductor mode-locked laser and a step recovery diode. The 60-ps electrical pulses from the step recovery diode are combined with a dc bias to drive the amplifier under test. The mode-locked laser generates 15-ps pulses whose timing, relative to the electrical pulse, can be adjusted by varying the phase of the laser RF drive signal. The maximum available pulse current of ~175 mA was used in conjunction with a variable dc bias. Gain measurements were performed while varying the timing of the optical pulses over a range of 1 ns, thereby mapping out the temporal shape of the gain. A typical result obtained for a 250 μm long amplifier is shown in Fig. 2 for three dc bias levels. The three cases correspond to absorption, transparency, and low gain when the electrical pulse is off. The maximum measured gain was 15.5 dB which corresponds to a chip gain of ~25 dB. This gain is 5-6 dB larger than the maximum possible gain for this amplifier under dc drive conditions.

REFERENCES

[1] J. M. Wiesenfeld, G. Eisenstein, R. S. Tucker, G. Raybon, P. B. Hansen, Appl. Phys. Lett. 53, 1239, (1988).

[2] I. W. Marshall, D. M. Spirit, M. J. O'Mahony, Electron. Lett. 23, 818, (1987).

[3] G. Eisenstein, P. B. Hansen, J. M. Wiesenfeld, R. S. Tucker, G. Raybon, Appl. Phys. Lett. 53, 1539, (1988).

[4] W. Lenth, Optics Lett. 9, 396, (1984).

[5] J. Hegarty, and K. A. Jackson, Appl. Phys. Lett. 45, 1314, (1984).

[6] G. Eisenstein, R. S. Tucker, I. P. Kaminow, T. P. Lee, and C. A. Burrus, Electron. Lett. 20, 624, (1984).

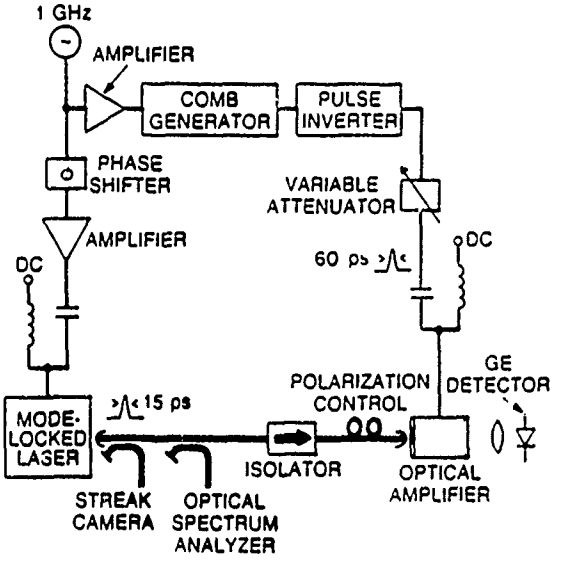

Fig. 1: Schematic diagram

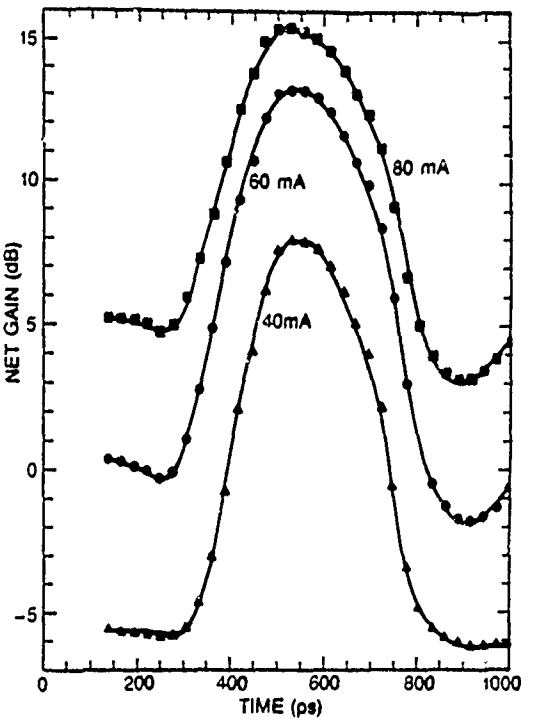

Fig. 2: Measured gain versus time

Ultrafast Nonlinearities in InGaAsP Diode Laser Amplifiers

K. L. Hall†, *E. P.Ippen*†, *J. Mark*†† and *G. Eisenstein**

†Department of Electrical Engineering and Computer Science and Research Laboratory of Electronics, Massachusetts Institute of Technology, Cambridge, MA 02139; ††Telecommunications Research Laboratory, Lyngsϕ Allé 2, DK 2970 Hϕrsholm, Denmark, *AT&T Bell Laboratories, Crawford Hill Laboratory, Holmdel, NJ 07733.

Semiconductor optical amplifiers are receiving increasing attention for possible applications to broadband optical communication and switching systems. Of particular interest are InGaAsP devices that can be tailored to the communication bands of 1.3 and 1.5 μm. Much is known about their linear and small signal characteristics, much less about their nonlinear and ultrafast dynamical properties. Studies of diode laser modulation characteristics[1], wave mixing[2,3] and picosecond pulse amplification[4,5] have provided information about population dynamics and gain compression. In this paper we present results from the first sub-picosecond investigations of InGaAsP laser amplifiers. They reveal strong nonlinearities due to nonequilibrium carrier distributions.

We performed pump-probe experiments using femtosecond pulses from a modelocked-color-center laser coupled to a nonlinear external resonator[6]. This laser is tunable from 1.48 to 1.54 μm and produces pulses of 100-200 fsec duration over this range, at a repetition rate of 100 MHz. Pump and probe pulses, with adjustable relative delay, are coupled into an active, traveling-wave InGaAsP amplifier. A short length of fiber terminated with a microlens is used for coupling into the diode to assure collinearity of pump and probe. Orthogonal polarizations are used, and a polarizer at the output selects the probe beam for detection.

Figure 1 shows typical data for the normalized probe transmission as a function of delay relative to the pump. The amplifier, which had a threshold of 13 mA as a laser before one facet was AR coated, was biased with a dc current of 30 mA. Pump and probe pulses, at identical wavelengths, were tuned into the gain bandwidth of the amplifier. The amplifier response is characterized by a transient gain compression (depletion) immediately following the pump pulse. Rapid, partial recovery of this compression occurs on a timescale of about 1 psec, too fast for population recovery due to transverse diffusion or current injection. Similar dynamics have been observed in AlGaAs lasers[7] and have been attributed to nonequilibrium carrier heating. An echo of this rapid transient is also apparent at the round-trip delay and is due to internal reflection from the imperfect AR coating. Complete recovery of the gain, associated with population recovery occurs on a nanosecond timescale.

These results clearly demonstrate strong, ultrafast gain nonlinearity due to a nonequilibrium carrier distribution. This is the first observation of nonequilibrium dynamics in these devices. It is evident that such dynamics can contribute significantly to the gain compression observed in the high frequency responses of diode lasers, and that they may produce intermodulation distortion in frequency multiplexed amplifiers. The picosecond recovery time seems commensurate with that required for carrier-lattice temperature equi-

libration and slower than that expected for the recovery of hole burning. Nevertheless, additional data are required for a more complete understanding of the underlying processes. Data taken at other wavelengths and different current levels will be described in our presentation.

We gratefully acknowledge collaboration with L. Y. Liu on the femtosecond color-center laser and support at MIT from AFOSR Grant No. 88C0089 and the Joint Services Electronics Program Grant No. DAAL03-86-K-0002.

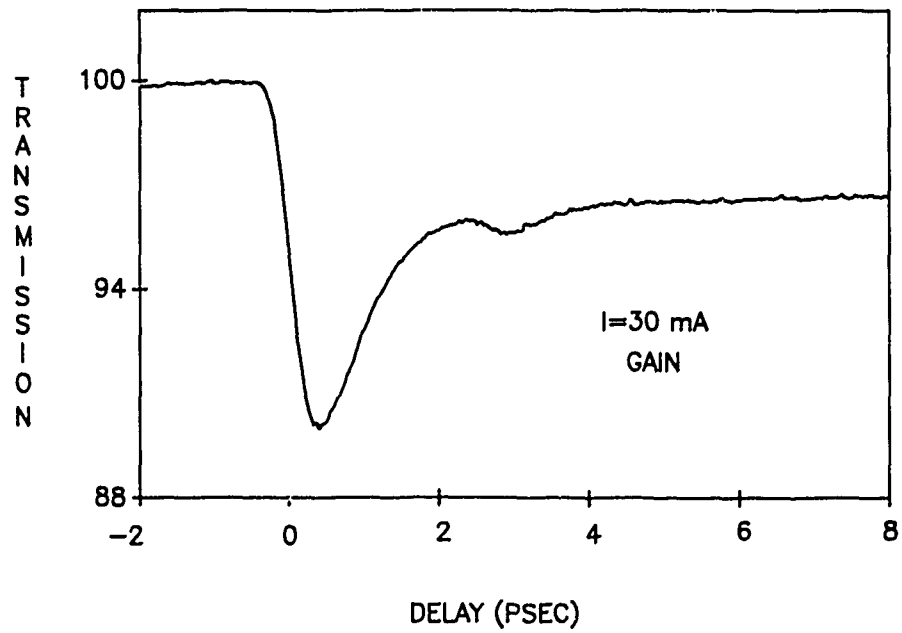

Figure 1. Probe transmission versus delay with respect to pump in a travelling wave InGaAsP amplifier.

References

1. R. S. Tucker, J. Lightwave Technol. LT-3, 1180 (1985).

2. K. Inoue, T. Mukai, and T. Saitoh, Appl. Phys. Lett. 51, 1051 (1987).

3. R. M. Jopson, T. E. Darcie, K. T. Gayliard, R. T. Ku, R. E. Tench, T. C. Rice, and N. A. Olsson, Electron. Lett. 23, 1304 (1987).

4. I. W. Marshall, D. M. Spirit, and M. J. O'Mahoney, Electron. Lett. 23, 818 (1987).

5. G. Eisenstein, P. B. Hansen, J. M. Wiesenfeld, R. S. Tucker, and G. Raybon, Appl. Phys. Lett. 53, 1539 (1988).

6. J. Mark, L. Y. Liu, K. L. Hall, H. A. Haus, and E. P. Ippen, Opt. Lett. (to be published, January 1989).

7. M. P. Kesler and E. P. Ippen, Appl. Phys. Lett. 51, 1765 (1987).

NOTES

WEDNESDAY, MARCH 8, 1989

SALON G

10:30 AM–12:15 PM

WB1–4

SUPERCONDUCTORS AND MODULATORS

L. Cooper, U.S. Office of Naval Research, *Presider*

RECENT DEVELOPMENTS IN HIGH T_c SUPERCONDUCTING FILMS AND DEVICES

R. A. Buhrman
School of Applied and Engineering Physics
Cornell University
Ithaca, N.Y. 14853-2501

The discovery of high temperature superconductivity (HTS) has created the opportunity for major extensions of current electron device applications of superconductivity, including opening up the possibility of integration of superconductivity with semiconductor devices. However, due to the difficult nature of the presently known HTS materials, the actual realization of this opportunity faces severe challenges. In this talk I will describe recent advances in, and current prospects for, the production of high quality, well-oriented HTS films with acceptable superconducting properties on technologically useful substrates, both insulating and semiconducting. Emphasis will be given to the discussion of new and improved techniques for the lower temperature growth and in-situ formation of the superconducting phase. The stability of current HTS materials will be discussed. I will also report on successful techniques for the formation of very low resistance contacts to HTS films and for the patterning of epitaxial films to micrometer, and possibly submicrometer, dimensions. The most recent results on the microwave and millimeter wave surface losses of high quality HTS material will be presented, as well as results on picosecond pulse propagation experiments on transmission lines formed from epitaxial HTS films.

Propagation of 1-ps Electrical Pulses on $YBa_2Cu_3O_{7-\delta}$ Superconducting Transmission Lines Deposited on $LaGaO_3$

Martin C. Nuss, P. M. Mankiewich, R. E. Howard, T. E. Harvey,
C. D. Brandle, B. L. Straughn and P. R. Smith
AT&T Bell Laboratories, Crawfords Corner Rd., Rm. 4C-330, Holmdel, NJ 07733
Tel. (201) 949-5358

The new high-temperature superconductors have triggered enormous interest not only because of the unique physics involved, but also because of their technical potentials like the promise for propagation of extremely short electrical pulses. Superconducting band gaps of ~20 THz are predicted assuming BCS-theory for the superconductor, making lossless propagation of electrical pulses as short as 50 fs possible.

Despite microwave measurements at low frequencies of several GHz, first studies at higher frequencies by Dykaar et al [1] have shown distortion-free propagation of 100 GHz electrical pulses on $YBa_2Cu_3O_{7-\delta}$ (YBCO) lines for ~ 5 mm propagation distance. Results were also reported for aluminum coplanar lines and a YBCO ground plane [2].

Here, we report the propagation of 1-ps electrical pulses (1 THz bandwidth) on YBCO coplanar transmission lines defined on lanthanum gallate ($LaGaO_3$) as a substrate. On $LaGaO_3$, YBCO grows highly oriented like on $SrTiO_3$. However, unlike $SrTiO_3$, $LaGaO_3$ has a much lower dielectric constant and small losses in the THz frequency range [3]. Electrical pulses of ~750 fs duration are generated in a radiation-damaged silicon-on-sapphire photoconductive switch integrated into a 20μm coplanar stripline with 10μm spacing and excited with 100 fs optical pulses from a CPM-laser. A ~1 THz bandwidth electrical contact is made to the YBCO coplanar stripline defined on $LaGaO_3$ using a "flip-chip" geometry. We find that electrical pulses broaden only from 750-fs to 1-ps with little loss in amplitude upon traveling through our flip-chip. Input and propagated electrical pulses are probed by electro-optic sampling in two small $LiTaO_3$-crystals separated by 3 mm.

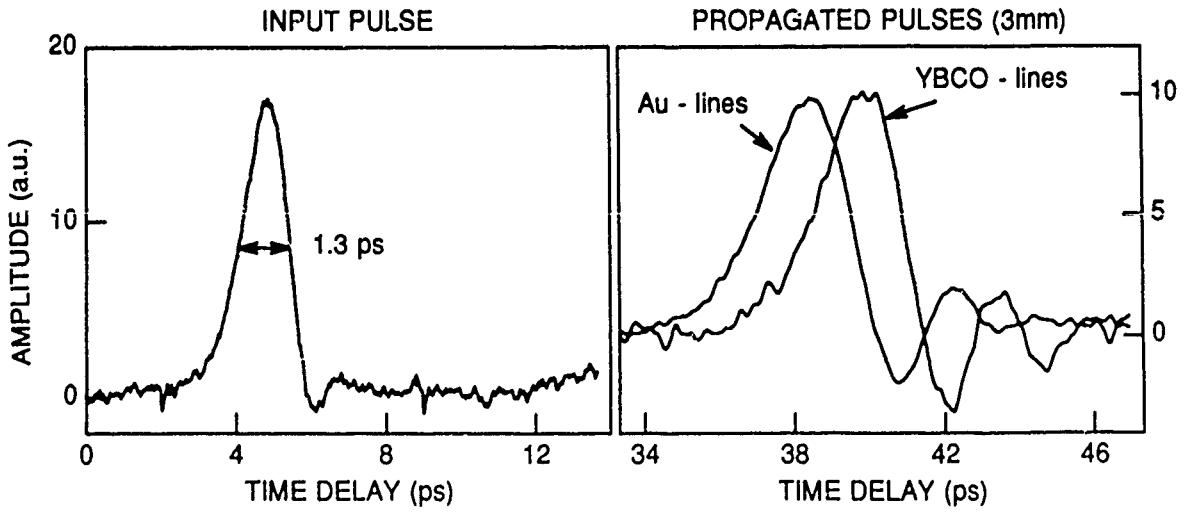

Fig. 1 displays input and propagated waveforms at a temperature of 12.5 K. As a reference, the propagated waveform on a gold stripline of identical dimensions on the same substrate is plotted in Fig. 2. The pulse on the YBCO line is slightly shorter than the one on the Au-line, demonstrating the capabilities of YBCO-lines for distortion-free propagation of even THz-bandwidth electrical pulses. The broadening from 1.3 ps to 2.3 ps is entirely accounted for by modal dispersion on the coplanar stripline due to the still relatively high dielectric constant of ~20. The shift of several picoseconds between the signal on Au-lines and YBCO-lines is due to the slower propagation velocity on superconducting lines.

The relatively low critical current density of $J_c \sim 10^3$ A/cm^2 at 65 K in our initial films on $LaGaO_3$ allows us to study the transient response of YBCO transmission lines to 1-ps pulses with currents close to and above the critical current density. The results are plotted in Fig. 2 for a fixed current density of 5×10^4 A/cm^2. Except for the lowest temperature, J_c is exceeded resulting in significant dispersion and attenuation. However, the attenuation is not by far as large as we would expect if the transmission line as a whole would become normal conducting. Furthermore, the increase in delay between input and propagated pulse with temperature still follows approximately the laws of a superconducting transmission line with T_c~90 K. We believe that this behavior stresses the importance of microlinks in YBCO transmission lines. Even in highly oriented films, the boundaries between grains represent tiny microlinks with a lower critical current than the grains themselves. The data in Fig. 2 therefore represent the case in which the critical current in the microlinks is exceeded, however the YBCO-grains still remain superconducting.

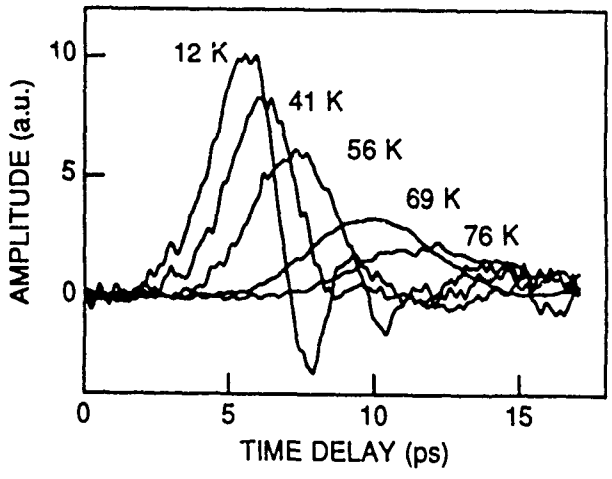

Fig. 2 Propagation of electrical pulses exceeding the critical current density of the transmission line.

We are currently studying the dynamic behavior of the microlinks as well as YBCO-transmission lines with higher critical current densities.

1. D. R. Dykaar, R. Sobolewsky, J. M. Chwalek, J. F. Whitaker, T. Y. Hsiang, G. A. Mourou, D. K. Lathrop, S. E. Russek and R. A. Buhrman, Appl. Phys. Lett. **52**, 1444 (1988)

2. D. Grischkowsky, I. N. Duling, OSA meeting, Rochester, NY (1987)

3. M. C. Nuss, C. D. Brandle, T. E. Harvey and P. R. Smith, to be submitted to Appl. Phys. Lett.

Spread Spectrum Integrated Optic Modulators

David W. Dolfi

Hewlett-Packard Laboratories

3500 Der Creek Road, Palo Alto, California 94303

In conventional integrated optic modulators, a trade-off exists exists between the drive voltage and bandwidth, due to the velocity mismatch between the modulating microwave voltage and the optical wave. This trade-off is normally controlled by the device length, whereby extended bandwidth can only be achieved by shortening the device active length, thereby increasing the drive voltage. One approach for overcoming this limitation involves the use of phase reversals in the microwave field to artificially advance the phase of the microwave field [1-3]. In this paper, we review the extension of this concept to the design of very wide band modulators whose phase reversals are patterned after spread spectrum sequences [4,5].

In the first part of the paper, the limitations of velocity mismatch in conventional modulator design will be reviewed, with examples. The operating principles of the spread spectrum, coded devices will be described in both the time and frequency domain, exhibiting both the advantages and limitations of these devices for various applications. In the second part of the paper, theoretical predictions and experimental results on specific spread spectrum modulator designs will be presented. These will be compared to conventional

electro-optic and other types of modulators. Measurement techniques used to characterize the frequency response of these devices will also be reviewed. Lastly, various applications of these devices will be discussed in light of their previously described advantages and disadvantages. Emphasis will be on applications in the area of high speed measurement. These application areas include - in the frequency domain - component evaluation, optical network analysis, and microwave mixing. In the time domain, applications to sampling of optical and electrical pulses will be discussed.

References:

[1] R.C. Alferness, S.K. Korotky, and E.A. Marcatilli, *IEEE J. Quant. Electron.*, vol. **QE-20**, pp. 301-309, (1984).

[2] A. Djupsjobacka, *Electronics Lett.*, pp. 908-909, (1985).

[3] D. Erasme and M.G.F. Wilson, *Opt. and Quant. Electr.*, **18**, pp. 203-211, (1986). [4] M. Nazarathy, D.W. Dolfi, and R.L. Jungerman, *J. Opt. Soc. Amer.*, **4**, pp. 1071-1079, (1987).

[5] M. Nazarathy, D.W. Dolfi, and R.L. Jungerman, *J. Lightwave Technol.*, **LT-5**, pp. 1433-1443, (1987).

Electro-Optical Synthesizing of Picosecond Optical Pulses.

Tetsuro Kobayashi and Akihiro Morimoto

Engineering Science, Osaka University
Toyonaka, Osaka 560, Japan

We will describe new electro-optical methods to generate arbitrarily shaped optical pulse signals in the picosecond range from cw lasers.

These methods are superior to ordinary methods utilizing passive modelocking and fiber pulse compression in controllability and stability, and probably more convenient for applications to high-speed electronics.

Direct generation of picosecond optical pulses from a cw laser by electrooptic modulation seems to be very difficult at first sight because a broad-band modulator with picosecond response is required. In our electro-optical synthesizing, however, we utilize frequency-domain control of optical sidebands produced by the modulation. For this case, what is required is not a broad-band modulator but widely spread sidebands. Fortunately it is possible to obtain the broad sideband as wide as 1THz by using even a narrow-band electrooptic modulator with the high modulation index[1]. Our method have potentialities to be applied to the subpicosecond range.

Here, we demonstrate three types of synthesizing : 1) by separation, control, and composition of each sideband component of the phase-modulated light using two gratings and a spatial filter, 2) by selection of produced sidebands using an FP filter, and 3) by control of near-field pattern of an elctro-optically deflected beam using a spatial filter and composition using a grating or a slit.

1. Method utilizing spatial control of PM sidebands [2]

Fig. 1 shows the basic construction of the synthesizer, which is basically equivalent to the method 3[3] and to Weiner's recent work[4]. This is one of the modifications of frequency-domain multiplexing. Sinusoidal phase modulation produces a series of side-band components at intervals of the modulation frequency. Each component can be separated spatially by a diffraction grating with optical Fourier transform system. Its amplitude and phase can be controlled individually by a spatial filter, or a modulato. array (c.f. for single shot pulse input with continuous frequency spectra[4]). Then the synthesized output is obtained after multiplexing with another set of Fourier transform optics and grating. The necessary amount of phase control is at most 2π.

We have done preliminary experiments using a cw Ar laser and a 9.35GHz $LiTaO_3$ phase modulator[1,5] and succeeded in synthesizing picosecond optical pulses[2].

2. Method with a Fabry-Perot Filter [6]

In this simple method, shaped pulses are obtained by selection of the proper sidebands using a Fabry-Perot interference filter as shown in Fig.2. The method can not apply to arbitrary shaping, but is suitable to get high-repetition pulse trains. In practice, we succeeded in generating of pulse trains at 9-112 GHz repetition rates[6].

3. Method with 10GHz EO Deflector

It is known that the instantaneous optical frequencies at the output plane of an electrooptic deflector depend linearly on the spatial positions in the beam cross section[3]. Accordingly, the output plane of the deflector corresponds to the frequency plane in Fig.1 and a type of optical synthesizing is realized by using the construction shown in Fig.3(a). It is known that this method has the function as a pulse compressor[3]. Pulse synthesizing is also possible if the grating is replaced by a slit at the cost of efficiency. In the experiment, we used new scheme of electro-optic deflector with the world record driving frequency of 9.35GHz as shown in Fig.3(b), where an optical beam passes through at the node of the standing electric wave. As results, 10ps pulse trains with 18.7GHz and 9.35GHz repetitions were obtained by using the slit and the grating, respectively.

References

1. K.Amano, T.Kobayashi, H.Yao, A.Morimoto, and T.Sueta: J. Lightwave Technology, LT-5, 1454 (1987).
2. T.Kobayashi, M.Doi, B.Y.Lee, A.Morimoto, and T.Sueta:in *Ultrafast phenomena VI*, eds. C.B.Harris, T.Yajima, and K.Yoshihara(Springer-Verlag, Berlin, 1988)/ *Dig.Jpn Soc.Appl.Phys.* 27p-F-12 (1986/9)/30p-ZG-14(1987/3).
3. T.Kobayashi, H.Ideno, and T.Sueta: IEEE J. Quant. Electron. QE-16, 132 (1980) / T.Kobayashi: *Japan Patent, No.1268338* (1977).
4. A.M.Weiner, J.P.Heritage, and E.M.Krishner: J. Opt.Soc. Am. B-5, 1563(1988).
5. T.Kobayashi, Y.Fukushima, H.Yao, K.Amano, A.Morimoto, and T.Sueta: IEEE J. Quant. Electron. QE-24, 382(1988).
6. A.Morimoto, H.Yao, T.Kobayashi, and T.Sueta: *IQEC '88*, ThH-6(1988).

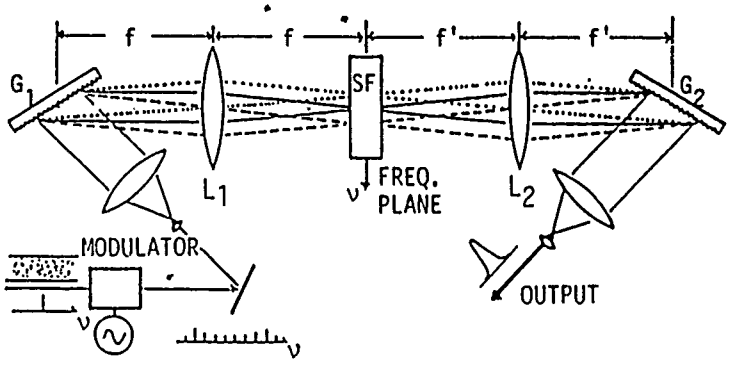

G1, G2 : Grating
L1, L2 : FT lens
SF : Spatial filter

Fig.1 Basic construction of optical synthesizer[2].

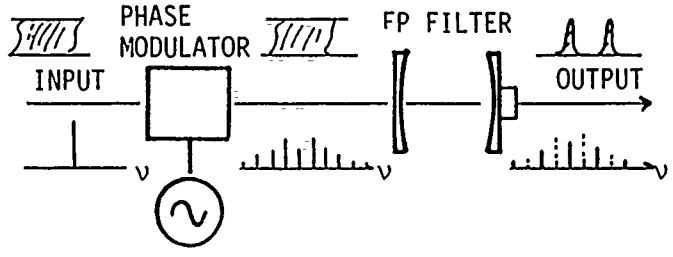

Fig.2 Optical pulse generation by selection of PM sideband using an FP filter.

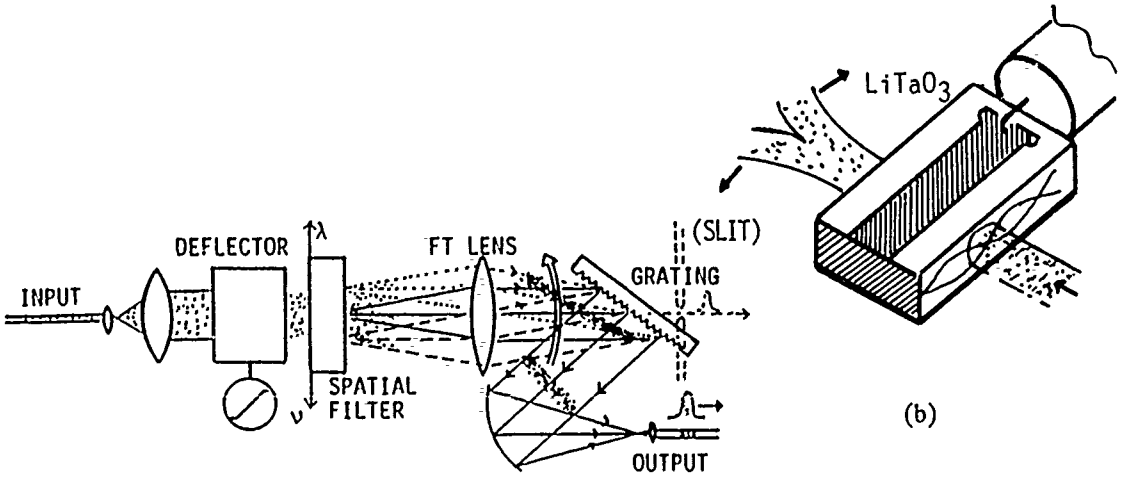

Fig.3 Pulse generation / compression / shaping by an EO deflector.

WEDNESDAY, MARCH 8, 1989

SALON G

1:30 PM–2:45 PM

WC1–4

JOINT SESSION ON TUNNELING AND RESONANT TUNNELING: 1

James S. Harris, Stanford University, *Presider*

ULTRAFAST OPTICAL STUDIES OF TUNNELING AND PERPENDICULAR TRANSPORT IN SEMICONDUCTOR MICROSTRUCTURES

Jagdeep Shah*
AT&T Bell Laboratories
Holmdel, N. J. 07733, U. S. A.

Novel electronic properties of superlattices, double barrier diodes and other semiconductor microstructures have generated considerable current interest from fundamental as well as device points of views. One of the driving forces behind this interest is the possibility of novel high speed devices; e.g. Sollner et al [1] have shown very high frequency response for double barrier diodes. There are also a number of very interesting fundamental issues as proposed in the original work of Esaki and Tsu [2]. Some of this work has been recently reviewed by Esaki [3] and Capasso et al [4].

The recent availability of ultrafast lasers in the femtosecond and picosecond time domain has made it possible to directly investigate some of the interesting phenomena associated with transport in superlattices and the dynamics of tunneling in semiconductor microstructures. This talk will review some basic concepts in optical studies of perpendicular transport [5] and then discuss recent experiments [6] on the measurement of tunneling times and perpendicular transport in semiconductor microstructures.

Tunneling times for electrons have been measured directly in asymmetric double quantum well structures using subpicosecond luminescence spectroscopy [6]. The tunneling times for electrons in the narrow well were measured for the non-resonant condition as well as for the resonant condition when the n=1 electron subband in the narrow well was at the same energy as the n=2 electron subband in the wide well. A sharp reduction in the tunneling time is observed at the resonance. The measurements will be discussed and compared with theoretical predictions.

These examples illustrate that optical spectroscopy provides a powerful means of obtaining quantitative information about tunneling and transport. Such information is relevant for picosecond electronic and optoelectronic devices and provides fundamental insights into the dynamics of tunneling and transport.

---

* work done in collaboration with D. Y. Oberli, T. C. Damen, C. W. Tu, T. Y. Chang, D. A. B. Miller, A. E. DiGiovanni, R. F. Kopf, N. J. Sauer, J. E. Henry

[1] T. C. L. G. Sollner, W. D. Goodhue, P. E. Tannenwald, C. D. Parker and D. D. Peck, Appl. Phys. Letters **43**, 588 (1983)

[2] L. Esaki and R. Tsu, IBM J. Res. Dev. **14**, 61 (1970)

[3] L. Esaki, IEEE J. Quantum Electronics **QE-22**, 611 (1987)

[4] F. Capasso, K. Mohammed and A. Y. Cho, IEEE J. Quantum Electronics **QE-22**, 1853 (1987)

[5] B. Deveaud, Jagdeep Shah, T. C. Damen, B. Lambert, A. Chomette and A. Regreny, IEEE J. Quantum Electronics **QE-24**, 1641 (1988)

[6] D. Y. Oberli, Jagdeep Shah, T. C. Damen, C. W. Tu, T. Y. Chang, D. A. B. Miller, A. E. DiGiovanni, R. F. Kopf, N. J. Sauer and J. E. Henry, to be published

Optical Detection of Resonant Tunneling of Electrons in Quantum Wells

by

G. Livescu, A.M. Fox, T. Sizer, W.H. Knox and D.A.B. Miller*

AT&T Bell Laboratories, Holmdel, NJ 07733

The investigation of vertical transport in superlattices (SL's) and multiple quantum wells (MQW's) has recently attracted much attention. Intense research was focused on basic quantum effects such as Bloch transport of electrons and holes in minibands,[1] coherent and incoherent, resonant, sequential and Zener tunneling[2] in double barriers,[3,4] SL's and MQW's of GaAs/AlAs,[5,6] GaAs/AlGaAs,[7] and InGaAs/InP.[2,8] In addition to the academic interest, the understanding of the mechanisms of escape from and travel through quantum wells is vital for the recently developed and constantly growing family of electro-optical devices using semiconductor quantum wells. Most of them are based on the quantum-confined Stark effect (QCSE), and they include bistable self-electro-optic effect devices (SEED's), tunable detectors, electro-absorption modulators and optical logic elements.[9] The basic unit of all of these is an epitaxially grown p-i-n diode, with the quantum well layers in the intrinsic region. By reverse biasing the diode, an electrical field is applied on the quantum wells, controlling its optical absorption spectrum. Since operating wavelengths are close to the excitonic absorption peaks, photoexcited charge is created in the quantum wells and is transported to the electrodes. The mechanisms by which this transport occurs are ultimately responsible for the intrinsic maximum speed or operating intensity of these devices.

The techniques used to investigate the dynamics of the photoexcited carriers have included transport (static[2,4-6] and time-resolved[4-6] photocurrent) as well as optical experiments (static[5,7,8] and time-resolved[1,3] photoluminescence, as well as time-resolved electroabsorption[10,11]). For the present work we chose the latter method, in which the picosecond pump-and-probe technique is used to study the photoexcited carrier escape rate, through the voltage changes induced on the electrodes upon their arrival. We find that the rise time of the induced change in absorption is extremely sensitive to the applied DC voltage, varying between 400 ps at low voltages and 25 ps at high voltages. It also exhibits a pronounced minimum at an intermediate voltage, for which the n = 1 electron level in one quantum well is in resonance with the n = 2 electron level in the adjacent one.

The sample used was a p-i-n structure grown by MBE, containing in its intrinsic region 75 periods of 65Å/58Å $GaAs/Al_{0.26}Ga_{0.74}As$ quantum wells. Using photolithographic techniques, contacts were made to the doped regions, with 200μm×200μm windows on the p side. The samples were antireflection coated and the substrate was etched away. The transmission spectrum at room temperature (Fig. 1) exhibits the excitonic peaks associated with the allowed n = 1 and n = 2 transitions. By applying a voltage (e.g. 10V, as in Fig.1), the allowed peaks shift to lower energy and broaden, while new peaks appear, associated with the forbidden transitions. The shift of the n=1 (heavy hole) hh and (light hole) lh excitonic peaks could be followed up to an applied voltage of 30 V (the breakdown voltage was 38V), and were found to be in reasonable agreement with those predicted by the QCSE theory.

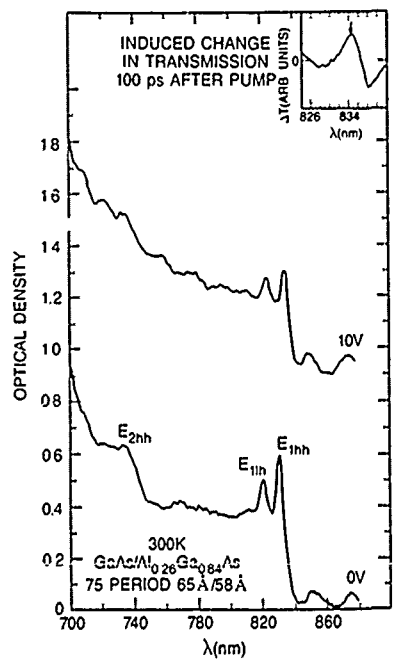

Fig.1. Absorption spectra of the MQW p-i-n modulator (vertically shifted for clarity). Inset: differential transmission at 10 V and 100 ps after the pump. Arrow: wavelength used for time-resolved measurements at 10 V.

For the time-resolved measurements we used a conventional pump-and-probe arrangement, exciting the photocarriers with a short laser pulse (pump), and monitoring the induced transmission changes with a second, time delayed pulse (probe). Both beams were derived from the same synchronously pumped Styryl 9 dye laser (6-10 ps pulse width, 780-870 nm tuning range). The geometry of the measurements is described in more detail elsewhere.[11]

The two beams were focused to ~25μm diameter spots coincident on the sample. The average optical powers were kept relatively low: 20-50 μW (0.24-0.6 pJ per pulse) for the exciting beam, and 5 μW for the probe. The number of photoexcited carriers per pulse was $(2-5)\times10^{15}cm^{-3}$. The carriers are created in *all* the wells throughout the sample, although their concentration becomes somewhat smaller as the exciting beam exits the sample. The carriers are generated with very small kinetic energy near the lowest allowed confined level. They are separated by the field, escape from the quantum wells and are swept towards the electrodes. Upon their arrival there (after a time τ) a voltage pulse ΔV is generated on the electrodes, which reduces the bias across the diode locally in the region of the spot, thereby inducing a change in the absorption, through the QCSE. We detected the changes in the intensity of transmitted probe using standard lockin techniques (the pump beam was chopped at 1.5 kHz). An example of the signal one obtains is shown in the inset of Fig. 1. Represented here is $-\Delta T$ (where ΔT is the change in transmission) as a function of wavelength, 100 ps after the exciting pulse. This signal is proportional to $\Delta\alpha$, and its shape indicates a blue shift of the E_{1hh} exciton ($\Delta\alpha < 0$ at long wavelengths), as well as an increase of the peak absorption ($\Delta\alpha > 0$ at shorter wavelengths). A similar, but weaker, signal is obtained also for wavelengths around the E_{lh} exciton. The differential absorption spectrum changes with the applied bias, because of the shift of the excitonic peaks. Therefore, when measuring the time dependence of $\Delta\alpha$ we always chose the wavelength corresponding to the largest positive $\Delta\alpha$ at that voltage. The magnitude of $\Delta\alpha$ is roughly proportional to ΔV, which, in turn, is determined by the total number of photoexcited carriers, thus by the power of the exciting beam. We have checked this proportionality over more than one order of magnitude. One can actually calculate ΔV (thus $\Delta\alpha$) for any exciting power; but the values obtained are at least one order of magnitude larger than the measured ones. We have shown in our previous work[11] that the reason for obtaining small $\Delta\alpha$ lies in the *fast recovery* of the initial voltage, or, in other words the *fast decay* of ΔV in the region of the exciting spot. This is due to the fact that ΔV quickly spreads over the area of the electrodes through a mechanism of diffusive electro-magnetic propagation. The diffusive time constant t_c is determined by the resistivity of the electrodes, the thickness of the intrinsic region of the diode, and the size of the exciting spot. For our sample and spot size, $t_c \sim 5$ ps. The magnitude of ΔV (hence $\Delta\alpha$) is thus the result of these competing processes: the build-up of the voltage pulse at the electrodes during a time τ, and its decay, with a time constant t_c. For $\tau \gg t_c$, ΔV will be much smaller than estimated; it increases for smaller values of τ. This is illustrated in Fig. 2, where the time dependence of the signal is plotted, for different values of τ. The experimental curves were measured at different applied voltages, but are normalized to the same exciting power, and the same value of the absorption coefficient. The dotted curves in Fig. 2 are calculated, using the diffusion model described before,[11] with a single set of parameters. Only the "transit times" τ (or "emission rates") are different for each curve, definitely proving that the faster rise time is always associated with a larger signal.

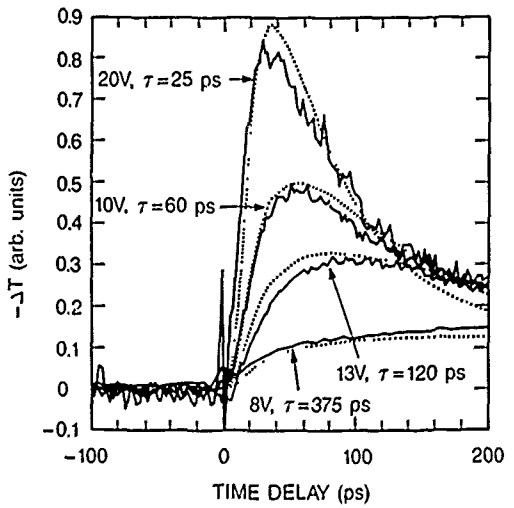

Fig.2. Differential transmission at different applied voltages, vs. time delay after excitation. Full lines: experimental. Dotted lines: calculated.

Our main emphasis in this work is the measurement of the rise times and their dependence on the applied voltage. A key result of our experiment is that the rise times do not depend monotonically on voltage (Fig. 2). We have repeated these measurements over a wider voltage range and in smaller voltage steps, and the results are plotted in Fig. 3. A sharp decrease of the rise times with increasing voltage is observed, with a clear minimum around 10.5V. The tunneling probability of a particle of mass m^* through a square potential barrier of height E_b and width L_b has the form $\exp[-(8m^*E_b/\hbar^2)^{1/2}L_b]$. In the presence of an applied field, the barriers become triangular, with an effective thickness proportional to 1/F (F = the applied field). Therefore, a strong increase of the tunneling probability is expected for larger applied fields, i.e. a sharp overall decrease of the "escape time" of the particles. Since the tunneling probability of the electron is about 500 times larger than that of a heavy hole, the electrons are the ones expected to tunnel. The presence of the minimum shows that resonant tunneling occurs, and its position is in agreement with the calculated "alignment" of the n = 1 electron level in one well with the n = 2 level in the adjacent well. However, the relatively large value of $\tau = 50$ ps cannot be compared with any of the calculated tunneling times. Once a carrier is in the conduction band, it only needs ~10 ps to traverse the whole structure at the saturated drift velocity. Assuming sequential tunneling, and assuming that an electron is recaptured in the next well after each successful escape attempt, one may divide this time by the 75 periods, to obtain 0.7 psec, which is a number closer to some theoretical estimates. More work is needed, however, to clarify the nature of this resonance, and the times associated with it. Preliminary low temperature (80K) measurements indicate that the rise times do not become longer, which strongly suggests that the dominant escape mechanism of the carriers is tunneling through the barriers, rather than thermionic emission, as previously proposed.[10,12]

In conclusion, our time-resolved electroabsorption measurements in a GaAs/AlGaAs p-i-n MQW diode suggest that the main escape mechanism of the photoexcited carriers is tunneling. By studying the dependence of the "sweep out" time on applied bias, we find evidence for resonant tunneling of electrons.

Our thanks are due to A.C. Gossard and J.H. English for the growth of the sample, to F. Beltram for illuminating dicussions on resonant tunneling, and to D. Oberli for sharing with us results of his most recent work on picosecond time resolved luminescence in GaAs/AlGaAs QW's.

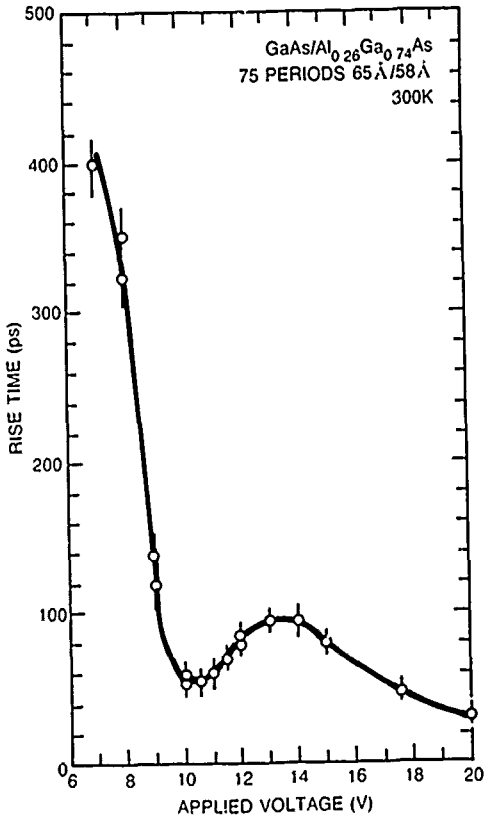

Fig.3. Differential transmission rise time vs. applied voltage.

REFERENCES

* Present address: AT&T Bell Laboratories, Murray Hill, NJ 07974.

1. B. Deveaud, J. Shah, T. C. Damen, B. Lambert and A. Regreny, Phys. Rev. Lett.58, 2582 (1987).
2. See the reviews in IEEE J. of Quantum Electron. 22 (1986) by E. Esaki (p. 1611) and F. Capasso, K. M. Mohammed, and A. Y. Cho (p. 1853).
3. M. Tsuchiya, T. Matsusue and H. Sakaki, Phys. Rev. Lett.59, 2356 (1987).
4. K. K. Choi, B. F. Levine, C. C. Bethea, J. Walker and R. J. Malik, Phys. Rev. Lett.59, 2459 (1987).

5. S. Tarucha and K. Ploog, Phys. Rev. B **38**, 4198 (1988).

6. H. Schneider, K. von Klitzing and K. Ploog, to be published in Superlattices and Microstructures (1989).

7. Y. Horikoshi, A. Fischer and K. Ploog, Phys. Rev. B **31**, 7859 (1985).

8. R. Sauer, K. Thonke, W. T. Tsang, Phys. Rev. Lett. **61**, 609 (1988).

9. For a recent review of electro-absorption devices see D. A. B. Miller, Opt. Eng. **26**, 368 (1987), and G. Livescu and D. A. B. Miller, in "Spatial light modulators and applications II" , SPIE, vol.825, p.69 (1987).

10. R. J. Manning, P. J. Bradley, A. Miller, J. S. Roberts, P. Mistry, M. Pate, Electronic Letters **24**, 854 (1988).

11. G. Livescu, D.A.B. Miller, T. Sizer. D.J. Burrows, J.E. Cunningham, A.C. Gossard and J.H. English, submitted to Appl. Phys. Lett.

12. A. Larsson, P.A. Andrekson, S.T. Eng and A. Yariv, IEE J. Quantum Electron.**24**,787 (1988).

Optical Evidence of Charge Accumulation in Double Barrier Diodes

N.VODJDANI, E.COSTARD, F.CHEVOIR, D.THOMAS, P.BOIS, S.DELAITRE
THOMSON-CSF LCR, Domaine de Corbeville, BP 10
91401 ORSAY Cedex, FRANCE

Tunneling is one of the basic quantum mechanical phenomena which plays a key role in many ultra thin semiconductor devices. Besides their potential for applications, double barrier heterostructures are also interesting for the understanding of tunneling-based transport processes (1) and their dynamics. Time-resolved photoluminescence (PL) has been used to determine the tunneling escape rate of electrons from a single quantum well through a thin barrier into a continuum (2) and to determine the electric field dependance of this tunneling rate (3).The charge accumulation in the quantum well can be estimated using magnetotunneling (4) or as recently demonstrated steady-state photoluminescence (5).

In this work, we present optical studies on DBD samples with large undoped spacer layers on each side of the barriers which are thought to be useful for high frequency operation (6).The steady-state electron accumulation in the quantum well is measured as a function of bias voltage and at the same time we observe an optical transition which corresponds to the build-up of an electron accumulation layer (EAL) in the emitter side spacer. These results are consistent with other magnetotunneling experiments (7) and support the idea that with spacer layers resonant tunneling can occur between localized states (8).

The sample was grown by molecular beam epitaxy on a $10^{18}cm^{-3}$ silicon doped substrate and consisted of the following layers : 300 nm GaAs n^+ (10^{18} cm^{-3}) buffer layer, 20 nm non-intentionally doped (nid) spacer, 10 nm (nid) $Al_{0.39}$ $Ga_{0.61}As$ barrier, 5nm(nid)GaAs Quantum well, 10nm(nid) $Al_{0.39}$ $Ga_{0.61}As$ barrier, 20 nm (nid) spacer layer and a 300 nm GaAs n^+ (10^{18} cm^{-3}) contact layer. In order to perform optical measurements under applied voltage 500 µm x 600 µm mesas were etched through the structure. AuGeNi-Au alloyed ohmic contacts were realized on the back side and on an annular contact on the mesa. This diode structure was designed to have low current densities compatible with large size mesas.

The sample was mounted in a variable temperature (4 K-300 K) optical cryostat. A 5 mW HeNe laser was focused on the Mesa.

Bias was applied on the sample using a four probe technique. For high pumping power densities the effect of the He-Ne laser illumination on the current voltage characteristic is to shift slightly the whole I (V) curve to lower (absolute) voltages and this for both positive (positive bias : electron injection from the substrate) and negative biases. It can be explained in the following way : light creates electrons which are captured in the EAL against the emitter barrier, while holes are captured against the collector barrier thus increasing the electric field in the well region. Then the situation in presence of light at a given bias is similar to the one

in the dark at a higher bias. For the experiments presented here care has been taken to work at low excitation power density ($1W/cm^2$) in order to minimize perturbations due to HeNe illumination.

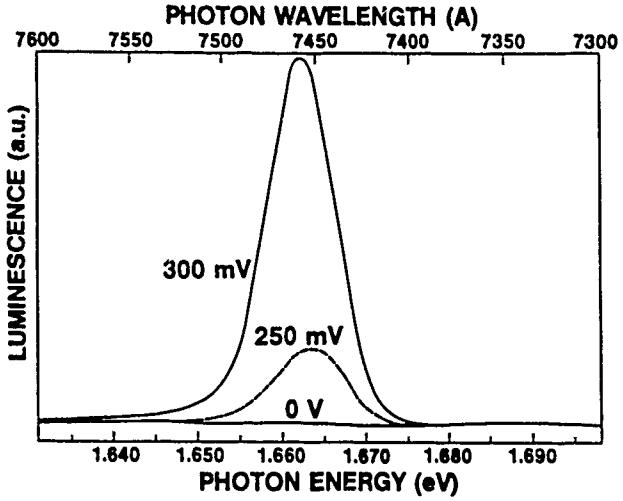

Fig. 1
5K PL spectra of the DBD quantum well under O mV, 250 mV and 300 mV applied Bias.

At zero bias, the photoluminescence of the QW (around 7450 A°) is hardly observable. Because the tunneling rate of electrons through the barriers is higher than the radiative recombination rate, in this experiment the main role of the HeNe illumination is to provide nonequilibrium free holes in the valence band of the QW and spacer layers.
Under applied bias electrons accumulate in the QW and recombine with the free holes optically injected. As a result the photoluminescence of the QW increases with current by more than two orders of magnitude as illustrated in fig. 1 which shows the Quantum Well photoluminescence for 0 mV, 250 mV and 300 mV at 5 K. The I-V curve of the DBD is shown in fig. 2a.

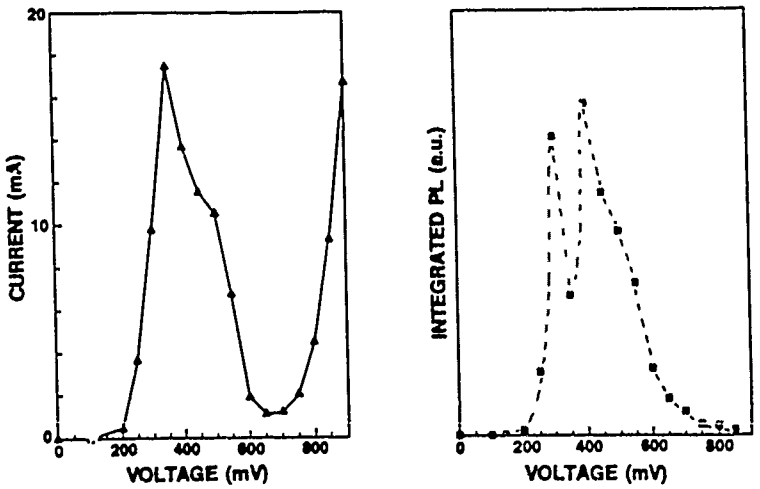

Fig.2
Current and integrated photoluminescence intensity of the DBD QW as a function of voltage.

In fig.2b for each voltage we have plotted the integrated QW luminescence. It can be seen that :

(i) the variation of integrated luminescence versus voltage follows roughly the current dependence up to 650 mV (5).

(ii) Above 650 mV the integrated QW luminescence intensity stays at the same level as at 0 bias and does not follow anymore the rise of current. This is because the 50 A° QW has only one electron quasi-bound state and above 650 mV the current rise is due to electrons flowing through extended states. These electrons do not accumulate in the QW and therefore do not contribute to the PL.

(iii) In the rise of integrated photoluminescence with bias there is a drop of intensity occuring at the maximum of current without any change of the QW photoluminescence shape. For higher optical pump power this "accidents" occur even more frequently, but are always located in the high current region of the I(V) curve. They can probably be associated with changes in radiative recombination kinetics. It appears therefore difficult in these conditions to give an accurate estimate of the steady state density of electrons accumulated in the QW and their characteristic escape time versus voltage.

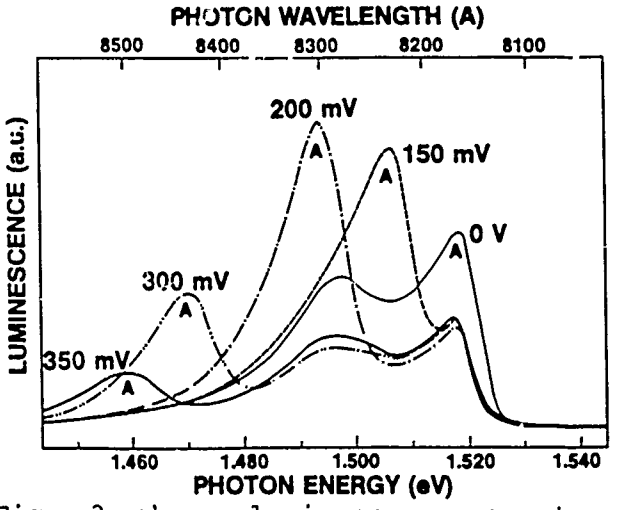

Fig.3
5K PL spectra for the region around GaAs band gap for different voltages.

Fig. 3 shows luminescence spectra in the region around GaAs bandgap for different applied biases. The "A" labelled transition shifts linearly towards lower energies and its intensity fades out with applied bias. The corresponding Stark shift at 350 mV applied voltage is about 60 mev.

To interpret these results, we have calculated the band structure of the device under bias by solving Poisson's equation self-consistently in the accumulation region. We have included space-charge effects in the well with a sequential tunneling model (9). Quantized state energies are given by resonances in the transmission coefficient. The calculation of the transmission coefficent includes the well, barriers, and the undoped spacer layers where band bending effects are taken into account.

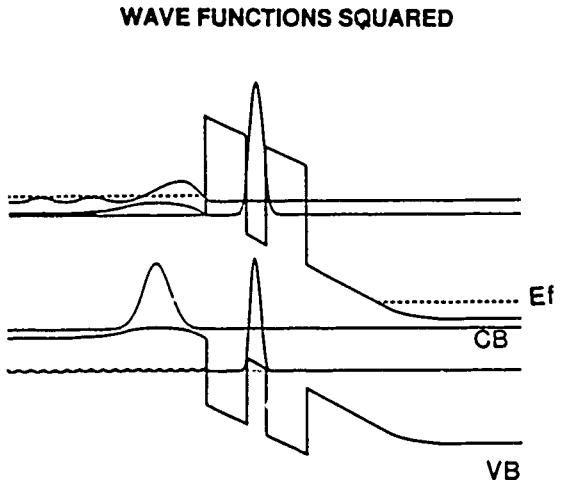

Fig.4
Calculated conduction and valence band structure of the DBD under bias, and squared wavefunctions for electron and heavy holes (the fundamental bound state) in the QW and in the emitter side spacer.

The results (see fig.4) show that as the EAL forms in the emitter side spacer layer when the device is biased, a trough develops in the valence band at the boundary between degenerate and undoped GaAs. Therefore, we believe that the "A" line is due to recombination of electrons in the EAL and holes in the trough. This important linear stark shift and the concomitant, quenching are due to spatial separations of charges.
The existence of localized states in the EAL observed in the emitter side of the DBD implies that at least part of the transport involves anti-crossing between two localized states of the EAL and QW rather than between 3D emitter and QW.
This mechanism allows current densities comparable to those obtained with thin spacer layers (7).

In summary using PL we have observed the charge build-up in the Quantum Well and EAL of a double barrier diode under operation. For large spacers the transport mechanism takes place between two localized states.

Acknowledgments : The authors would like to thank B. VINTER, C. WEISBUCH and J. NAGLE for fruitful discussions.

References

(1) R. Tsu, L. Esaki, Appl. Phys. Lett. 22, 562, 1973.
(2) M. Tsuchiya, T. Matsusue, H. Sakaki, Phys. Rev. Lett. 59, 20, 1987 (2356).
(3) M. Tsuchiya, T. Matsusue, H. Sakaki, Proceedings Ultrafast Phenomena, Kyoto, July 1988.
(4) L. Eaves et al., Appl.Phys.Lett., 52,212, (1988).
(5) J-F. Young et al., Phys. Rev. Lett., 60, 2085, (1988)
(6) V.Kesan et al., IEEE Trans.on. El.Dev., ED-35, p.405, (1988)
(7) D.Thomas, F. Chevoir, P. Bois, E. Barbier, Superlattices and Microstructures (1988) (in press).
(8) B. Ricco and Y. Azbel, Phys. Rev. B 29, 1970 (1984)
(9) F.W. Sheard and G.A. Toombs, Appl. Phys. Lett., 52, 1228 (1988).

Fabrication of Resonant Tunneling Diodes for Switching Applications

S.K. Diamond, E. Özbay, M.J.W. Rodwell, D.M. Bloom
Edward L. Ginzton Laboratory, Stanford University, Stanford, CA 94305-4085.

Y. C. Pao, E. Wolak and J.S. Harris
Department of Electrical Engineering, Stanford University, Stanford, CA 94305-4055

For digital circuit applications such as binary and multi-level logic circuits, device isolation is required to integrate several devices on chip. Microwave circuit applications such as mixers, and frequency multipliers require a low loss nonconducting substrate for on-chip integrations of high quality transmission lines and other passive microwave structures. We have demonstrated a fabrication process which produces high quality RTD's with a maximum frequency of oscillation above 200 GHz in a process suitable for switching applications, integrations of devices and microwave structures

Devices were grown on a 2-in. semi-insulating GaAs substrate. A .9μm 10^{18} silicon doped n^+ layer was grown on the substrate, followed by a 700 Å undoped GaAs spacer layer and a RT double barrier. The latter consists of a 16 monolayer GaAs well sandwiched between two 6 monolayer AlAs barriers. This was followed by a shorter 100 Å undoped spacer layer and a .45μm n^+ layer.

Devices were fabricated with a four step masking process resulting in a RTD structure as shown in device cross section Fig. 1. Initially two rectangular holes are etched down to the bottom n^+ region and $Ni/Ge/Au$ is deposited for the bottom ohmic contact. The etch serve to define the RTD active region in one dimension. $Ni/Ge/Au$ is then deposited on the narrow island formed between the two previous etch holes to form the top ohmic, and the contacts are annealed. Definition of the active area in the other dimension and rendering of the GaAs nonconducting is achieved through proton isolation. The proton isolation step consists of masking the top ohmic contact and the majority of the bottom ohmic with 1 μm of polyimide followed by 1.6 μm of Au. High energy protons are then implanted. Ti/Au metallization can be deposited directly on the GaAs and devices can be connected with "random" wiring as in digital circuits or with coplanar transmission lines. Other passive microwave structures may also be incorporated at this step.

Fig. 2 shows typical room-temperature and 77 K static current-voltage (I-V) characteristics. The I-V curve is asymmetric as would be expected from the asymmetric spacer layers used in growth. The devices exhibit current densities in the range of .9-1.3x10^5 A/cm^2 with PVR's of 2-2.5. At 77 K, current densities increase to 1.5-1.7x10^5 A/cm^2 with PVR's of 5.2-6.1. These devices are unique, for the GaAs/AlAs system, in their high current densities and simultaneous high PVR's.

A number of the devices were connected to bond pads compatible with microwave wafer probes and S_{11} measurements were made from 45 MHz to 26.5 GHz, for several bias voltages. Measured S_{11} data was compared with modeled S_{11} values from an RTD equivalent circuit and agreement to within 5% was obtained. The S_{11} measurements were also used to obtain circuit parameters and from these f_{max} was estimated at 230 GHz.

To measure the large signal switching performance of these devices, voltage step form-

ing structures were fabricated. The structure consists of a 50 Ω input transmission line before a RTD shunted to ground followed by another 50 Ω line terminated in 50 Ω's. A few GHz sine wave is applied to the input transmission line. The input amplitude is sufficient to switch the RTD from a state before resonance to a one past resonance. As the device switches, a voltage step travels down the transmission lines. Switching measurements were tried with 25 μm^2 devices which had a negative differential resistance of 26.8 Ω and a series resistance of 9.2 Ω. With the parallel combinations of transmission lines, the effective load impedance was 34.2 Ω's (25 + 9.2). An analysis of switching transition times for this value of load impedance and negative resistance predicts switching times of $10R_nC$=8.5 ps [1]. Measured switching times were on the order of 10 ps. With an optimal load resistance across the device, the minimum obtainable risetime should be $4.5R_nC$=3.8 ps. Structures with a more appropriate load line are currently being fabricated.

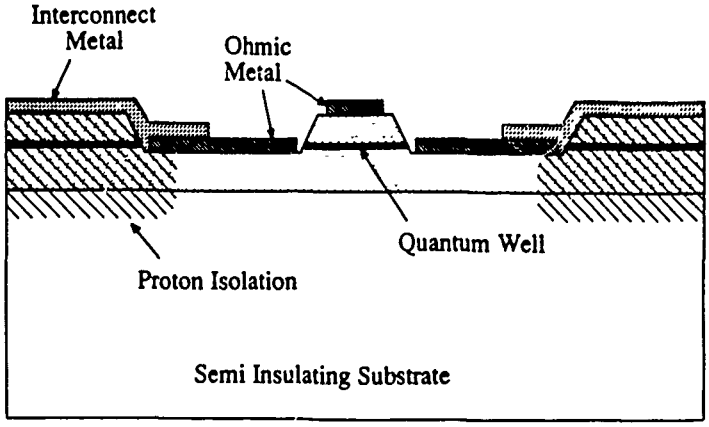

Fig.1 Device cross section of proton implanted, microwave compatible RTD process.

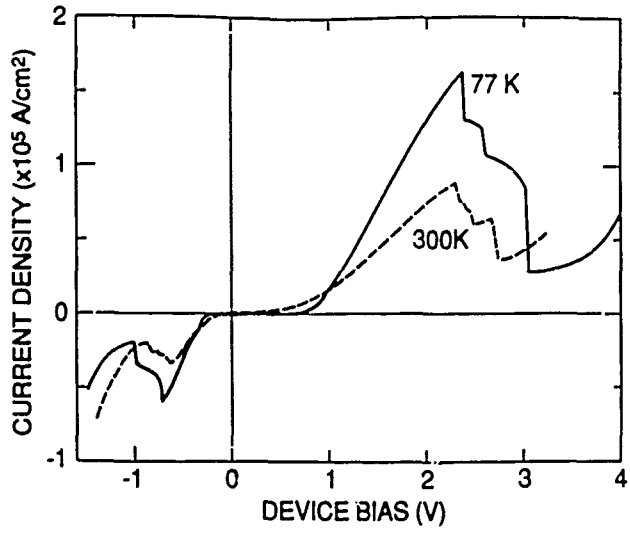

Fig. 2 Static I-V curves for typical devices at room temperature and 77 K.

[1] S.K. Diamond, E. Özbay, M.J. Rodwell, Y.C. Pao, J.S. Harris and D.M. Bloom, To be published Appl. Phys. Letters

This work was supported by Office of Naval Research contract N00014-86-K-0530.

NOTES

WEDNESDAY, MARCH 8, 1989

SALON G

3:15 PM–4:45 PM

WD1–5

JOINT SESSION ON TUNNELING AND RESONANT TUNNELING: 2

James S. Harris, Stanford University, *Presider*

Tunneling Dynamics and Resonant Coupling of Electrons in GaAs/AlAs Coupled Double Quantum Well Structures under Electric Fields

T. Matsusue[(a)], M. Tsuchiya[(a)*] and H. Sakaki[(a)(b)]
Institute of Industrial Science, University of Tokyo[(a)]
7-22-1 Roppongi, Minato-ku, Tokyo 106, JAPAN
Research Center for Advanced Science and Technology, University of Tokyo[(b)]
4-6-1 Komaba, Megro-ku, Tokyo 153, JAPAN

Resonant tunneling(RT) phenomenon in double-barrier(DB) heterostructure[1,2] has a conceptual similarity to a transmission of optical waves in Fabry-Perot (FP) resonator and involves time delay. Its dynamics should be investigated since they limit the ultimate speed of RT devices. Such a study will also clarify similarities and differences between electronic and optical waves. In our previous work[3], we investigated the tunneling escape process of electrons from AlAs/GaAs/AlAs DBRT structures. The measured escape rate was well explained by the idealized theory of FP-like model, which predicts the tunneling escape time τ in DBRT structures is given by $|t|^2 v_k/Lw$, when $|t|^2 \ll 1$, where t is the transmission coefficient through the barrier, v_k is the group velocity of electrons and Lw is the well width. This predicted escape time is equal to the one calculated by the sequential tunneling model, suggesting that the tunneling escape time is not strongly dependent on the coherency of electron waves. This simple relation may not hold for the tunneling process between quantum wells(QW), where resonant coupling effect plays a more sophisticated role. To clarify the resonant tunneling phenomena between QWs, we report, in this paper, our study on electron dynamics in several different double GaAs QW structures separated by thin AlAs barrier, where the coupling condition between QWs was varied by electric fields. Tunneling process was studied at ~20K by measuring time resolved photoluminescence(PL). Picosecond pulses of a mode-locked dye laser were used to generate electron hole pairs in QWs, and the subsequent PL from particular QWs was monitored by a streak camera to determine the time variation of electron density in the QWs. Note that the electrons are lost either by recombination (radiative[4] and nonradiative) and/or by tunneling process. Since the mass of heavy hole is quite heavy, hole tunneling can be neglected at least in the initial phase of tunneling.

1. Electron Dynamics in Coupled Resonant Tunneling Structures

We investigated first the effect of resonant coupling on tunneling process in coupled QW structures of Fig.1, where $L_{B1}=L_{B2}=31.1$A, $L_{W1}=70.5$A, and $L_{W2}=50.8$A. We measured the variation of tunneling rates at different bias voltage Va applied to the semi-transparent Schottky contact formed at the surface. The photon energy of laser was chosen to be 1.771eV to generate carriers in both wells. Under the flat band condition (Va~+0.6V), the electrons in QW2 have the highest energy, and therefore, transfer to QW1 or escape rightwards to outside. When the ground levels of QW1 and QW2 are in resonance(Va~-0.6V), interwell tunneling is enhanced. When Va is made further negative, resonance breaks down, and tunneling from QW1 to QW2 comes to be allowed. In addition, change in potential shape by electric field may affect tunneling process, and radiative recombination lifetime also change gradually with electric field. Measured PL decay time and time-integrated PL intensity I are shown in Fig.2 as a function of Va. Their variations with Va indicate large change in tunneling dynamics as will be described below.

*currently at Dept. of Electrical and Computer Engineering, Univ. of California, Santa Barbara, CA 93106, USA

Before the resonance is achieved(Va>-0.1V), the ground level E1(QW1) of QW1 is far lower than that E1(QW2) of QW2. The PL decay time of QW1 (τ_1) in this case is 400ps, which is nearly equal to radiative recombination lifetime τ_R. In contrast, the decay time of QW2 (τ_2) is 50ps. This decay rate $1/\tau_2$ is equal to the sum of two escape rates $1/\tau_{23}$, $1/\tau_{21}$ which correspond to the tunnel escape from QW2 to outside and to QW1, respectively. The former (τ_{23}) is estimated to be ~100ps by the measured data of Fig.1 with the use of relation $\tau_T \propto L_W^4$. Hence the latter τ_{12} is expected to be also ~100ps. Note that this tunneling process was clearly observed also in photoluminescence excitation(PLE) spectrum of QW1, where the structure associated with QW2 exciton appeared. With these time constants, PL efficiency η_1 of QW1 and that η_2 of QW2 are expected to be ~1 and ~0.1, respectively, since $\eta_2=\tau_2/\tau_R$. The expected values agree well with the data.

When E1(QW1) and E1(QW2) are brought close together but slightly separated(-0.4V<Va<-0.1V), QW1 and QW2 get weakly coupled, which allows a slow electron transfer(injection) from QW1 to QW2. This leads to the increase in τ_2. When the two levels are at resonance(-0.7V<Va<-0.4V), interwell tunneling gets frequent and large variations in decay time and PL intensity appeared. The fact that both the PL lifetime $\tau_1 \sim \tau_2$ and the intensity $I_1 \sim I_2$ in this region indicates that the interwell tunneling time τ_{12} is much faster than τ_{23}(~100ps). The fact τ_{12} is far smaller than τ_{23} is understood by considering that the tunneling rate is of the order of $\exp(-\kappa L_B)$[5] for coupled QW and $\exp(-2\kappa L_B)$ for DBRT structures, where κ is electron wave decay constant ($\sqrt{2m(V-E)}/\hbar$) in the barrier and L_B is the barrier thickness. Indeed, when barrier height is 1.13eV, τ_{23} is calculated to be 100ps for L_W=7.1nm and L_B=3.1nm, while τ_{12} is predicted to be 0.62ps from the calculated energy splitting $\Delta E(\sim\hbar/\tau_{12})$ for coupled QW with $L_{W1}=L_{W2}$=62A and L_{B1}=31A.

Hence, under such a condition quasi-equilibrium is reached between N1 and N2, the electron density of each well. The total density N(=N1+N2) is then likely to be dominated mainly by the tunneling escape process and, therefore, written as $dN/dt=-N2/\tau_{23}=-N/(1+R)\tau_{23}$, where R is the ratio N1/N2 of electron densities. This indicates that the lifetimes τ_1 and τ_2 get equal each other and are given by $(1+R)\tau_{23}$, while the PL efficiencies are given $2R\tau_{23}/\tau_R$ for QW1 and $2\tau_{23}/\tau_R$ for QW2. Therefore, one expects that τ_1 equals τ_2, and that $\eta_1/\eta_2(\sim R)$ decreases as Va decreases. This prediction agrees with the data. Since τ_{23} is expected to change with Va less sensitively than R does, τ_1, τ_2 and η_1 should decrease, and η_2 is nearly constant as Va decreases.

Note here also that τ_R or τ_{NR} (nonradiative recombination lifetime) do not change appreciably with Va in this region for the following reasons; the measured sum of PL intensity from QW1 and QW2 in this region varies with Va in proportion to $\tau_1(\sim\tau_2)$, indicating that τ_R is nearly constant. In addition, the remarkable increase in PL intensity of QW2 at resonance indicates that the non-radiative path remained small here.

When Va gets more negative beyond the resonance (Va<-0.7V), the tunneling rate from QW2 to QW1 gets negligible and that from QW1 to QW2 is also somewhat reduced because of the breakdown of resonance. This mechanism explains the increase in τ_1 and τ_2, and change in PL intensity. The data indicate τ_{12} increases to ~500ps since $\tau_1(=(1/\tau_R+1/\tau_{12})^{-1})$ goes up to ~230ps. The value is reasonable considering the dependence of τ_T on L_W.

2. Electron Dynamics in Coupled Double Quantum Well Structures

To focus mainly on the tunneling process through the interwell barrier, we next investigated the electron dynamics in three different coupled double QW structures which are sandwiched on both ends by thick (L_{B2}=100A) barriers.

These thick barriers prevent the tunneling escape process to outside of the coupled QWs and allow the investigation of interwell coupling only. The thicknesses of the interwell barriers of three samples ranges from 31.1 to 100A. With the application of electric field, the behavior similar to that in coupled RT structure described in Sec.1 takes place, except for the reduction of escape process to outside. Figure 3 shows PL decay time and the time integrated PL intensity of QW1 and QW2 of three samples as a function of Va. The physical interpretations are given below.

In the sample with L_{B1}=31.1A, the PL intensity I_1 and I_2 of QW1 and QW2 show the sharp structure when plotted as a function of Va. Under the flat band condition and/or before the resonant condition (Va>~0v), the lifetime τ_1(~300-400ps) and the PL intensity I_1 are nearly constant, which indicates that electrons in QW1 is not allowed to tunnel into QW2 and that τ_1 is determined by recombination lifetime. As Va decreases from ~1V to ~0V, I_2 gradually increases and τ_2 decrease, which results from the change in tunneling process from QW2 to QW1. Indeed, at Va>0.8V, fast initial decay component, which is ascribed to tunneling process from QW2 to QW1, appeared in time resolved PL from QW2 and was reduced with decrease in Va. Note that this tunneling process was clearly observed in PLE spectrum of QW1, where the structure associated with QW2 exciton appeared. The gradual increase in I_2 comes from the change in ratio of thermal distribution of N1 and N2.

When Va goes near the resonant condition, τ_1 and I_1 decreases. Though the measured τ_1 at Va=-0.4V is ~70ps, the presence of initial faster transfer process is suggested since the fact that the peak intensity of time resolved PL from QW1 was reduced by factor of ~4 is explained by convoluting the faster decay component (τ~20ps) with the detection time resolution (σ~30ps). As to τ_2 and I_2, clear dip structure were not observed as a function of Va; this suggests that the fast tunneling from QW2 to QW1 occurred even under flat band condition. When the bias is beyond the resonance (Va<~-0.6V), measured τ_1 and I_1 increase again τ_1 reaches up to ~300ps, which indicates tunneling process from QW1 does not play an important role. In contrast, τ_2 and I_2 decrease with decrease in Va. Although the mechanism of the decrease is not clear, increase in tunneling rate through rightside barrier with strong electric field may take place.

In the sample with L_{B1}=56.6A, both τ and I showed only the gradual change with Va without clear resonant behavior. The suppression of resonant coupling was confirmed by the fact that peak associated with QW2 exciton was small in PLE spectrum of QW1. When Va<-0.7v, however, a small evidence of tunneling component was observed in the time dependence of PL intensity from QW2, where the shoulder of delayed PL component appeared. In the case of L_{B1}=100A, we observe only gradual change in τ and I and no clear evidence of electron tunneling between QWs.

In all the samples, oscillatory behavior of PL intensity with time predicted by S. Luryi was not observed. This is reasonable since our detection time resolution is about several ten ps, which is much larger than the coherent time.

In summary, electron dynamics in coupled RT and coupled QW structures were investigated. A drastic change in tunneling processes was observed as the coupling condition was varied by applying bias voltage. In the coupled RT structure with barrier thickness of 31.1A, a large enhancement in interwell tunneling was observed at resonance, where the dynamic processes within two QWs are under quasi-equilibrium. The enhancement was successfully explained by calculating the tunneling rate for coupled QW and DBRT structures. The

tunneling into the other well was observed under the off resonant condition. In coupled QW structures with different barrier thickness, the systematic variation of electron dynamics was demonstrated as a consequence of the varied strength of coupling condition. When $L_{B1} \geq 56.6A$, tunneling rate was found to be small.

References

1. L.L. Chang, L.Esaki, and R.Tsu, Appl.Phys.Lett. 24, 593 (1974)
2. T.C.L.G.Sollner, W.D.Goodhue, P.E.Tannenwald, C.D.Parker, and D.D.Peck, Appl.Phys.Lett. 43, 588 (1983)
3. M.Tsuchiya, T.Matsusue, and H.Sakaki, Phys.Rev.Lett. 59, 1934 (1987)
4. T.Matsusue and H.Sakaki. Appl.Phys.Lett. 50, 1429 (1987)
5. E.O.Kane, "Tunneling Phenomena in Solids", ed. by E.Burstein and S.Lundqvist (Plenum Press, New York, 1969) p.1

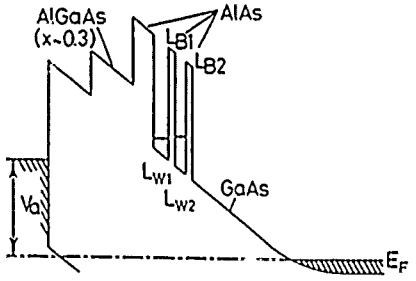

Fig.1 Band diagram of coupled QW structures

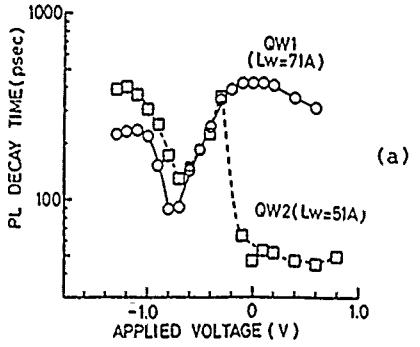

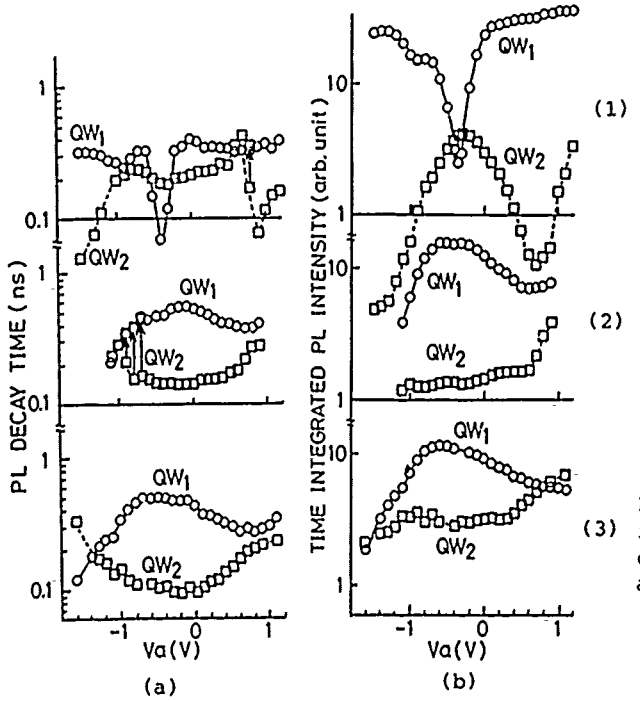

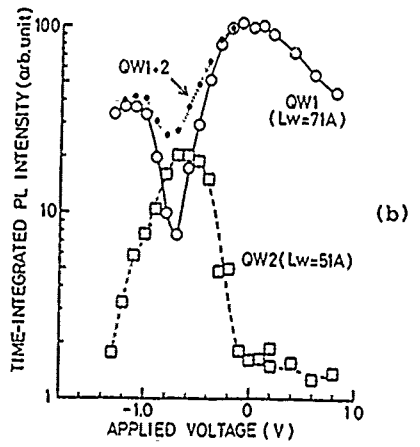

Fig.2 PL decay time(a) and time-integrated PL intensity(b) in coupled resonant tunneling structure as a function of applied voltage

Fig.3 PL decay time(a) and time-integrated PL intensity(b) in coupled QW structures as a function of applied voltage with interwell barrier thicknesses of 31.1A(1), 56.6A(2), and 100A(3). Arrows in (a) indicate presence of two decay components, where decay time changes according to the arrow. Note that relative magnitude of PL intensity between two QWs is arbitrary.

Time-Resolved Observation of Luminescence from a Charge-Transfer State in Double Quantum Wells

T.B. Norris, Laboratory for Laser Energetics and Dept. of Physics and Astronomy, University of Rochester, 250 E. River Road, Rochester, NY 14623;
N. Vodjdani, B. Vinter, and C. Weisbuch, Thomson-CSF, Laboratoire Central de Recherches, Domain de Corbeville, BP10, Orsay, France; and
G.A. Mourou, Dept. of Electrical Engineering and Computer Science, University of Michigan, Ann Arbor, MI 48109.

Time-resolved techniques have lately been applied to the study of the dynamics of tunneling in semiconductor quantum well (QW) structures.[1,2] The physics of tunneling in coupled QW structures has also been a topic of much recent interest.[2,3] We have applied the technique of time-resolved photoluminescence (PL) spectroscopy to investigate tunneling in a novel asymmetric GaAs/AlGaAs double QW structure. We report in this paper the direct observation of PL from a "charge-transfer" (CT) state, which is built up by electron and hole tunneling in opposite directions between the QW's.

The double-QW's are designed so that under flat band conditions the electron levels of the two wells are close to resonance, but the hole levels are sufficiently different that the PL energies of the two wells are well separated. This is accomplished by using an asymmetric double QW, where the wider QW has an Al composition that is adjusted so that the electron levels will be close to resonance.[4] Specifically, a 58 Å $Al_{0.15}Ga_{0.85}As$ QW (QW1) is coupled to a 26 Å GaAs QW (QW2) through a 43 or 86 Å $Al_{0.45}Ga_{0.55}As$ barrier. For the thin barrier sample, the electrons are somewhat delocalized over the two wells; for the thick barrier they are strongly localized in each well. There is a semitransparent Schottky contact on the top surface so the effect of an electric field could be studied. The samples were held in a cryostat at a temperature of 6 K.

Electron-hole pairs were generated in each QW at t = 0 by picosecond pulses from a synchronously pumped dye laser. The time-dependent PL spectrum was monitored with a monochromator and synchroscan streak camera with two-dimensional detector. Time-resolved spectra for the thin (43 Å) barrier sample are shown in Figs. 1 and 2 for 0 V and -4.75 V bias. The low field spectrum shows the scattered pump light, a PL line corresponding to transitions in QW1, and at lower energy a line from QW2. The high field spectrum reveals a third PL line that is strongly Stark shifted to lower energy. The decay times of the PL lines corresponding to QW1 and QW2 are streak-camera-limited. The decay time of the third PL component is extremely long; it exceeds the 10 ns time interval between pump pulses and synchroscan sweep cycle time. The Stark shift of this line is approximately linear with applied field. These observations lead us to the conclusion that this PL line originates from radiative recombination of electrons in QW1 with holes in QW2, which we refer to as the CT state. The charge separation occurs by electron and hole tunneling in opposite directions.

The time-dependent PL spectra for the thick (86 Å) barrier sample do not show the development of a CT state. The spectra show only the two PL lines corresponding to transitions within QW1 and QW2; the Stark shifts of these lines are as expected for isolated QW's in an electric field. Time-integrated (cw) PL spectra of this sample reveal that there is in fact some charge separation occurring; it is not observable on the time-resolved spectra because incomplete charge separation takes place, so the instantaneous intensity of the CT PL is much less than that of QW1 and QW2.

We finally note that the long decay time of the CT state causes a dc charge buildup in each well, which screens the applied field and reduces the Stark shift of the CT PL line. Thus by comparing the CT Stark shift with the calculated value from the external field, we have been able to estimate the separated charge density and hence the CT state lifetime. We find that this lifetime depends on the injected carrier density, and ranges from 20 ns to 1 μs for our experiments on the 43 Å barrier sample.

ACKNOWLEDGMENT

This work was supported by the sponsors of the Laser Fusion Feasibility project at the Laboratory for Laser Energetics and by the U.S. Air Force under contract F49620-87-C-0016.

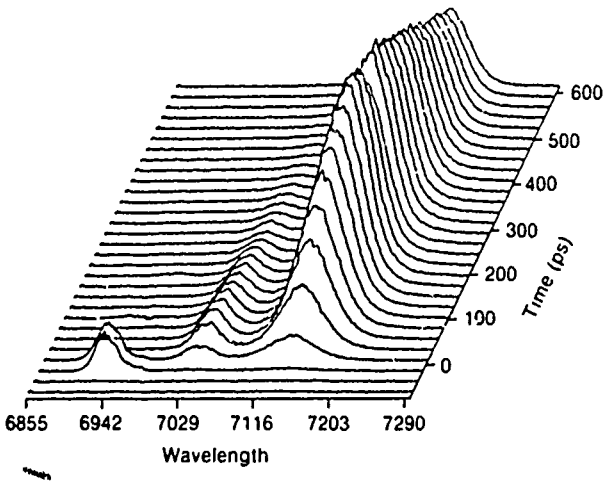

Figure 1.

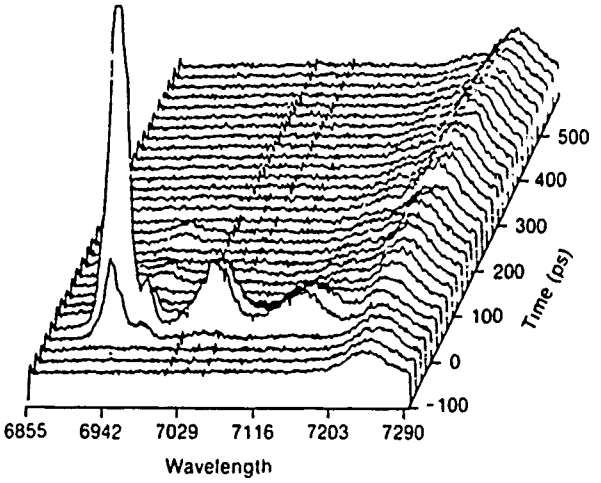

Figure 2.

REFERENCES

1. M. Tsuchiya, T. Matsusue, and H. Sakaki, Phys. Rev. Lett. 59, 2356 (1987).
2. T. Tada, A. Yamaguchi, T. Ninomiya, H. Uchiki, T. Kobayashi, and T. Yao, J. Appl. Phys. 63, 5491 (1988).
3. R. Sauer, K. Thonke, and W. T. Tsang, Phys. Rev. Lett. 61, 609 (1988).
4. G. Wicks, private communication (1986).

Electron Tunneling Times in Coupled Quantum Wells

D. Y. Oberli, J. Shah, T. C. Damen, C. W. Tu and D. A. B. Miller
AT&T Bell Laboratories, Holmdel, N.J. 07733, U.S.A.

The work by Esaki and Tsu on tunneling in superlattices[1] has generated a considerable interest for the potential application of tunneling to real devices. The rapid progress of epitaxial growth techniques has led to the creation of novel semiconductor structures which exhibit quantum-size effects and tunneling such as the double-barrier resonnant tunneling structures or the superlattice p-i-n diodes[2]. Transport studies in these structures demonstrated Bloch transport through the superlattice minibands[3], negative differential resistance in double barrier diodes[4], field induced localization[5]. More recently, optical measurements have been performed in double barrier structures in order to gain some insight on space-charge buildup[6] and escape rates[7].

We have investigated the fundamental times characterizing the process of tunneling through a single semiconductor barrier by time-resolved luminescence spectroscopy. For this purpose, we have used an asymmetric double well structure and measured tunneling time from the luminescence decay of the narrow quantum well. By applying an electric field perpendicular to the layers, we observe a drastic reduction of the tunneling time at a voltage corresponding to the resonant coupling of the n=1 level of the narrow quantum well with the n=2 level of the wide one (Fig.1).

The samples were grown by MBE on a n-doped GaAs substrate. Eight periods of two quantum wells of approximately 60 and 90 Å width separated by a 55 Å (or 65Å) $Al_{0.3}Ga_{0.7}As$ layer are placed in the center of a p-i-n diode structure. The n- and p-type doped layers were both made of 2000 Å thick of $Al_{0.3}Ga_{0.7}As$. Spacer layers of undoped $Al_{0.3}Ga_{0.7}As$ were grown on either side of the intrinsic region. The sample is processed in an array of 200 μm x 200 μm mesas. An important consideration in the design is the position of the narrow well versus the wide well relative to the p^+ contact. In order to eliminate current heating of the structure and maintain field uniformity, the diode is biased in the reverse direction only . Thus, the narrow well follows the wide well in the growth sequence.

Time-resolved luminescence is measured by the energy up-conversion in a $LiIO_3$ crystal of a photon from the photoexcited luminescence with a photon from the pump laser pulse. Short optical pulses of 750 fs tunable over the range of 7200-7800 Å are generated by synchronously pumping a dye laser (Styryl 8) with the compressed and frequency doubled output of a CW modelocked Nd-YAG laser. The sample is placed in an optical cryostat and maintained at a temperature of 20 K for the photoluminescence and 50 K for the photocurrent measurements.

Without any applied bias, the luminescence decay times in a 55 Å barrier structure are equal to 3 ns and 75 ps for the wide and narrow wells respectively. The long luminescence lifetime of the 90 Å well implies that non-radiative recombination processes have been eliminated to a large extent. Therefore the short luminescence decay time in the narrow well is attributed to the existence of tunneling through the barrier separating the two wells. This conclusion is supported by the data in the 65 Å barrier structure for which the decay time has increased to 150 ps. Since tunneling rates for heavy holes are much smaller because of their larger effective mass, electron tunneling is responsible for the shorter decay time of the luminescence.

The measured tunneling times show a striking dependence on the applied voltage (Fig.2). The main features are: 1) nearly constant value of the tunneling time between flat band conditions (at 1.8 V) and -2.0 V 2) an abrupt reduction of the tunneling time at the onset of resonance (-2.4V) and 3) an increase of the decay time behond -3.2 V. The non-monotonic behaviour of the luminescence decay time clearly demonstrates the occurence of a resonant coupling between the two quantum wells. We also note that the luminescence decay time in the wide well is slowly decreasing as a function of the applied bias, reaching a minimum of 100 ps at -3 V.

In our interpretation, a question of primary importance is whether the resonance occurs at the correct value of the electric field. Our approach has been to compare the prediction of the QCSE theory[8] with the energy shift of the heavy hole exciton peak measured from the photocurrent spectrum at very low densities (Fig.3). At a -2.75 V bias, the Stark shift is equal to 10 meV, which is then associated with an electric field of 7.0×10^4 V/cm. A numerical calculation of the energy position of the electronic subbands predicts resonant coupling at 6.4×10^4 V/cm. The assignement of the sharp decrease of the decay time to resonant tunneling is thus well confirmed by this comparison. The remaining difference points to the existence of a space-charge buildup across the two wells. By reducing the laser excitation density on the sample by a factor of two, we observed a significant shift of the resonant position to a lower voltage (-2.4 V). At a carrier density of 2.0×10^{10} cm^{-2} used in the luminescence experiment, we estimate that a 3×10^3 V/cm field exists as a result of the transfer of all the electrons from the narrow to the wide quantum well. The charge buildup is a complicated dynamical process, which occurs simultanuously with the resonant tunneling of the electrons. Its relevance to the dynamic evolution of tunneling has been discussed by Ricco and Azbel[9].

In conlusion, we have measured directly the tunneling times of electrons in an asymmetrical double well structure. The application of an electric field perpendicular to the layers led to the resonant coupling of the two wells and to a large reduction of the tunneling time to 7.5 ps for a 55 Å barrier width.

Acknowledgement

This work would not have been possible without the technical assistance of A. E. DiGiovanni and J. E. Henry.

[1]R. Tsu and L. Esaki: Appl. Phys. Lett. **22**, 562 (1973); see also the review by E. Esaki in IEEE J. of Quantum Electron. **QE-22**, 1611 (1986).
[2]F. Capasso, K. Mohammed , and A. Y. Cho: IEEE J. of Quantum Electron. **QE-22**, 1853 (1986).
[3]B. Deveaud, J. Shah, T. C. Damen, B. Lambert and A. Regreny: Phys. Rev. Lett. **58**, 2582 (1987).
[4]T. C. L. G. Sollner, W. D. Goodhue, P. E. Tannenwald, C. D. Parker, and D. D. Pack: Appl. Phys. Lett. **43**, 588 (1983).
[5]E. E. Mendez, F. Agullo-Rueda and J. M. Hong: Phys. Rev. Lett. **60**, 2462 (1988).
[6]J. F. Young, B. M. Wood, G. C. Aers, R. L. S. Devine, H. C. Liu, D. Landheer, and M. Buchanan, A. J. SpringThorpe and P. Mandeville: Phys. Rev. Lett. **60**, 2085 (1988).
[7]M. Tsuchiya, T. Matsusue, and H. Sakaki: Phys. Rev. Lett. **59**, 2356 (1987).
[8]D. A. B. Miller, D. S. Chemla, T. C. Damen, A. C. Gossard and W. Wiegmann, T. H. Wood and C. A. Burrus: Phys. Rev. B 32, 1043 (1985).
[9]B. Ricco and M. Ya. Azbel: Phys Rev. B **29**, 1970 (1984).

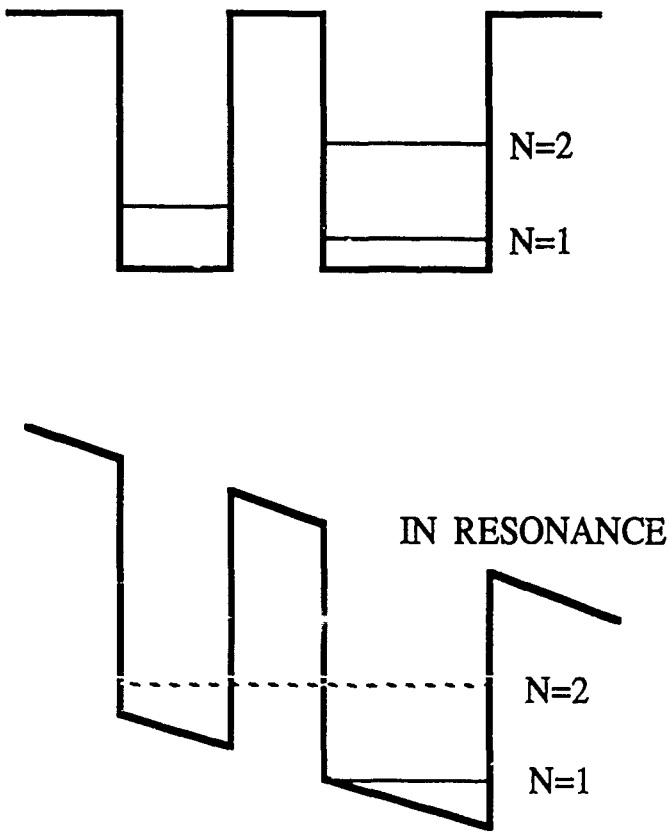

Fig.1: Energy potential profile of the conduction band edge of asymmetric double quantum wells: away from resonance (top) and at resonance (bottom).

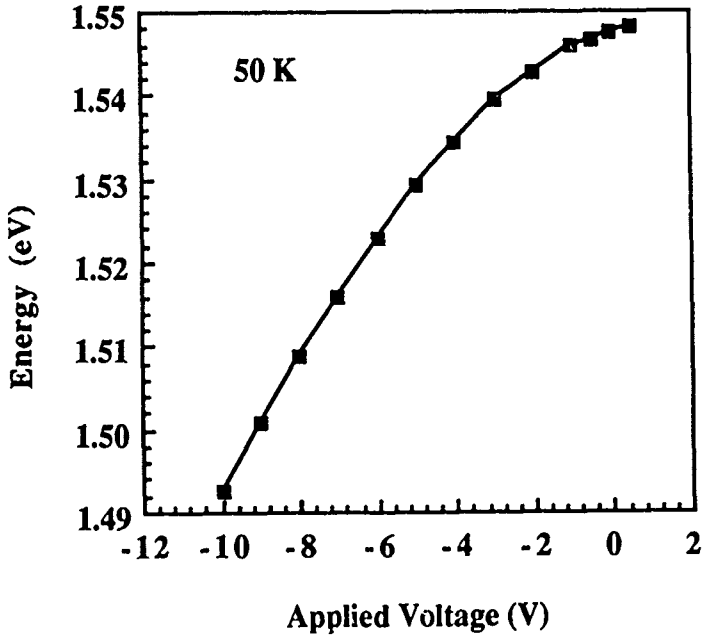

Fig.3: Energy shift of heavy hole exciton in wide quantum well versus applied voltage.

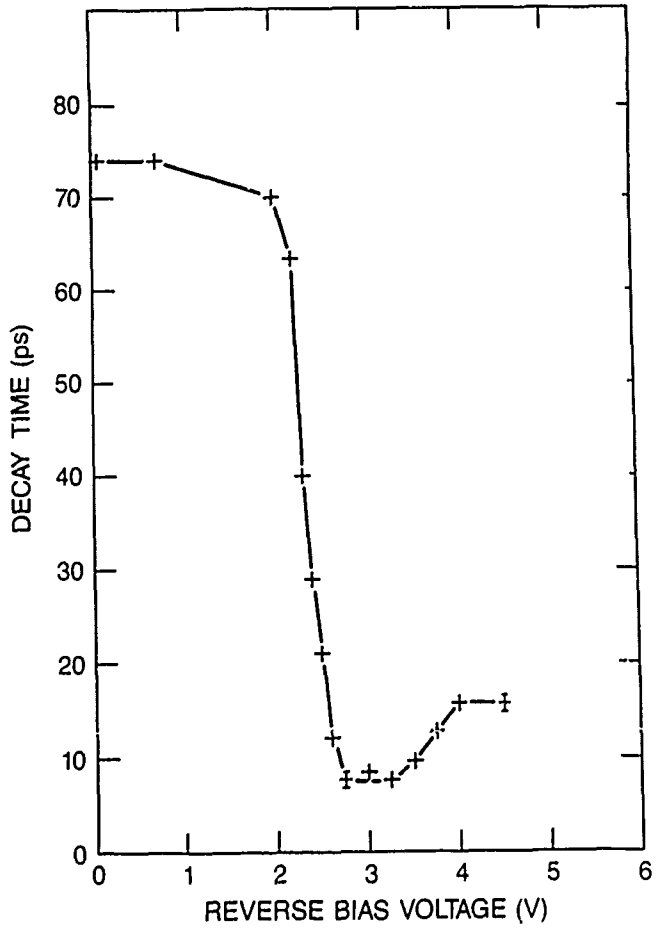

Fig.2: Luminescence decay time of narrow quantum well versus.applied voltage.

The Effect of Quasibound State Lifetime on the Speed of Resonant-Tunneling Diodes

E.R. Brown, C.D. Parker, and T.C.L.G. Sollner
Lincoln Laboratory, Massachusetts Institute of Technology
Lexington, MA 02173-0073

C.I. Huang and C.E. Stutz
Air Force Wright Aeronautical Laboratory
Wright-Patterson Air Force Base, OH 45433-6543

Recent optical experiments have directly measured the quasibound-state lifetime in resonant-tunneling structures [1]. The results indicate that this lifetime is close to that predicted by the coherent model of the process. The present paper deals with the effect of this lifetime on the electrical response of the double-barrier diode at high frequencies.

Intuitively, one would expect a finite lifetime to cause the conduction current through a double-barrier diode to lag behind the time-varying voltage applied across it. We quantify this by analyzing the electrical current response to a voltage step function within the coherent picture of resonant tunneling. In the "sudden" approximation [2], the applied voltage step instantaneously determines a new quasibound-state energy; however, the Schrödinger equation demands that the wavefunction at each point in the structure be continuous in time. We assume that both the wavefunction and the current approach their new steady-state values in the same manner as the charge in the well, i.e., exponentially with a time constant τ equal to the quasibound-state lifetime. This leads to the conduction-current response, $i(t) = I_1\theta(-t) + [I_2 + (I_1 - I_2)\exp(-t/\tau)]\theta(t)$, where $\theta(t)$ is the unit step function, and I_1 and I_2 are the initial and final dc currents, respectively. Near the center of the negative differential resistance region, linear-response analysis then yields the conduction-current impedance in the form [3], $Z(\omega) = R + i\omega L$, where R is the differential resistance and $L = R\tau$. The displacement-current reactance is represented by an ideal capacitance C, because the electrostatic potential throughout the structure is determined primarily by the static space-charge density on the anode side. The complete equivalent circuit is shown in the inset of Fig. 1, where R_S comprises various parasitic series resistance components.

We have tested this equivalent circuit by measuring the oscillation power and the small-signal terminal impedance Z_T as a function of frequency in the microwave and millimeter-wave bands. To observe clearly the effect of the quasibound-state lifetime, the experiments were performed on double-barrier diodes that were designed to make τ much greater than the RC time constant of the diodes, $(R_S|R|)^{1/2}C$. This is accomplished by growing relatively thick (5 - 6 nm) $Al_{0.42}Ga_{0.58}As$ barriers that yield a ground-state lifetime τ_1 between about 5 and 50 ps, and by asymmetrically doping the regions immediately outside the structure to simultaneously achieve low specific capacitance and high current density. Shown in Fig. 1 is the experimental curve of maximum oscillation power versus frequency for an 8-μm-diameter diode consisting of 5.1-nm-thick AlGaAs barriers and a 5.1-nm-wide GaAs quantum well. The experimental points fall toward zero near 40 GHz, which is just below the maximum theoretical oscillation frequency f_{RCL} = 51 GHz. This is the value above which $Re(Z_T)$ becomes positive and is calculated with the following parameters: R = -21 Ω, C = 77 fF, R_S = 5 Ω, and τ_1 = 6.0 ps (L = -0.125 nH). Also shown in Fig. 1 is the theoretical oscillation-power curve derived from a large-signal analysis of the RCL circuit. It displays nearly the same rolloff behavior as the experimental curve. To demonstrate the importance of

the inductance in the model, we also plot the theoretical power and maximum oscillation frequency f_{RC} for L = 0. The difference between f_{RC} = 177 GHz and the largest measured frequency (38 GHz) cannot be explained by experimental error. Rather, we believe that these results serve as the first indication of a strong inductive effect in resonant-tunneling. Although our circuit model is a simple one, we believe that it is qualitatively correct and that more accurate analyses will also predict an inductance (possibly a frequency-dependent one) in the equivalent circuit. Finally, we point out that this effect is by no means limited to double-barrier diodes and should apply to coherent resonant tunneling through any superlattice-like structure.

This work was sponsored by the U.S. Army Research Office, the U.S. Air Force, and NASA.

References

[1] M. Tsuchiya, T. Matsusue and H. Sakaki, *Phys. Rev. Lett.* **59**, 2356 (1987).

[2] L.I. Schiff, *Quantum Mechanics*, 3rd ed. (McGraw-Hill, New York, 1968), p. 292.

[3] E.R. Brown, C.D. Parker and T.C.L.G. Sollner, submitted to *Appl. Phys. Lett.*

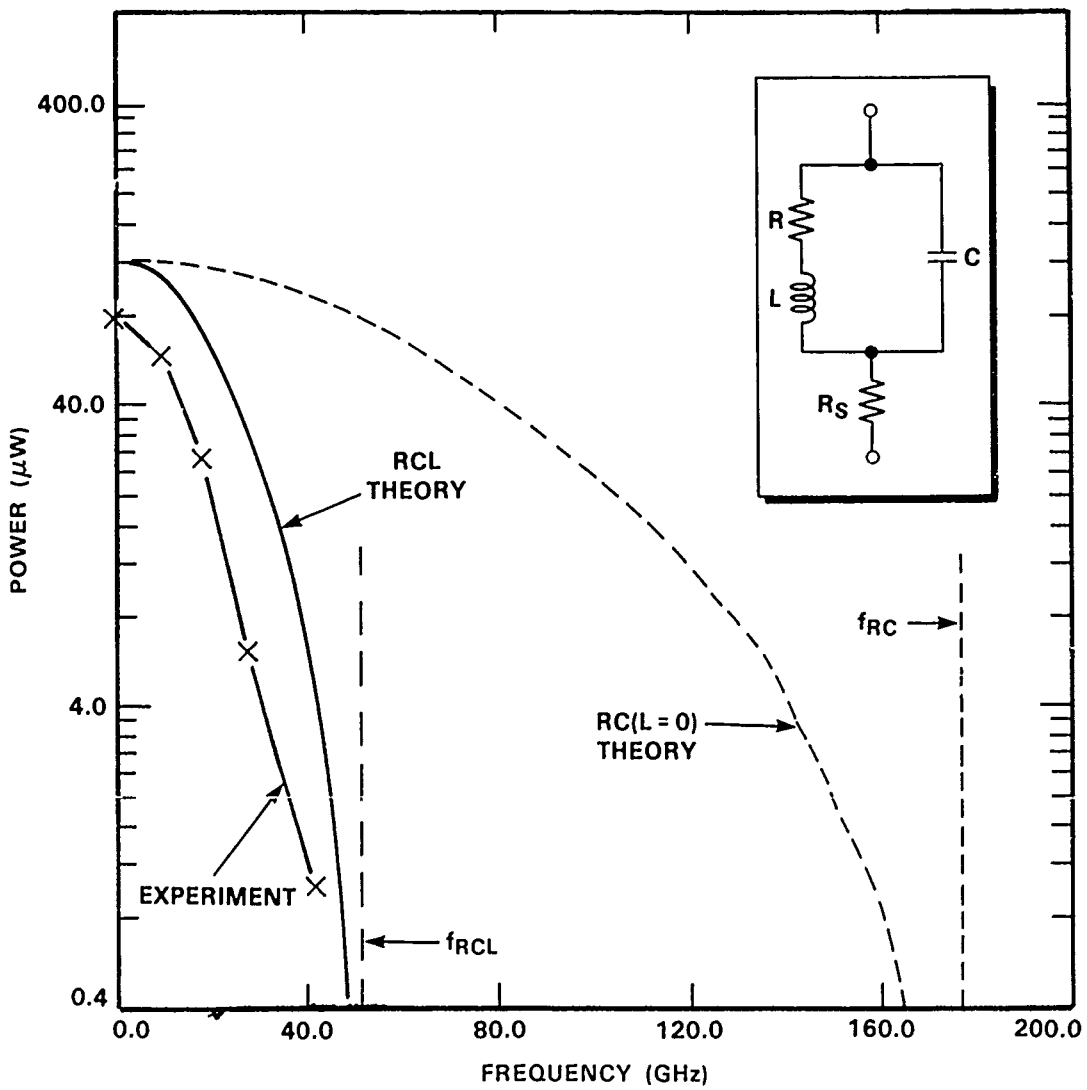

Electric Field Dependence of the Tunneling Escape Time of Electrons from a Quantum Well

T.B. Norris, Laboratory for Laser Energetics and Dept. of Physics and Astronomy, University of Rochester, 250 E. River Road, Rochester, NY 14623;
X.J. Song, G. Wicks, W.J. Schaff, and L.F. Eastman, The School of Electrical Engineering, Cornell University, Ithaca, NY 14850; and
G.A. Mourou, Dept. of Electrical Engineering and Computer Science, University of Michigan, Ann Arbor, MI 48109.

Tunneling of electrons through thin barriers in semiconductor heterostructures is usually studied via the tunnel current through multiple barrier structures.[1,2] Time-resolved photoluminescence has also been used to investigate the tunneling escape rate of an electron from a quantum well (QW) bounded on each side by a thin barrier.[3] We have applied the same technique to investigate the electric field dependence of this tunneling.

The sample nominally consisted of a single 30 Å GaAs QW bounded on the top by a thick $Al_{0.3}Ga_{0.7}As$ barrier and on the bottom by a thin barrier, as shown in Fig. 1. The thickness b of this barrier was set so that the tunneling decay time would be between the recombination time (subnanosecond) and the experimental temporal resolution (20 ps); for the experiments reported here b = 86, 111, and 121 Å. The tunneling structure was situated in the intrinsic region of a p-i-n diode so that the effect of an electric field applied along the growth direction could be studied. The samples were held in a cryostat at a temperature of 6 K.

Electron-heavy-hole pairs were generated in the QW by a picosecond pulse from a synchronously pumped dye laser. The QW photoluminescence was filtered by a monochromator and detected with a synchroscan streak camera. The luminescence decay was fitted by a single exponential; the decay time vs. electric field is shown in Fig. 2.

The solid lines of Fig. 2 are from a simple semiclassical model. The tunneling time under flat band conditions is expressed as $\tau_T(0) = (\upsilon T)^{-1}$, where υ is the oscillation frequency of the electron in the well, and T is the transmission coefficient of the barrier. We find that $\tau_T(0)$ = 809, 277, and 17 ps for b = 121, 111, and 86 Å, respectively. The field dependence is expressed as

$$\tau_T = c \exp\left(\frac{2}{\hbar}\int_0^b \sqrt{2m(V-E-Fz)}\,dz\right)$$

where b is the barrier thickness, F is the field, and c is a constant obtained from the tunneling time at zero field. The agreement with experiment is quite good, except for the 86 Å barrier zero-field decay time. Therefore we have plotted that theoretical curve with $\tau_T(0)$ = 65 ps. Evidently the field-dependence of the tunneling rate is properly given by the expression above. It is important to note that it is extremely difficult to fit the data quantitatively because small variations in the assumed sample parameters will result in large differences in the calculated tunneling rate, due to the exponential dependence of the rate on the barrier height, thickness, and effective mass.

ACKNOWLEDGMENT

This work was supported by the sponsors of the Laser Fusion Feasibility Project at the Laboratory for Laser Energetics and by the U.S. Air Force under contract F49620-87-C-0016.

p+	$Al_{.3}Ga_{.7}As$	2000 Å
i	$Al_{.3}Ga_{.7}As$	2000 Å
i	GaAs	30 Å
i	$Al_{.3}Ga_{.7}As$	b
i	GaAs	1000 Å
n+	GaAs	1 μm

Figure 1.

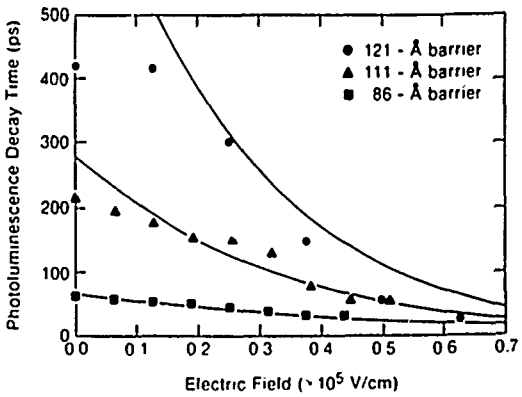

Figure 2.

REFERENCES

1. T. C. L. G. Sollner, W. D. Goodhue, P. E. Tannenwald, C. D. Parker, and D. D. Peck, Appl. Phys. Lett. 43, 588 (1983).
2. F. Capasso, K. Mohammed, and A. Y. Cho, IEEE J. Quant. Electron. QE-22, 1853 (1986) and references therein.
3. M. Tsuchiya, T. Matsusue, and H. Sakaki, Phys. Rev. Lett. 59, 2356 (1987).

NOTES

WEDNESDAY, MARCH 8, 1989

SALON D

5:30 PM–7:00 PM

WE1–12

POSTER SESSION

Intersubband Relaxation of Electrons and Holes in $Al_xGa_{1-x}As$/GaAs Quantum Wells During Photoexcitation

Stephen M. Goodnick
Department of Electrical and Computer Engineering
Oregon State University
Corvallis, OR 97331
and

Paolo Lugli
Dipartimento di Ingegneria Meccanica
II Universita' di Roma
Via O. Raimondo
00173 Roma, Italy

Here we report on Monte Carlo simulation of ultra-fast optical intersubband relaxation experiments[1,2]. Oberli et al.[1] found very long time constants(in excess of 100ps) using Raman scattering for relatively wide quantum wells in which the intersubband spacing was less than the optical phonon energy. Seilmeier et al.[2] reported time constants of 11-14ps in narrow 50Å modulation doped wells studied using time resolved intersubband infrared absorption spectroscopy. Such times are in excess of the expected relaxation times based on simple consideration of the intersubband polar optical phonon transition rates.

We have modeled these experimental studies using an ensemble Monte Carlo simulation of a multi-subband single quantum wells system. In this simulation, we include the dynamics of photogenerated electrons, holes, and nonequilibrium polar optical slab mode phonons. For confined phonons, the momentum perpendicular to the well is quantized so that only discrete q_z modes are excited through hot carrier phonon emission. Since the phonon modes are spatially localized, problems associated with the phonon normalization(in the case of bulk mode)[3] are circumvented.

Results of our calculation for the experimental parameters of Oberli et al.[1] are shown in Figs. 1 and 2. Here an aerial density of $4x10^{11}/cm^2$ electrons are injected just above the second subband(2) which is separated by 26meV from the ground subband(1). We plot the average carrier energy and fraction of carriers in 2 as a function of time after the initial pulse. Without hot phonons, the population in 2 decays rapidly and is quite small after 10ps. With hot phonons, however, the electron population is heated, thus maintaining a thermal population in 2 even after 50ps suggesting that the observed long time constant observed experimentally is due to hot phonon effects.

1. D.Y. Oberli, D.R. Wake, M.V. Klein, J. Klem, T. Henderson, and H. Morkoc, Phys. Rev. Lett. 59, 696(1987).
2. A Seilmeier, H.J. Huebner, G. Abstreiter, G. Weimann, and W. Schlapp, Phys. Rev. Lett. 59, 1345(1987).
3. P.J. Price, Physica 134B, 164(1985).

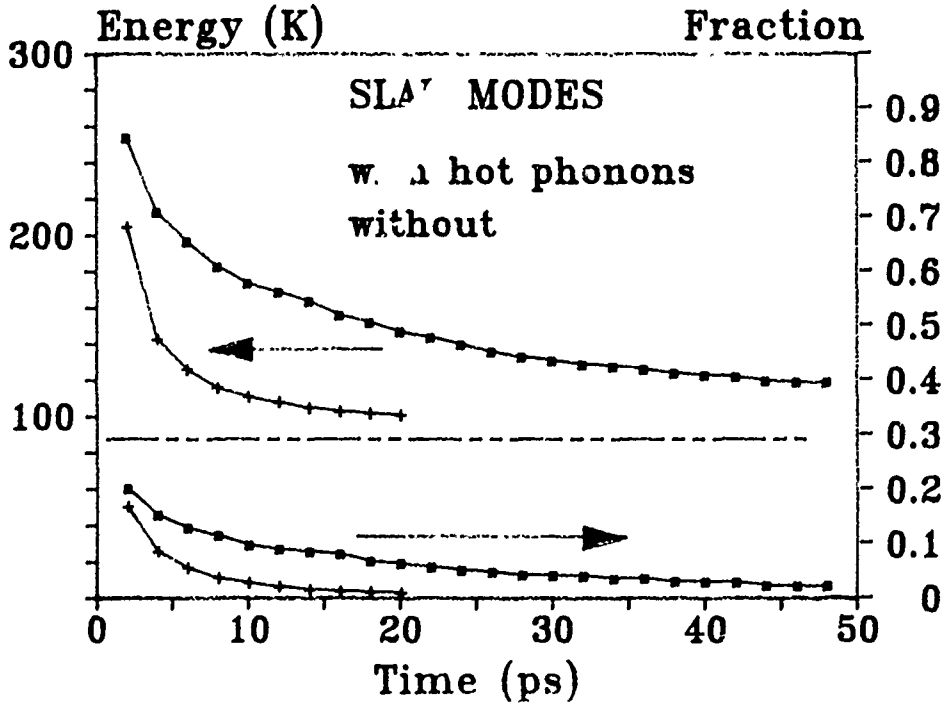

Fig. 1. Average energy and fraction of carriers in 2 as a function of time for a 230Å well and injection energy of 40meV.

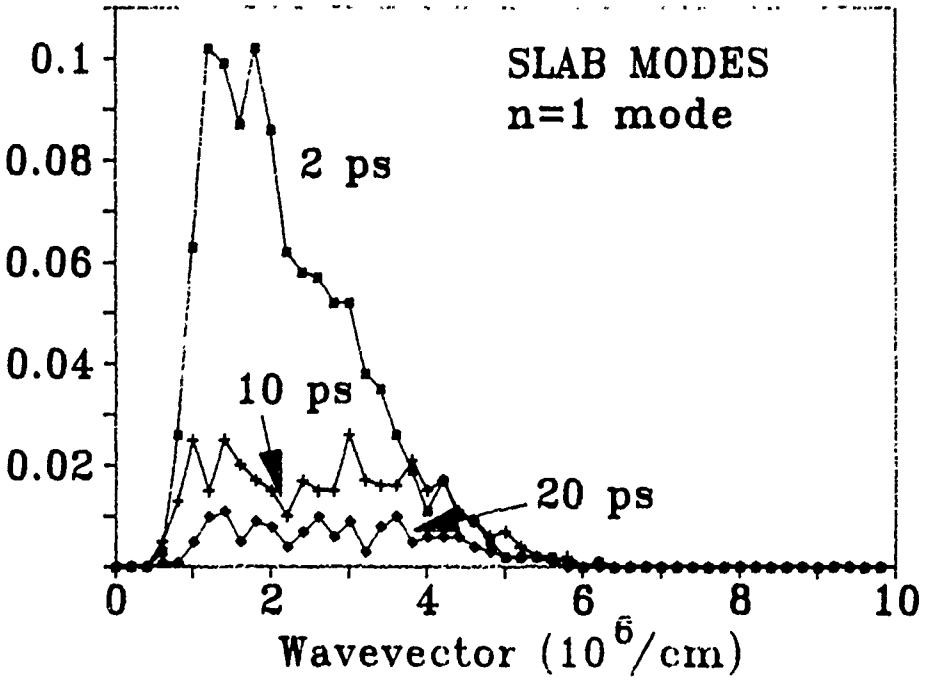

Fig. 2. Phonon population(N_q) versus parallel wavevector for the lowest perpendicular slab mode for the parameters of Fig. 1.

Phonons and Phonon Interactions in Layered Semiconductors

G. Mahler
Institut für Theoretische Physik I, Universität Stuttgart
Pfaffenwaldring 57, D-7000 Stuttgart 80, FRG
and
A. M. Kriman and D. K. Ferry
Center for Solid State Electronics Research
Arizona State University, Tempe 85287-6206, USA

In semiconductor heterostructures, the eigenmodes of phonon as well as electron fields are expected to exhibit confinement effects, and these should also influence the respective transition rates induced by external perturbations. Despite the complexity of any detailed treatment of a realistic interface, simplified interface models in terms of boundary conditions, like the infinite barrier model for electrons in quantum wells, have proven useful in providing intuitive understanding and even quantitative estimates. For acoustic and optical phonon fields no such interface models exist, and while models of coupling to the electron field are well established, the anharmonic interaction appears to be very involved: No attempt has been made to date to study the influence of phonon confinement. In this paper, we describe the first attempts to do so, in a framework useful for studies of picosecond excitation in quantum wells.

Within a systematic continuum approach,[1] we derive generalized equations of motion for the acoustic and optical displacement fields. As our immediate interest is in the interactions, rather than the details of the dispersion relations, we specialize these equations to isotropic symmetry and retain gradients up to second order, in which case both fields decouple into longitudinal and transverse parts. In this way, the *ad hoc* model proposed in Ref. 2 can be derived systematically. We then show that model boundary conditions can be introduced which lead to confined modes but which nevertheless do not introduce mode conversion between the longitudinal and transverse parts. As a consequence, simple confined modes appear even for polar displacement fields.

For specific point symmetries, we derive explicit analytical anharmonic coupling models. Coupling coefficients are estimated from scaling arguments.[3] The low temperature phonon lifetimes thus obtained are in satisfactory agreement with picosecond experiments. In particular, we show that[4] $\tau \sim q^{-5}$ (q is the phonon wave vector) for acoustic modes, $\tau \sim q^{-1}$ for optical modes and O_h symmetry, and $\tau \sim$ const. for optical modes and T_d symmetry (to leading order). For typical semiconductor materials of T_d symmetry the $q \to 0$ LO phonon lifetime is found to vary in the range of 5 psec to 50 psec; the corresponding zone-edge phonon lifetimes are estimated to be shorter by one order of magnitude.

We show that the lifetime of *confined* LO phonons decaying into *delocalized* acoustic modes does not depend significantly on the confinement length: The reduction of overlap with increasing confinement length is counterbalanced by the weakening of the selection rules governing the

coupling. This is reminiscent of the fact that typical radiative lifetimes of "zero-dimensional" electronic states (atomic levels) are usually of the same order of magnitude as the extended states of, e.g., direct-gap semiconductors.

Our results are applicable to a number of experimental situations:

a. Phonon linewidth[5] as seen, e.g., in a Raman experiment,

b. Electron-hole energy relaxation in bulk semiconductors,[6]

c. Electron-hole energy relaxation in quantum wells[7]

d. Electron-hole energy relaxation in mixed crystals, in the range where they become indirect.[8]

The energy relaxation is dominated by the LO phonon lifetime if that is the slowest process, but still the most effective cooling mechanism. For higher excitation the hot phonon effect[9] limits the cooling rate. This effect is less pronounced if large q-vector phonons are excited, as is the case for intervalley scattering,[8] because of their shorter lifetimes.

---

1. A. Atkins: Lattice Dynamical Foundation of Continuum Theories, (World Scientific, 1985).
2. M. Barbiker, J. Phys. C19, 683 (1986).
3. V. L. Gurevich: Transport in Phonon Systems, (North Holland, 1986).
4. A. Berke, A. P. Mayer and R. K. Wehner, Solid State Commun. 54, 395 (1985).
5. P. F. Tua and G. D. Mahan, Phys. Rev. B26, 2208 (1982).
6. J. Shah, Solid State Elec. 21, 43 (1978).
7. J. Shah, A. Pinczuk, A. C. Gossard and W. Wiegman, Phys. Rev. Lett. 54, 2045 (1985).
8. K. Leo, Thesis, Stuttgart 1988, unpublished.
9. W. Pötz and P. Kocevar, Phys. Rev. B28, 7040 (1983).

Observation of Low Power-Level Picosecond Pulses Using Single-Photon Counting Technique

M.Hamana, A.Kimura, T.Shioura, T.Umeda and Y.Cho
The Institute of Scientifc and Industrial Research, Osaka University
Mihogaoka 6-1, Ibaraki, Osaka, 567 Japan

M.Kanda
R and D group, Sumitomo Electric Industries, Ltd.
Shimaya 1-1, Konohana-ku, Osaka 554 Japan

Recently, reliable and stable picosecond pulses became available from semiconductor lasers with mode-lockings by forming an absorbing section in the active layer [1] or by inserting a saturable absorber such as an MQW platelet into the external cavity [2], or chirp-compensation technique [3]. Semiconductor laser may offer a unique regime in the field of ultrafast measurements, because of its compactness and reliability. Peculiarity of ultrafast measurements using those picosecond pulses available from semiconductor lasers is its associated low level power. Corresponding to this low handling power level, pulse detection process must be reconsidered. For example, if we attempt to make a time-resolved measurement utilizing the correlation or sampling technique by a certain nonlinear process with using pulses from semiconductor lasers, signal levels inevitably become low because the conversion efficiency of the nonlinear process drops excessively.

Here in this paper, we report results of our investigation of finding out the possibility of application of single-photon counting technique onto a low level picosecond pulse measurement based on the cross-correlation or sampling scheme using a nonlinear crystal.

To measure the sensitivity of cross-correlation measurements using single-photon counting technique, we tested an unbalanced autocorrelation measurement. A chirp-compensated picosecond pulse (pulsewidth 7 - 18 ps) train from a mode-locked semiconductor laser (λ=830 nm) was split into two unbalanced pulse trains. Smaller one served as a signal, while larger one served as a pumping (or as a local oscillator). After receiving a mutual variable delay τ, they were introduced onto a nonlinear crystal of $LiIO_3$ with a non-collinear configuration. Second harmonic signal generated in the crystal was counted by a single-photon counting photomultiplier as a function of τ, thereby unbalanced autocorrelation traces were obtained as shown in Fig.1. From these traces, the signal to noise ratio S/N as a function of input signal level I_s, with keeping the pumping power level constant, was measured as shown in Fig.2. It is seen that, while the signal level is small, S/N is proportional to the input signal, and for sufficient signal levels, it becomes to be proportional to the square root of the signal. These results means that the main cause of the noise was thermal and partition noise [4] included in a photomultiplier tube used at low signal levels and it was masked by the shot noise at higher signal levels. Sensitivity, determined as a power level giving unity S/N, is found to be ~1μW peak power for λ=830 nm pulse with a pumping peak power I_p of 5 mW and a gate time t_g of 5 seconds.

For the nonlinear crystal we used, conversion efficiency to the second harmonic was estimated to be ~$3\times10^{-11}\times I_p$ (I_p in watts) with considering the nonlinear coefficient of $LiIO_3$ and used optical geometry. Observed photon count numbers agree well with this conversion efficiency when quantum efficiency of the photomultiplier tube used is taken into account. Since the observed minimum detectable power level is determined by the thermal and the partition noise of the photomultiplier tube, cooling of the photocathode

will improve the sensitivity.

Responding to the recent availability of picosecond pulses from semiconductor lasers, measurement capability utilizing those low power level pulses based on a combination of nonlinear process and single-photon counting technique has been demonstrated.

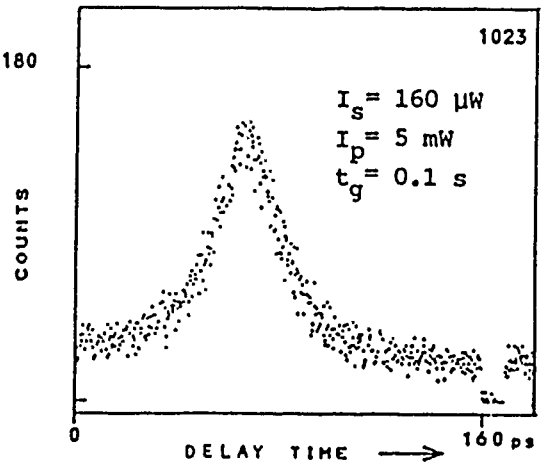

Fig.1 An example of single-photon counted unbalanced autocorrelation trace.

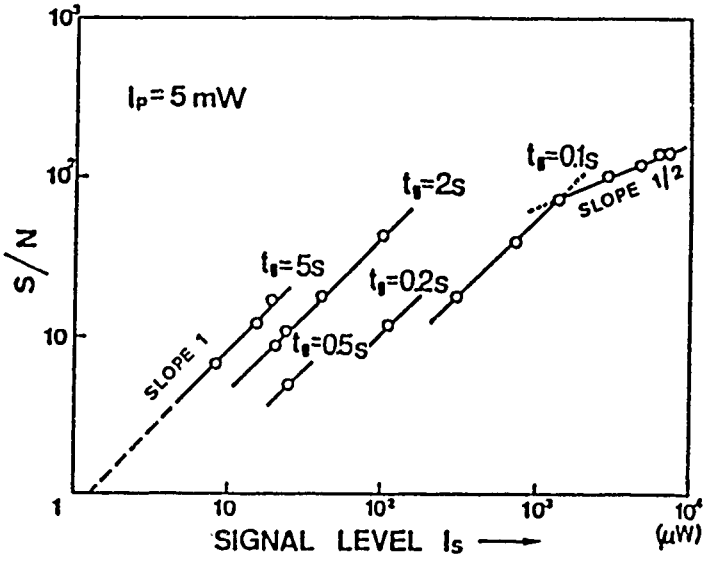

Fig.2 Variarions of signal to noise ratio as functions of signal level.

References

[1] P.P.Vasil'ev, V.N.Morozov, Y.M.Popov, A.B.Sergev, IEEE Jour. Quant. Electron. QE-22, 149 (1986).
[2] Y.Silberberg, P.W.Smith, D.J.Eilenberger, D.A.B.Miller, A.G.Gossard and W.Wiegmann, Optics Lett., 9, 507 (1984).
[3] A.Takada, T.Sugie and M.Saruwatari, Electron. Lett., 22, 1347 (1986).
[4] N.Hirano, Trans. Instit. Electron. Commun. Engineers, Jpn. J61, 371 (1978).

Investigation of picosecond time-resolved photoluminescence in gallium arsenide with 3 µm spatial resolution

Thomas A. Louis

Heriot-Watt University, Physics Department, Riccarton,
Edinburgh EH14 4AS, UK

A novel instrument, the Photoluminescence Lifetime Microscope Spectrometer (PLµS), was developed for the investigation of highly spatially resolved and picosecond time-resolved photoluminescence (TRPL) in gallium arsenide (GaAs) materials and devices. The PLµS is a time-correlated single photon counting (TCSPC) instrument based on a modified optical microscope and uses only solid state components, a pulsed diode laser (≤35ps (FWHM), 785nm, $5mW_{peak}$) source and a silicon single photon avalanche diode (SPAD) detector. Recently, it was shown that decay times of the order of 10ps can be resolved with ±2ps accuracy in a TCSPC setup with an instrumental response width of 70ps (FWHM) by means of convolution analysis[1]. In the PLµS, with an instrumental response width of below 75ps (FWHM), the time resolution is therefore comparable to a synchroscan streak camera. The PLµS, however, is several orders of magnitude more sensitive especially in the 800-950nm GaAs wavelength range. In semi-insulating GaAs substrates, e.g., at excitation densities as low as $10^{15}cm^{-3}$, a TRPL signal-to-noise ratio of better than 1000:1 is easily obtained at room temperature. The high sensitivity of the PLµS permits, for the first time, to measure the TRPL signal from microscopically small sample regions, where typically less than one external luminescence photon is generated per excitation pulse. Novel applications include TRPL spatial mapping of inhomogeneous GaAs materials and testing of small, highly integrated GaAs devices. The high statistical accuracy of the TCSPC data and excellent linearity of the detection system allow accurate fitting of complex decay models to the experimental data by convolution analysis. As an example of typical TCSPC data obtained with the PLµS, the TRPL signal of a homojunction GaAs solar cell is shown in the figure below. The dotted curves in the top left diagram show the instrumental response and the TRPL decay data. A three exponential decay model was convoluted with the instrumental response and fitted to the TRPL decay by nonlinear iterative least squares reconvolution analysis. The fitted model (impulse response function) is shown in the diagram on the right. The quality of the fit is excellent as seen from the value of chi-square (XSQ=1.16) and the random distribution of residuals (bottom left).

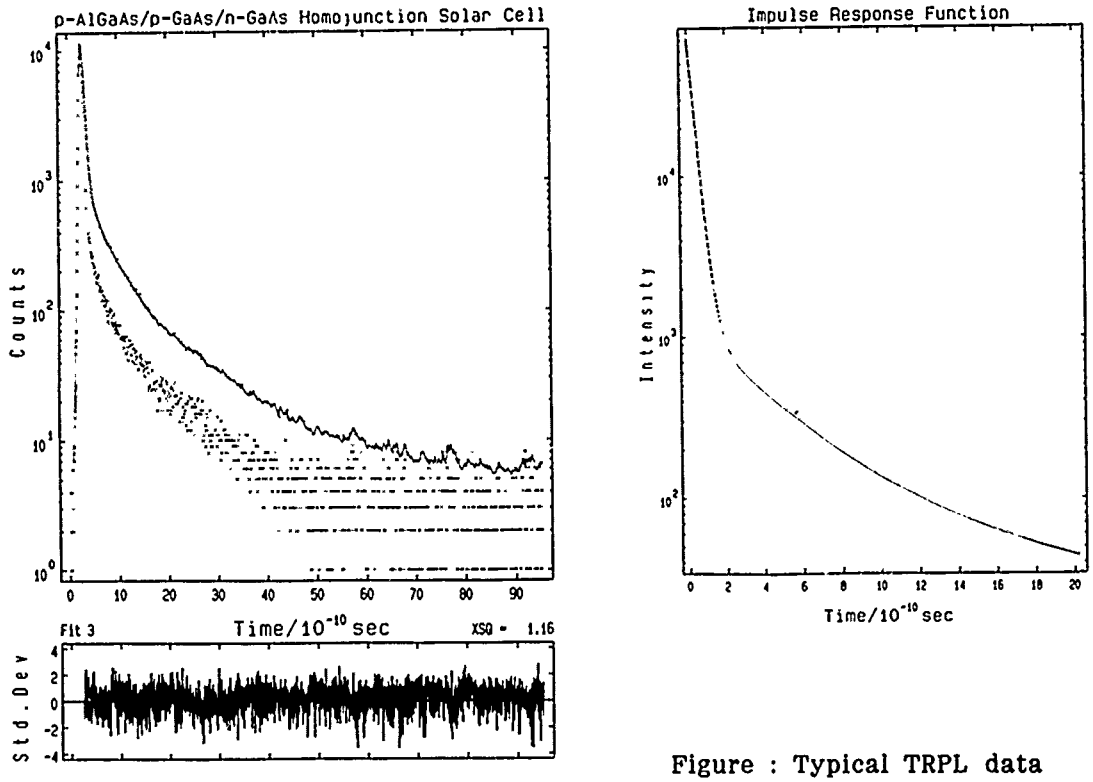

Figure : Typical TRPL data obtained with the PLμS

Although the three exponential decay model is not an analytical solution of the corresponding transient diffusion equation, it can, however, be seen as an exponential series expansion of the unknown solution. The fit parameters may therefore not have a simple physical interpretation, but a smooth impulse response function is nevertheless accurately extracted from the noisy experimental data and can now be interpreted qualitatively : The dominating, rapid initial decay with a time constant of 36ps is due to efficient collection of minority charge carriers at the shallow junction, whereas the much weaker slow component with a time constant of around 1.4ns is due to carrier recombination via deep levels in the field free base region below the depletion layer edge. Obviously, whenever an analytical solution of the transient diffusion equation for a particular sample is known, this should be used as the kinetic model. Physical parameters such as the minority carrier lifetime, surface recombination velocity, diffusion coefficient etc. can then be extracted from the experimental data.

Reference

1 T. Louis, G.H. Schatz, P. Klein-Bölting, A.R. Holzwarth, G. Ripamonti, S. Cova, "Performance comparison of a single-photon avalanche diode with a microchannel-plate photomultiplier in time-correlated single photon counting", Rev.Sci.Instrum. 59 (7), July 1988

Photoconductive and Photovoltaic Picosecond Pulse Generation Using Synthetic Diamond Films

S. T. Feng, J. Goldhar and Chi H. Lee

Electrical Engineering Dept.
University of Maryland
College Park, MD20742

Because of its unique electrical and mechanical properties, such as high breakdown filed, highest known thermal conductivity, etc., diamond is an excellent candidate semiconductor material for many high power and high speed electronic and optoelectronic devices. Recent developments in synthetic diamond film technology made it possible to grow high quality polycrystaline films with many characteristics of natural diamond.(1) In order to learn more about this new material we conducted series of experiments with a simple switch shown in figure 1. Diamond films of approximately one micron thickness were grown on heavily p-doped silicon substrates by Crystallume Corporation. Silicon provided one electrode, and a thin aluminum coating ($\sim 100\mathring{A}$) provided second semitransparent electrode. We observed sensitivity to light over a wide range of wavelength from 0.25 μ to 1.05 μ.

Figure 2 shows the peak pulse voltage observed when the switch was illuminated by $\sim 10\mu J$, 10 psec pulses at 1.05 μ generated by a c.w. mode locked glass laser and regenerative amplifier.(2) Over wide range of bias voltages the signal is independent of bias. This signal is due to photovoltaic effect at silicon-diamond junction. Since no bias is required in this regime simple pulse forming networks for generation of "clean" electrical pulses were demonstrated.

At bias voltages greater then 40 V strong photoconductive effect resulted in short short duration electrical pulses. Reliable operation of 400 H_z with average electric field $\sim 1MV/cm$ in the diamond film was observed. In this regime the signal was proportional to square root of incident laser intensity. This nonlinear behavior is being used in a two pulse experiment to measure directly switch response time. The results will be presented at the conference.

References

1. Diamond Technology Initiative Symposium, July 12-14 1988, Crystal City, Arlington, Va.

2. "An Actively Mode-locked Continuous Wave Nd: Phosphate Glass Laser Oscillator and Regenerative Amplifier," L. Yan, J. D. Ling, P. T. Ho, Chi H. Lee, and J. Burdge, *IEEE J. of Quant. Electr.*, QE-24, 418-426, 1988.

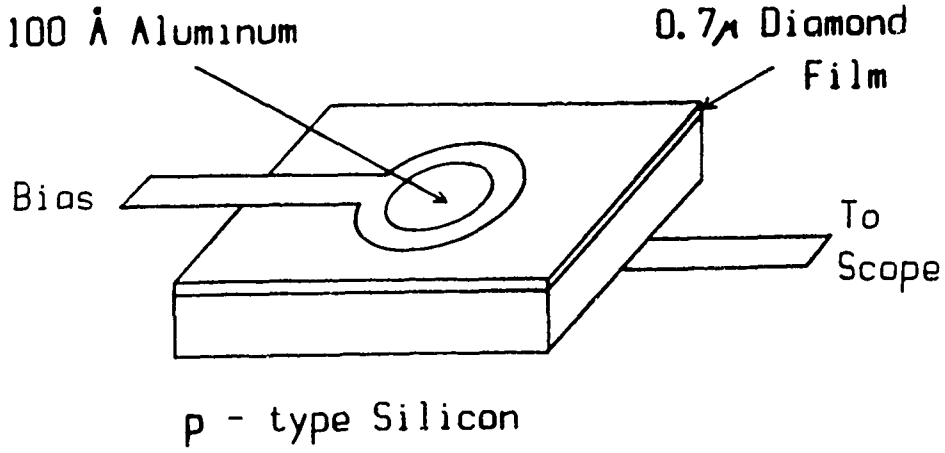

Figure 1.

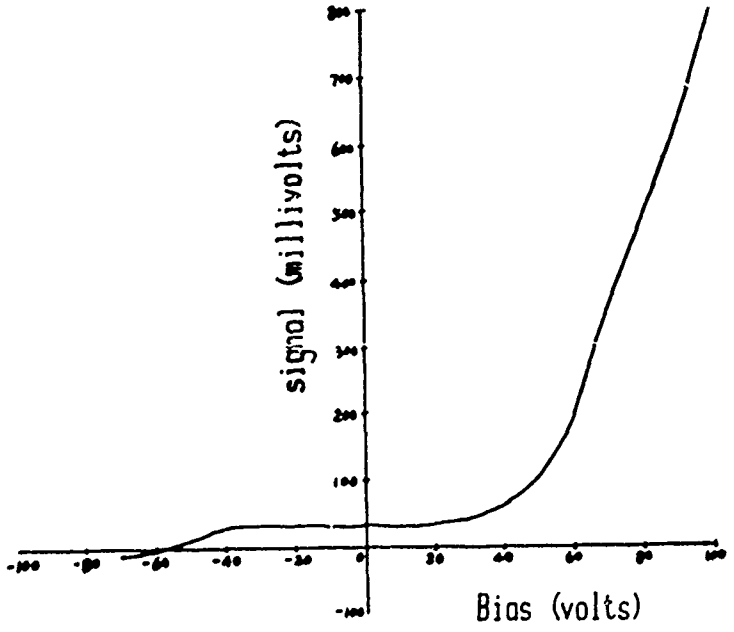

Figure 2.

Beryllium-bombarded $In_{0.53}Ga_{0.47}As$- and InP-Photoconductors with High Responsivity and Picosecond Resolution

R. Loepfe, A. Schaelin and H. Melchior
Institute for Quantum Electronics
Swiss Federal Institute of Technology, Zurich, Switzerland

The technique of ion bombardement of semiconductor photoconductors has led to detectors with large bandwidths and response times in the picosecond and even subpicosecond range[1,2]. Although these devices show very high speeds of response, their sensitivity is severely limited by implantation damage. Of major interest is the improvement of the responsivity while maintaining the response speed.

Two different kinds of photoconductors are investigated: epitaxial $In_{0.53}Ga_{0.47}As$-layers for the infrared range up to $1.6\mu m$ and semi-insulating Fe:InP bulk material for the visible to $0.9\mu m$ range. Thin light absorbing layers of 1 to $2\mu m$ in thickness on semi-insulating substrates were processed into 4×4 and $16 \times 16\mu m^2$ mesa structures with Ni/Ge/Au ohmic contacts. For extraction of the photoresponse over broad electrical bandwidths, these devices were integrated into tapered coplanar 50Ω microwave transmission lines.

To improve the response speed from the nanosecond range down to the low picosecond range the devices are bombarded with Beryllium ions. Implantation was done with a tandem accelerator with ion energies in the MeV-range. To reach a broad defect profile over the entire thickness of the active photoconductive layers the ions were slowed down with a tungsten foil to ion energies below $800\,keV$. Doses are scaled between $10^{11}cm^{-2}$ and $10^{15}cm^{-2}$.

For an evaluation of the speed of response of these devices, we used Carruther's optical pulse-mixing technique[3]. A sequence of two partially overlapping high-speed laser pulses is directed onto the detector. Relying on the slight nonlinearities inherent in high-speed photoconductors the nonlinear mixing part in the response is then registered in the form of an autocorrelation function[4]. Response times of the samples with doses above $10^{14}cm^{-2}$ reach values as low as $2\,ps$ to $4\,ps$, compared to 0.1 - $2\,ns$ before bombardement.

Investigations of the relations between implantation dose, responsivity and response speed (see Fig.2) as well as mobility and dark conductance give an indication of the major scattering and recombination mechanisms in these devices.

1. D. Grischkowsky, C.C. Chi, I.N. Duling III, W.J. Gallagher, N.H. Halas, J.M. Halbout and M.B. Kitchen in *Picosecond Electronics and Optoelectronics II*, ed. F.J. Leonberger (Springer,Berlin,1987).
2. P.M. Downey, J.E. Bowers, C.A. Burrus, F. Mitschke and L.F. Mollenauer, Appl. Phys. Lett. **49**, 430 (1986).
3. T.F. Carruthers and J.F. Weller, Appl. Phys. Lett. **48**, 460 (1986).
4. R. Loepfe, A. Schaelin, H. Melchior, M. Blaser, H. Jaeckel and G.L. Bona, Appl. Phys. Lett. **52**, 2130 (1988).

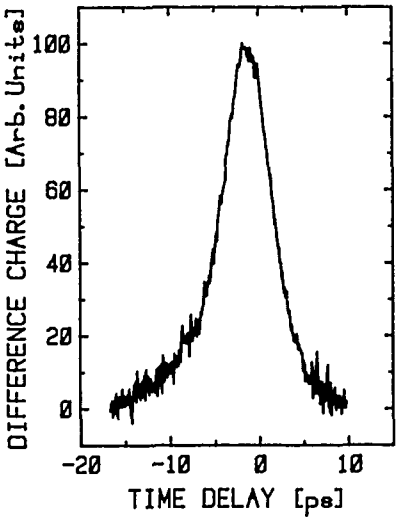

Fig.1
Autocorrelation-trace of a $10^{14} cm^{-2}$ Be^{3+}-bombarded Fe:InP-photoconductor with $16 \times 16 \mu m^2$ active area biased at 30V. From the autocorrelation-FWHM of $6.5\,ps$ a pulse response of $4\,ps$ is deduced. Excitation pulse was at $583\,nm$. Pulse energies were $10\,pJ$ and had pulse widths of $1\,ps$.

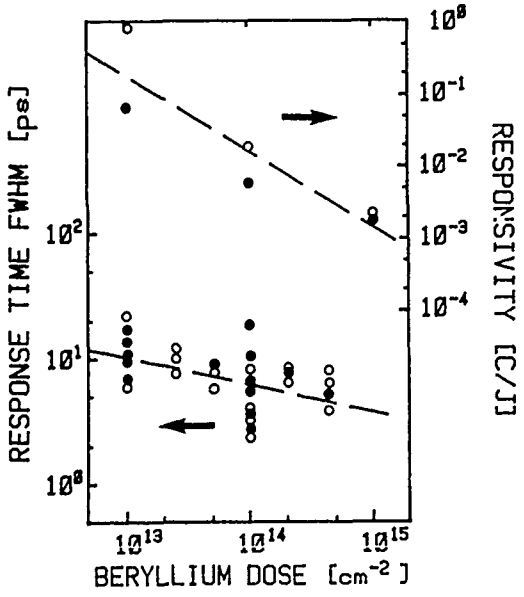

Fig.2
Responsivity and response FWHM vs. Be^{3+}-dose.
○ $In_{0.53}Ga_{0.47}As$-photoconductors biased at $1.25 \times 10^3 kV/cm$.
● Fe:InP-photoconductors biased at $6.25 \times 10^3 kV/cm$.
Pulse widths at $583\,nm$ were deduced from autocorrelation traces assuming single sided exponentials. Responsivities were measured at $830\,nm$ using $20\,ps$ semiconductor laser pulses with energies of $30\,fJ$.

Photocurrent-Voltage Characteristics of Ultrafast Photoconductive Switches, S. Moss, J. Knudsen, R. Bowman, P. Adams, and D. Smith, Aerospace Corporation, P.O.B. 92957, Los Angeles, CA 90009 and M. Herman, Charles Evans & Associates, 301 Chesapeake Dr., Redwood City, CA 94063.

We have measured the photocurrent-voltage characteristics (PIV) of ultrafast photoconductive switches (UPS) fabricated on GaAs, Si with a buried oxide layer (SIMOX), and SOS. Switches were fabricated by forming microstrip transmission lines in an optoelectronic autocorrelation configuration with gaps exposing the semiconductor material[1]. In all materials, the metalization was 175 μm wide with 20 μm wide UPS gaps. These measurements were performed for each material with various ion-implantation dosages to probe effects of amorphization on PIV linearity and temporal response. We varied the order of the implantation and the metalization fabrication steps. Samples implanted before metal had contacts to a highly damaged semiconductor material. Samples implanted after metal had contacts to fairly crystalline semiconductor. Linearity of response was dependent on the extent of ion-induced damage and, in this respect, was fairly consistent with reports in the literature[2]. However, linearity of response was also dependent upon the order of ion-implantation and metalization steps and was inconsistent with recent literature reports[2].

The UPS were pumped by pulses from a picosecond dye laser. A triangle wave varying linearly from -15 to +15 V was applied to one sidearm of each of our samples. The photocurrent produced was detected by a lock-in amplifier and digitized in a microcomputer.

Results for UPS fabricated on GaAs are shown in Figs. 1(a) and 1(b). The GaAs wafers were 450 μm thick {1,0,0} undoped. The metalization was 0.5 μm Al. Damage was induced by a quadruple implant 200/100/50/20 keV $^4He^+$ with total dosages of $7x10^{12}$, $7x10^{13}$, $7x10^{14}$, or $7x10^{15}$ ions/cm^2. Results in Fig. 1(a) are for wafers implanted before metalization. Those in 1(b) are for wafers implanted after metalization. We show only the results for the $7x10^{15}$ implant because the other results are qualitatively similar. While neither result is linear over the range of applied bias switches implanted after metalization exhibit a more linear response. Switches implanted before metalization display saturation at the higher biases similar to that reported recently for other GaAs photoconductive devices[3].

Results for UPS fabricated on SIMOX are shown in Figs. 1(c), 1(d). The SIMOX wafers were 350 μm thick {1,0,0} Si with a 2200 Å Si epilayer over a buried 3500 Å SiO_2 layer. The metalization was 0.5 μm of Au on a 200 Å thick barrier layer of Ti/W. Damage was induced by a triple implant of 25/75/125 keV $^{28}Si^+$ at dosages of $1x10^{14}$ or $3x10^{14}$ ions/cm^2. The results in Fig. 1(c) are for wafers which were implanted before metalization, while those in 1(d) are for wafers which were implanted after metalization. While neither result is linear over the range of applied bias the switches implanted after metalization exhibit a more linear response.

Our results for UPS fabricated on SOS are shown in Fig. 1(e) and 1(f). The SOS wafers were 175 μm thick {1,0,0} with a 0.5 μm thick Si epilayer. The metalization was 0.5 μm of Au on top of a 200 Å thick barrier layer of Ti/W. Damage was induced by a triple implant of 100/200/400 keV $^{28}Si^+$ at dosages of $1x10^{14}$ (wafers B2 and A1) or $1x10^{15}$ (wafers B3 and A2) ions/cm^2. Wafer B1 was implanted with a 375 keV $1x10^{15}$ $^{28}Si^+$ cm^{-2}. The results in Fig. 1(e) are for wafers which were implanted before metalization, while those in 1(f) are for wafers which were implanted after metalization. The wafers implanted before metalization show that the PIV become more linear at higher levels of ion-implantation induced damage. Conversely, the response of the switches ion-implanted after metalization are linear.

We measured the bias dependence of the dark current and the response as a function of optical power. Measurements to characterize the degree of crystallinity include Raman spectra, electron-beam modulated electro-reflectance, photoreflectance, RBS, and x-ray rocking curves. We discuss the physical mechanisms which affect the PIV including carrier transport, generation, recombination, space-charge, and the barriers produced during contact formation.

1. D.H. Auston, A.M. Johnson, P.R. Smith, and J.C. Bean, Appl. Phys. Lett. 37, 371(1980).
2. D.H. Auston, *Picosecond Optoelectronic Devices*, Ed. C.-H. Lee (Acad. Press,New York,1984).
3. G.W. Anderson, et al, Appl. Phys. Lett. 53, 313(1988).

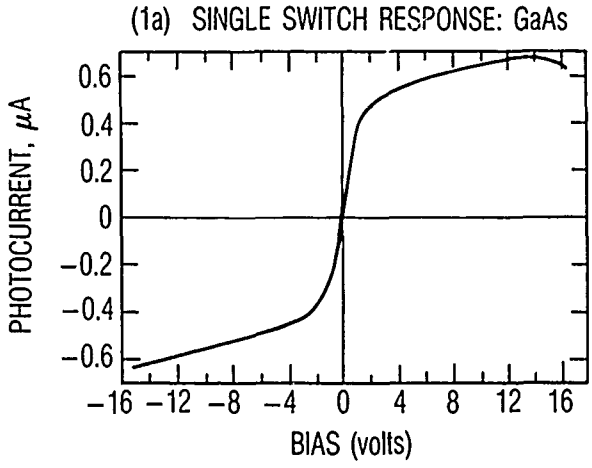
(1a) SINGLE SWITCH RESPONSE: GaAs
PHOTOCURRENT, μA
0.6
0.4
0.2
0
−0.2
−0.4
−0.6
−16 −12 −8 −4 0 4 8 12 16
BIAS (volts)

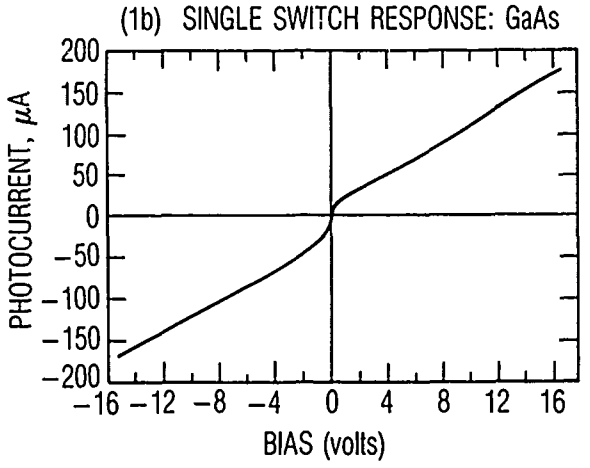
(1b) SINGLE SWITCH RESPONSE: GaAs
PHOTOCURRENT, μA
200
150
100
50
0
−50
−100
−150
−200
−16 −12 −8 −4 0 4 8 12 16
BIAS (volts)

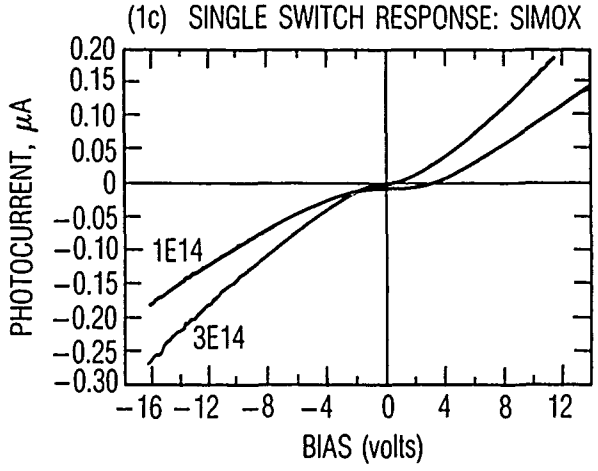
(1c) SINGLE SWITCH RESPONSE: SIMOX
PHOTOCURRENT, μA
0.20
0.15
0.10
0.05
0
−0.05
−0.10
−0.15
−0.20
−0.25
−0.30
1E14
3E14
−16 −12 −8 −4 0 4 8 12
BIAS (volts)

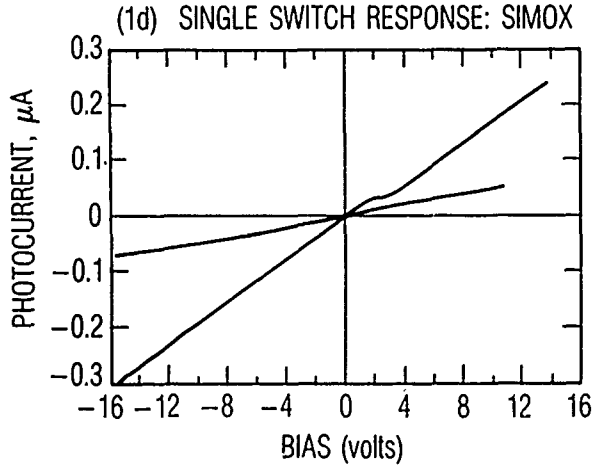
(1d) SINGLE SWITCH RESPONSE: SIMOX
PHOTOCURRENT, μA
0.3
0.2
0.1
0
−0.1
−0.2
−0.3
−16 −12 −8 −4 0 4 8 12 16
BIAS (volts)

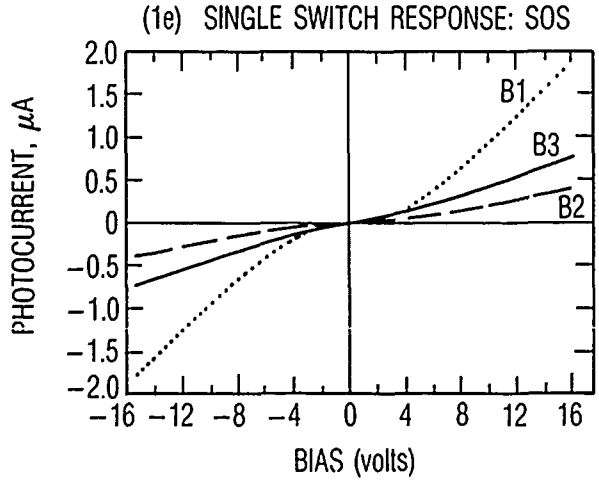
(1e) SINGLE SWITCH RESPONSE: SOS
PHOTOCURRENT, μA
2.0
1.5
1.0
0.5
0
−0.5
−1.0
−1.5
−2.0
B1
B3
B2
−16 −12 −8 −4 0 4 8 12 16
BIAS (volts)

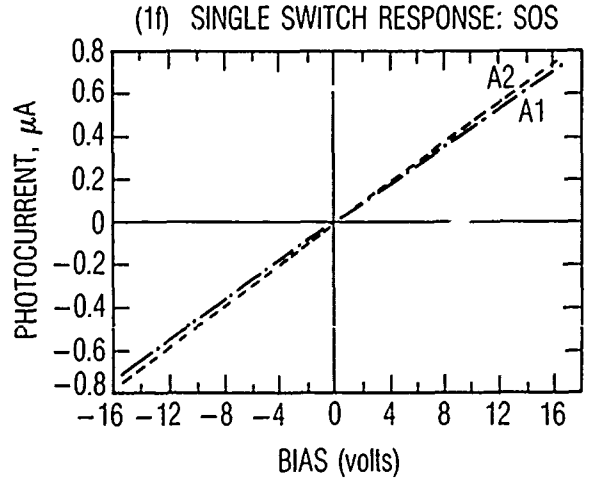
(1f) SINGLE SWITCH RESPONSE: SOS
PHOTOCURRENT, μA
0.8
0.6
0.4
0.2
0
−0.2
−0.4
−0.6
−0.8
A2
A1
−16 −12 −8 −4 0 4 8 12 16
BIAS (volts)

The use of tandem photoconductive switches for measuring picosecond turn-on delay of laser diodes.

P. Blixt*, E. Adomaitis, A. Krotkus

Semiconductor Physics Institute of the Lithuanian Academy of Sciences, 232600 Vilnius, Lithuania, U.S.S.R.

**Department of Physics II, Royal Institute of Technology, S-100 44 Stockholm, Sweden.*

The turn-on delay of laser diodes is an important parameter in two respects. Firstly, in high bit-rate optical communication systems employing gain-switched laser diodes it is important to minimize the turn-on delay. This can be accomplished by applying a current pulse with a steep leading edge and an amplitude of more than ten times the threshold current. For lasers with ultralow threshold, the turn-on delay (20-50 ps) is shorter than the rise-time of the current pulse (100 ps) [1]. Secondly, turn-on delay measurements have been employed for calculating carrier lifetime and bimolecular recombination coefficient [2,3]. Dixon and Joyce have shown theoretically that with an accuracy of tens of picoseconds in the turn-on delay measurements, both radiative and nonradiative carrier lifetimes could be unambiguously deduced [4].

The difficulty in using photoconductive switches to produce the short turn-on delay has been the necessary trade-off between the electrical pulse width and amplitude. When shortening the fall-time of the switch by carrier lifetime reduction, the mobility and, consequently, the current will decrease [5]. One way to avoid this trade-off is to use a single-gap photoconductor and two different laser wavelengths. A short wavelength to turn the switch on and a long wavelenght to shorten the signal to the ground [6]. This gives a very limited choice of switch substrate and lasers. In the present article, a novel technique for measuring the turn-on delay, using a tandem photoconductive switch, is described.

Experimentally, the carrier lifetime τ and the differential or small-signal lifetime τ' can be calculated by plotting the delay time T versus $\ln\{I/(I-I_t)\}$, were I is the injection current and I_t is the threshold current, at two extreme limits [4]:

$$T \sim \tau \ln\left(\frac{I}{I-I_t}\right) \text{ when } I \to \infty \tag{1}$$

and

$$T \sim \tau' \ln\left(\frac{I}{I-I_t}\right) \text{ when } I \to I_t. \tag{2}$$

The following relations connect the nonradiative recombination time τ_n and the radiative recombination time τ_r with the lifetime τ and the differential lifetime τ' [4]:

$$\frac{1}{\tau_n} = \frac{2}{\tau} - \frac{1}{\tau'} \text{ and } \frac{1}{\tau_r} = \frac{1}{\tau'} - \frac{1}{\tau}. \tag{3}$$

In Fig.1, a sketch of the experimental set-up is presented. A passively mode-locked and frequency doubled Nd^{3+}:YAG laser produced pulses of 23 ps duration at a wavelength of 0.53 μm and with pulse energy of 100 μJ. The repetition rate was 12 Hz and a single-pulse selection system was used. The laser beam was split into two parts with equal intensity, illuminating two photoconductive switches in a tandem configuration [7]. The switches were connected to a common microstrip transmission line and were biased to the same voltage but with opposite polarity. When illuminating the switches, two step-like current pulses were launched into the

microstrip-line. A negative and a delayed positive pulse, of equal magnitudes, were superimposed producing a rectangular pulse with a variable pulse duration. Pulses of durations ranging from approximately 25 ps to 1 ns were generated in this way. The pulse amplitude remained constant when altering the pulse duration. At one end of the microstrip-line a laser diode was mounted together with a resistor (R) for impedance matching and suppression of the reflected pulse. The laser was an LPE-grown, etched-mesa buried-heterostructure diode made by Ericsson Components AB. The doping concentration in the active layer was ~10^{17} cm^{-3}. The threshold current was 24 mA (one facet was antireflection-coated, with reflectivity of 1%). At the other end of the microstrip-line, the signal was monitored by a high-speed real-time oscilloscope with a bandwidth of 6 GHz.

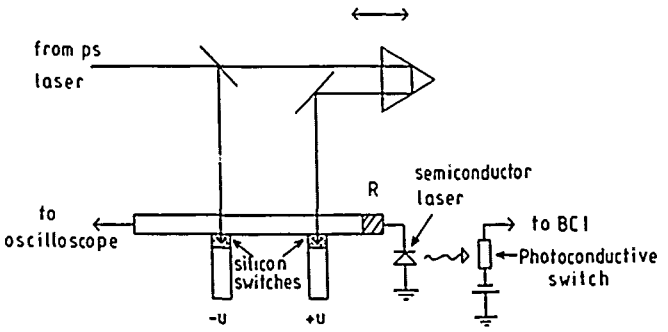

Fig.1 *Experimental set-up with photoconductive switches in tandem configuration.*

The switches were made from high-ohmic single crystal silicon. The rise time was 15 ps, limited by the laser pulse duration, and the fall-time was of the order of microseconds. The switches were fed by two coaxial cables with 50 Ω impedance matching to the bias power supply. Hence, each switch would produce a step pulse with a duration determined by the cable length. The cable of the negatively biased switch was a few centimetres longer than the other to avoid reverse biasing of the diode by the second pulse.

The maximum magnitude of the electric pulse on the 50 Ω microstrip-line was 50 V. These pulses have a much higher amplitude and shorter duration than those employed in previous experiments to feed a laser diode, *viz.*, a single-gap photoconductor which produced pulses with less than 2 V amplitude and 60 ps FWHM [8]. A tandem structure switch made from InP was able to produce pulses of 3 V and 40 ps FWHM [7]. An InGaAsP ($\lambda = 1.3\mu m$) photoconductive switch connected to a transmission line and a boxcar integrator was used to detect the signal from the laser diode. The signal measured by the boxcar integrator was proportional to the total number of photons emitted by the semiconductor laser during a 200 ps interval after turn-on.

We increased the pulse duration by an increment of 10 ps and measured the signal at each step. When the pulse width was equal to the turn-on delay time, the boxcar integrator gave a non-zero signal. By this method we had a turn-on delay time accuracy of 15 ps, determined primarily by the photoconductor rise-time. This was measured at different injection current magnitudes. Typical experimental curves are shown in Fig.2. The laser turn-on delay time T was established from the onset of the steep increase in output signal. The slope of the experimental curves was steeper as the injection current increased. Some curves showed a more complicated behaviour, which was probably due to relaxation oscillation phenomena in the laser emission.

Turn-on delay times down to 60 ps were measured. This is nearly three times lower than the shortest delay times found in previous investigations [9]. This time-resolution has allowed us to plot the T versus $\ln\{I/(I - I_t)\}$ dependence at extremely high injection currents ($I/I_t = 42$). This dependence is shown in Fig.3 together with the nanosecond delay time data obtained by conventional pulse technique. It is seen that the experimental points make a good fit to the theoretical linear depencies, as found in equations (1) and (2), at both low and high injection

current limits. From the slopes of the T vs $\ln\{I/(I-I_t)\}$ dependence at these limits, the differential life time τ' and the lifetime τ were established. From Fig.3, we obtain $\tau' = 2.475$ ns and $\tau = 3.346$ ns. By using the relations (3), the radiative lifetime τ_r and the nonradiative lifetime τ_n were found to be 9.5 ns and 5.2 ns, respectively.

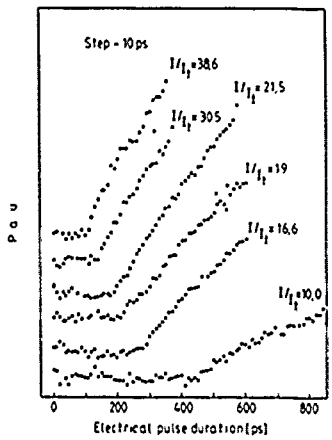

Fig.2 *Typical experimental data obtained from the boxcar integrator. Relative current (I/I_t) is shown for each curve and the time increment was 10 ps.*

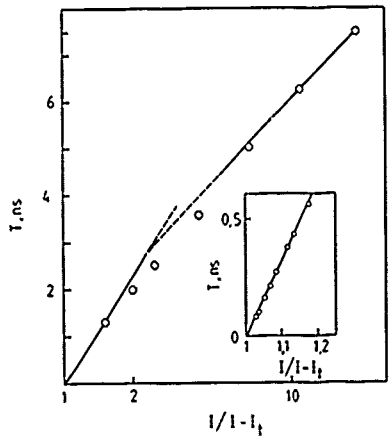

Fig.3 *The lifetimes* τ and τ' *are found by measuring the slopes of T vs* $\ln\{I/(I-I_t)\}$ *at the two extreme limits.*

In conclusion, we have demonstrated a new method to measure turn-on delay times of laser diodes with an accuracy of 15 ps by using tandem photoconductors. This makes it possible to deduce radiative and nonradiative carrier lifetimes unambiguously. The new features of the switch are the extremely high pulse magnitude (50 V) together with the variable pulse duration with constant amplitude. The rectangular pulses had both 15 ps rise and fall times. The response of the rectangular pulse excitation is easier to interpret than the corresponding response of the mathematically more complicated pulses produced by single-gap photoconductors or electrical pulse generators.

References.

1. K.Y. Lau, N. Bar-Chaim, P.L. Derry and A. Yariv, Appl. Phys. Lett. **51,** 69 (1987).
2. G.W. 'tHooft, Appl. Phys. Lett. **39**, 389 (1981).
3. K. Konnert and C. Lanza, Appl. Phys. Lett. **4**, 120 (1964).
4. R.W. Dixon and W.B. Joyce, J. Appl. Phys. **50**, 4591 (1979).
5. D.H. Auston, IEEE J. Quantum Electron. **QE-19**, 639 (1983).
6. D.H. Auston, Appl Phys. Lett. **26**, 101 (1975).
7. Y. Hori, J. Paslaski, M. Yi and A. Yariv, Appl. Phys. Lett. **46**, 749 (1985).
8. E.O. Göbel, G. Veith, J. Kuhl, H.U. Habermeier, K. Lübke, and A.Perger, Appl. Phys. Lett. **42**, 25 (1983).
9. D. Bimberg, E.H. Böttcher, K. Ketterer, H.P. Vollmer, H. Beneking and P. Roentgen, Appl. Phys. Lett. **48**, 83 (1986).

Differential Sampling with Picosecond Resolution using Bulk Photoconductors

J. Paslaski, A. Yariv
California Institute of Technology 128-95
Pasadena,CA 91125
(818) 356-4830

The success of photoconductive sampling has critically depended on the ability to reduce carrier lifetimes to attain sufficiently short temporal resolution. We present an alternate approach which achieves a sampling resolution limited only by the RC circuit response of charging the photoconductive gap.

The result of a typical sampling measurement, $V_{meas}(\tau)$, can be expressed as the correlation between the signal to be measured, $V_{sig}(t)$, and a sampling function, $f_{samp}(t)$[1]:

$$V_{meas}(\tau) \equiv V_{sig} \circ f_{samp} = \int dt V_{sig}(t) f_{samp}(t-\tau) \tag{1}$$

Neglecting the finite optical pulse width and mobility transients, f_{samp} is itself a correlation between the gap conductivity $G(t)$ and a gap charging transient $h(t)$ which is typically fast(a few ps at most). If the conductivity $G(t)$ is very short, then $V_{meas} \simeq V_{sig}$ to the extent that f_{samp} approximates a delta function. If instead,the conductivity has a a slow decay, then V_{meas} will be approximately the integral of V_{sig} (for sufficiently short V_{sig}) and it is recovered by a derivative operation. As such, consider the following:

$$\Delta V_{meas}(\tau) \equiv V_{meas}(\tau) - \alpha V_{meas}(\tau + \Delta\tau) = V_{sig} \circ [h \circ (G(t) - \alpha G(t - \Delta\tau))] \tag{2}$$

The expression in [ ] is a new sampling function composed of a sharp "spike" followed by an equal area negative tail which becomes negligible if it is much longer than the signal being measured. In the special case that $G(t)$ is an exponential decay, this tail can be eliminated altogether by an appropriate choice of the factor α. This effective sampling function is plotted in Fig. 1 for various values of $\Delta\tau$, using exponential decays for $h(t)$ and $G(t)$(dotted line) with respective time constants of 2ps and 150 ps. It is seen that very short sampling windows can be achieved which are independent of the carrier decay, and limited only by the circuit transient $h(t)$.

The experimental set-up used is diagrammed in Figure 2. The electrical signal is fed to a microstripline and two opposing photoconductors sample it with a relative delay, $\Delta\tau$, set by the positioning of mirror M_2. The correlation variable τ is swept by moving mirror M_1. The low frequency average currents from the two sampling electrodes are then subtracted with the balancing factor α, and the result is synchronously detected with a lock-in amplifier. The simultaneous measurement of the two sampling signals minimizes effects due to low frequency noise of the optical pulse source which degrade simpler schemes such as just shifting the stored result of a single gap measurement and subtracting it from itself(this does work rather well). The center microstripline and two sampling electrodes were designed for 50Ω impedance and were separated by $50\mu m$ gaps which had a dark resistance of 80MΩ. The substrate was ordinary semi-insulating InP:Fe and the metallization was AuGe:Au with a 5 minute anneal at 340 °C. A modelocked dye laser operating at 100 MHz, λ=600 nm, and a pulse width of 2ps illuminated the photoconductors as well as a *pin* photodiode which generated the electrical signal.

The result of a sampling measurement of the *pin* photodiode is shown in Figure 3. A sampling oscilloscope measurement of the same signal confirms the shape and calibrates the amplitude with a peak signal level of 60 mV. The resolution is believed to be a little over the fixed delay, $\Delta\tau$, which is 10 ps here; although it is unfortunately not demonstrated here, presumably due to the lack of fast features in the measured signal. This is a substantial improvement over the single gap capabilities which had a photoconductive decay of 150 ps. Also, the optical power incident on each photoconductor was only 5μW which is quite low for typical optoelectronic sampling.

A major advantage of this scheme is that it achieves picosecond resolution without the need for a technique to reduce carrier lifetimes. This is especially useful in situations where such techniques (usually

involving material damage) are undesirable or for materials for which such techniques are not developed. It also means that mobility does not have to be sacrificed which can improve sensitivity in some cases, although the long carrier lifetimes cause increased Johnson noise from the photoconductors. Another feature is that the adjustment of $\Delta\tau$ offers a selectable trade-off between resolution and sensitivity since a wider sampling window gives a stronger signal. Finally, the application of this scheme to a coplanar, "sliding contact" geometry[2] could result in resolutions well below a picosecond.

References

[1] D. H. Auston, IEEE J. Quant. Electron., **QE-19**, 639, (1983)
[2] D. R. Grischkowsky, M. B. Ketchen, C.-C. Chi, I. N. Duling,III, N. J. Halas, J.-M. Halbout, and P. G. May,IEEE J. Quant. Electron., **QE-24**, 221, (1988)

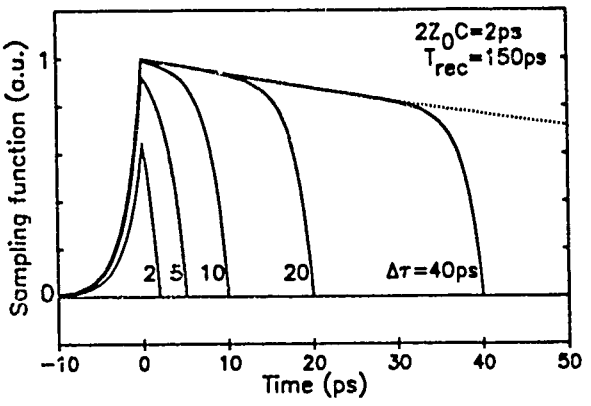

Fig. 1- Effective sampling function curves

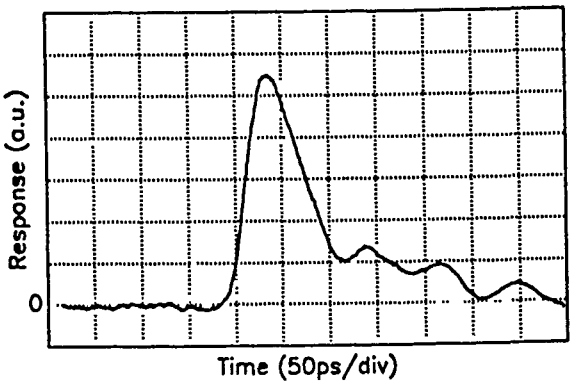

Fig. 3- Differential sampling trace of pin response

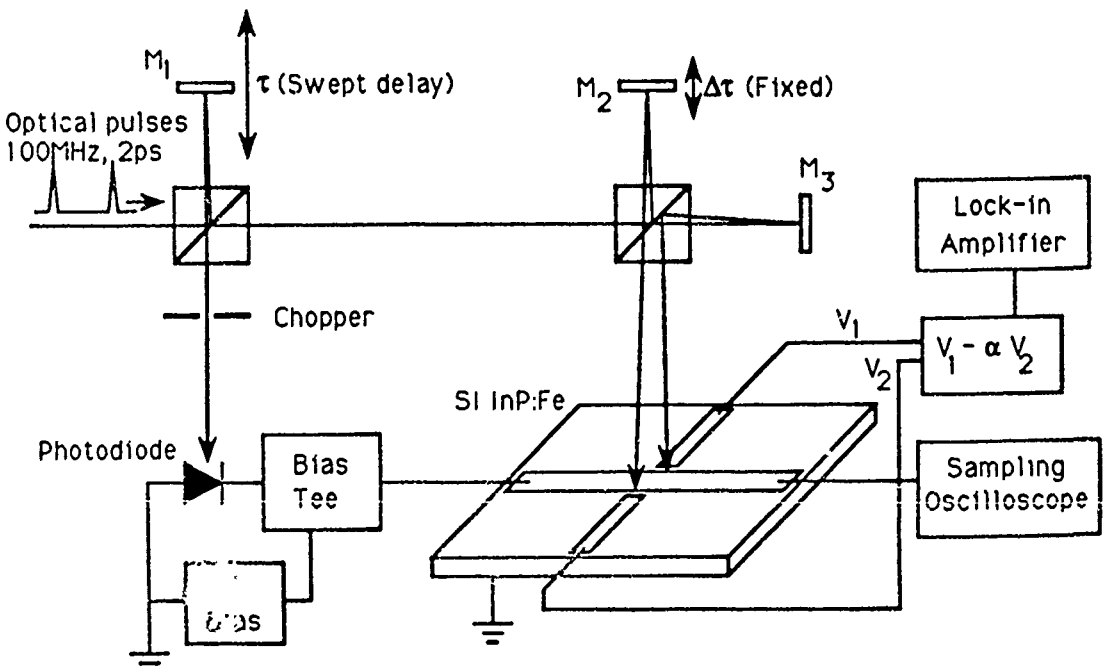

Fig. 2- Experimental set-up

Timing Jitter in Repetitively Pulsed Semiconductor Lasers

by
Ruixi Yuan and Henry F. Taylor
Department of Electrical Engineering
Texas A&M University
College Station. TX 77843

Timing jitter can limit the accuracy of data obtained by optical sampling using repetitively pulsed semiconductor lasers. When the optical sampling is used for real-time analog-to-digital conversion, for example, the maximum allowable jitter is typically 20-40 times less than the maximum permissible pulse width[1]. Timing jitter in semiconductor lasers has been studied experimentally[2,3], but a predictive model has not heretofore been available.

In this paper, we present results of an analysis of timing jitter in free-running and in external-cavity-coupled semiconductor lasers driven with repetitive current waveforms. The analysis is based upon a quantum amplifier model[4] of the laser, in which spontaneous emission, stimulated emission, absorption, and scattering of light are treated as Poisson processes which produce random fluctuations in photon and carrier densities. By solving rate equations with appropriate random (Monte Carlo) variables[5], the temporal variation of output power is simulated. The effect of an external mirror is analyzed by incorporating delayed feedback into the model.

We have studied the effect of variations in key system parameters (facet reflectances, bias current, modulating current waveform, and external cavity length and mirror reflectance) on the average pulse width and the root-mean-square timing jitter. Some representative results are shown in Figs. 1 and 2 for a laser with a 20 mA threshold current. Sinusoidal modulation at a frequency f_m of 2.2 GHz with a peak-to-peak current amplitude of 80 mA is superimposed upon a dc bias of 50 mA. In Fig. 1(a) the full-width at half-maximum of the laser pulse is shown as a function of external cavity length L for front-facet reflectances of .35 (without AR coating) and .01 (with AR coating) and an external mirror reflectance r of .04. As reported by other authors[6], shortest pulse widths are obtained when the modulation frequency is slightly less than the reciprocal of the round-trip transit time for the external cavity. The results in Fig. 1(b) indicate that timing jitter is very sensitive to external cavity length and that lower jitter (much less than 1 ps) is obtained with the AR-coated laser. Fig. 2 shows a monotonic decrease in pulse jitter with increasing external mirror reflectance r - but at the higher reflectance values the pulses become broadened and distorted.

Results for modulation with short pulses such as those produced by a comb generator will be included in the presentation. In one case, for example, it was found that the laser pulse jitter in an external cavity was less than 1

ps even when a simulated jitter of 4 ps was present in the modulating pulse train.

To summarize, a quantum amplifier model has been applied to the calculation of pulse jitter in semiconductor lasers. The pulse jitter is very sensitive to external cavity length and feedback level. The results suggest that it may be possible to produce optoelectronic "clocks" which show better short-term stability than their all-electronic counterparts.

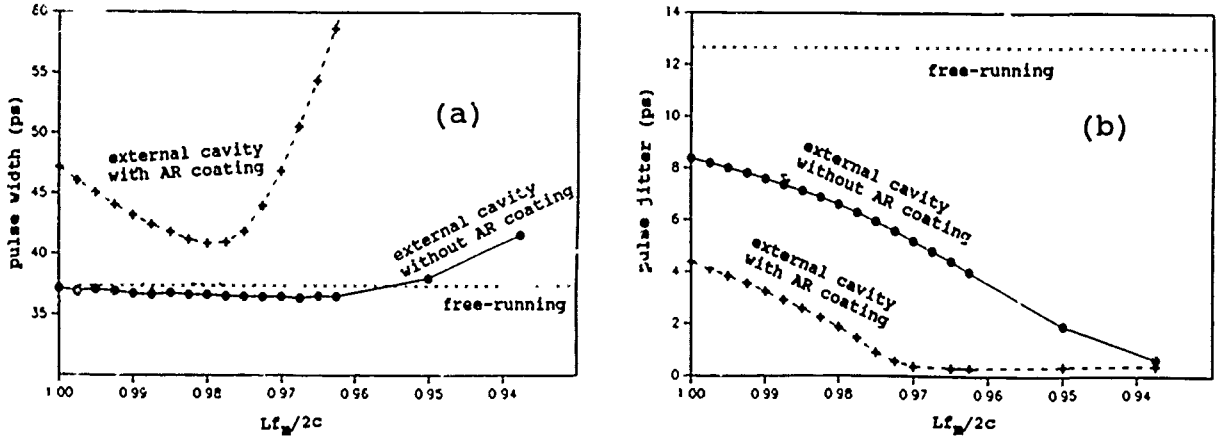

Fig. 1. Dependence of pulse width (a) and pulse jitter (b) on external cavity length, for r=.04.

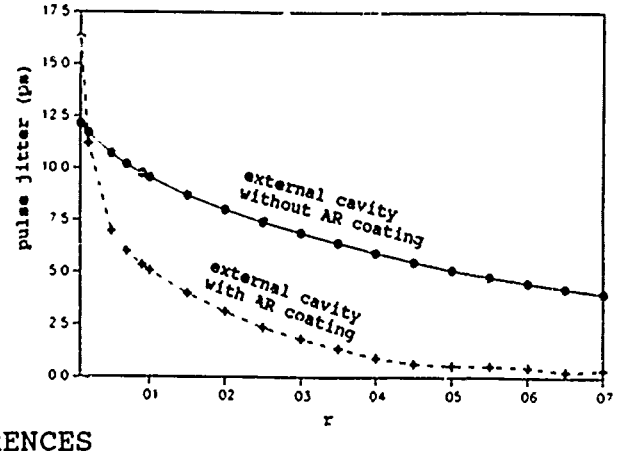

Fig. 2. Dependence of pulse jitter on external mirror reflectance, for $Lf_m/2c = .975$.

REFERENCES

1. H. F. Taylor, IEEE J. Quant. Electron. QE-15, 210 (1979).
2. F. Mengel, C. Lin, and N. Gade, Opt. Commun. 54, 103 (1985).
3. A. J. Taylor, J. M. Wiesenfeld, G. Eisenstein, and R. S. Tucker, Appl. Phys. Lett. 49, 681 (1986).
4. A. M. Yurek, H. F. Taylor, L. Goldberg, J. F Weller, and A. Dandridge, IEEE J. Quant. Electron. QE-22, 522 (1986).
5. D. Marcuse, IEEE J. Quant. Electron. QE-20, 1139 (1984).
6. J. C. Goodwin and B. K. Garside, IEEE J. Quant. Electron. QE-19, 1068 (1983).

Timing Jitter of Colliding Pulse Modelocked (CPM) Lasers

G.T. Harvey, M.S. Heutmaker
AT&T Bell Laboratories, P.O Box 900, Princeton NJ 08540
P.R. Smith - AT&T Bell Laboratories, Murray Hill
and J.A. Valdmanis - University of Michigan

An excellent source of stable subpicosecond pulses, the balanced colliding pulse modelocked (CPM)[1] dye laser represents an attractive source for electrooptic sampling. Being a free running laser, the CPM must act as the master oscillator of the system, to which any electrical signals must be synchronized. This is in contrast to actively mode-locked systems where the laser is locked to the frequency of an external oscillator by modulating the gain or loss in the laser cavity. Acting as the master clock, the CPM is a source of both amplitude and phase noise in the system. The absolute phase noise of the laser, however, is not as critical as the relative phase noise between the laser and the oscillator which results in jitter between the two sources and a reduction in temporal resolution. Our experiments deal with both the absolute phase noise of the laser and the synchronization of the laser to commercial frequency synthesizers.

We have used a high-speed photodetector and RF spectrum analyzer to measure the absolute timing jitter of pulses[2] from a free-running CPM laser. We distinguish phase noise from amplitude noise by the fact that phase noise power in a sideband grows as the square of the harmonic number, while the amplitude noise is constant. Fig. 1 shows the spectrum from the photodetector pulses at the fundamental (100 MHz) and the tenth harmonic. The fundamental spectrum contains a noise continuum and a set of peaks spaced by 60 Hz around the central (carrier) peak. At 1 GHz, the noise continuum within about 500 Hz of the carrier has increased markedly, and rises sharply with decreasing frequency offset.

We calculate the timing jitter on the fundamental by integrating the power in the phase noise continuum at the nth harmonic, and dividing by n^2. From the ratio of integrated phase noise power to the carrier power, we find the rms phase jitter and convert it to timing jitter. From two sets of data at the fifth and tenth harmonic the jitter (integrated from 50 Hz to 500 Hz) is found to be 3.5±1.5 milliradian, or about 5 ps at 100 MHz.

To measure the relative phase noise between a CPM and an external oscillator we use the phase detector method[3]. Fig. 2 is a block diagram of the experimental set up. The divider generates a 10 MHz square wave from the 100 MHz output of a PIN detector monitoring the laser pulses. Output from the divider is used as an external reference for a low phase noise RF synthesizer. To test the synchronization between the synthesizer and the laser, another part of the PIN signal is low pass filtered and combined with a 100MHz signal from the synthesizer in a double balanced mixer. The signal from the PIN is also attenuated to prevent harmonic generation in the mixer. A low pass filter eliminates the high frequency components of the mixer output and the signal is amplified and fed into both a low frequency spectrum analyzer and an oscilloscope. For proper phase detection, the phase shifter in the synthesizer arm is adjusted for quadrature by nulling the DC mixer output on the oscilloscope.

The low frequency spectrum analyzer takes the Fourier transform of the signal to calculate the power spectral density of the noise. To find the mean square phase noise density (both side bands), the power spectral density is divided by the carrier power and by a factor of 2 to account for the base band conversion. Integrating and taking the square root gives the rms phase noise which is used to calculate the jitter. A number of synthesizers were tested with the lowest phase noise caculated at 1.13 mrad over a 2 Hz to 1 kHz band, corresponding to a jitter of 1.8 ps.

Locking an RF synthesizer to the CPM laser pulses can clearly be done with less relative

phase noise than the absolute phase noise of the CPM. The residual 1.8 ps jitter seen in our experiments is probably due to amplitude to phase noise conversion in either the divider, the mixer, or the phase detector of the synthesizer. Noise in the mixer presents only a measurement problem while the divider or phase detector could perhaps be optimized to reduce jitter.

1. R.L. Fork, B.I. Greene, and C.V. Shank, Appl. Phy. Lett. **38**, 671 (1981).

J.A.Valdmanis and R.L Fork, IEEE JQE **QE 22**, 112 (1986).

2. M.J.W. Rodwell , D.M. Bloom, and K.J. Weingarten, "Subpicosecond Laser Timing Stabilization", to be published in J. of Quantum Electron.

J. Kluge, D. Wiechert, and D. Von Der Linde, Optics Comm. **51** 271 (1984).

3. Hewlett Packard Product Note 11729B-1.

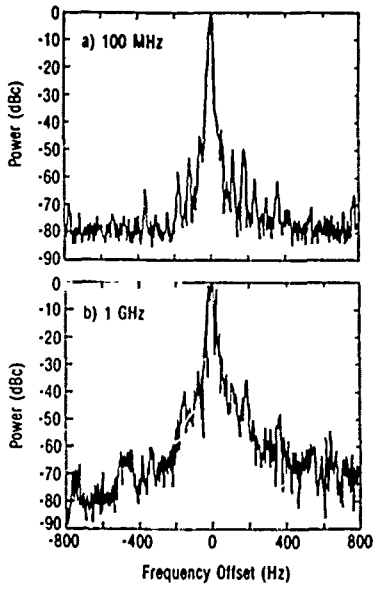

Fig. 1

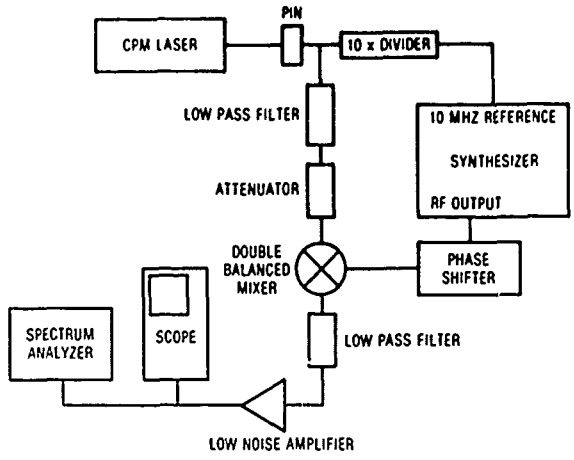

RELATIVE JITTER MEASUREMENT

Fig 2

Comparison of Electro-Optic and Photoconductive Sampling Using a 28-GHz Monolithic Amplifier.

E. Chauchard, G. Treacy, K. Webb, Chi H. Lee
University of Maryland, Department of Electrical Engineering, College Park, MD 20742

H.-L. A. Hung, H.C.Huang
COMSAT Laboratories,Clarksburg, MD 20871-9475

P. Polak-Dingels
University Research Foundation, 6411 Ivy Lane, Suite 110, Greenbelt, MD 20770

Electro-optic sampling and photoconductive sampling have been used by different groups [1,2] to evaluate the performance of high speed electronic circuits. No one has yet quantitatively compared the two techniques using the same device. In this paper, we will evaluate the performance of a 28-GHz monolithic microwave integrated circuit (MMIC) using both techniques and compare the results to network analyzer measurements. We utilize a unique approach for characterizing the MMIC. A short electrical pulse with wide frequency content is analyzed in the time domain before and after passing through the device. The transfer function of the MMIC is then obtained by Fourier Transformation.

The device evaluated consisted of a 28-GHz MMIC mounted between two sets of photoconductive switches fabricated on a proton-implanted GaAs substrate. See Figure 1 for a schematic diagram of the device. This design permits both techniques to be utilized to study the performance of the MMIC. The MMIC was sampled by 0.532 and 1.06 micron pulse trains having a typical pulse duration of 5-6 psec.

For photoconductive sampling, the 0.532 micron pulse train is split into two separate pulse trains. One is directed to Port a of the device to generate a voltage pulse on the input microstrip line; the second pulse train is used to sample the input waveform to the MMIC at Port b or the output waveform of the MMIC at Port d. For electro-optic sampling, the input waveform is also generated at Port a using the 0.532 micron laser pulse train . The sampling of the waveforms is performed with the 1.06 micron pulse train using the electro-optic effect in GaAs . For a valid comparison of the two techniques, the input and output waveforms were sampled at the same positions on the microstrip line.

Figure 2 shows the input waveforms as sampled by these two techniques. These waveforms which reflect the photoconductive switch response time were very short because the GaAs substrate has been proton implanted. The Fourier transforms of the input and output waveforms were performed using a numerical FFT routine. The transfer function of the MMIC, both magnitude and phase, were calculated by a ratio of the output and input Fourier transforms and corrected for the RF loss and phase shift of the GaAs transmission lines. Figure 3 shows the transfer function calculated from the photoconductive sampling data. These results are compared to those obtained with a HF3510 network analyzer.

By comparing Figures 2a and 2b, one can see an immediate difference between the two techniques. In photoconductive sampling, the waveform is sampled by a gate whose temporal characteristics are dominated by the switch response time.

For the input waveform, this results in an autocorrelation of the switch response time. In electro-optic sampling, the waveform is sampled by a gate whose shape is that of the laser pulse. Therefore the temporal resolution of electro-optic sampling is better than that obtained by photconductive sampling.

In comparing both methods, we found that it is more difficult to implement electro-optic sampling because of its lower sensitivity. For our device, the ratio of the detected signal voltage to the sampled voltage is 2×10^{-5} for electro-optic sampling and 3×10^{-3} for photoconductive sampling. In order to obtain a quantitative measurement of the voltage on the line, a calibration of the sampling configuration is necessary. We found this calibration more difficult to obtain with electro-optic sampling because the signal is very sensitive to the position of the sampling beam next to the microstrip line. Electro-optic sampling requires only one photoconductive switch since sampling can be done anywhere along the microstrip line and even "on-chip", within the integrated circuit. However photoconductive sampling can be performed on any substrate while electro-optic sampling is limited to GaAs.

Our results indicate that the transfer functions obtained by these two techniques and network analyzer measurements show the same main features, for example gain at 28 GHz. However, some differences exist which determine the range of applicability of each technique.

References:

1. K. J. Weingarten, M. J. W. Rodwell and D. M. Bloom. IEEE J. Quantum Electronics. QE-24, (1988), 198.

2. D. A. Auston. IEEE J. Quantum Electronics. QE-19, (1983), 639.

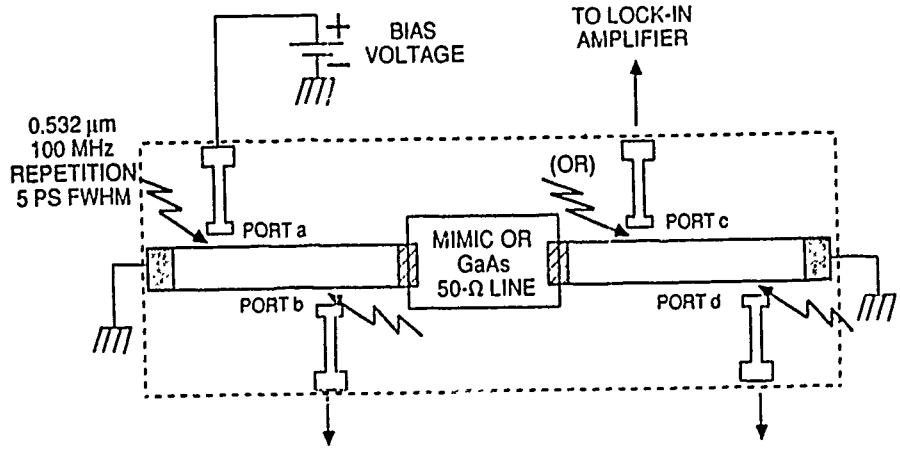

Figure 1: Schematic diagram of the device.

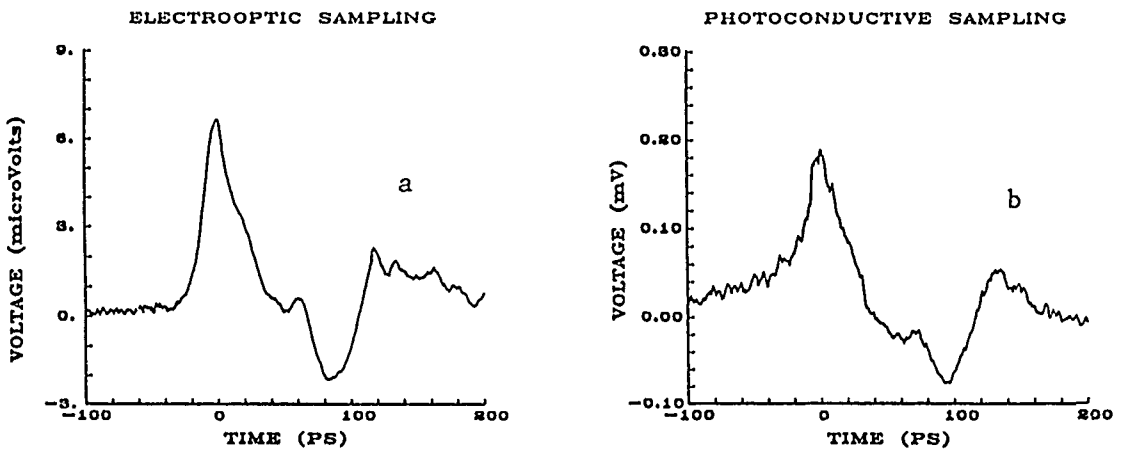

Figure 2: Input waveform obtained at Port b by (a) electro-optic sampling and (b) photoconductive sampling.

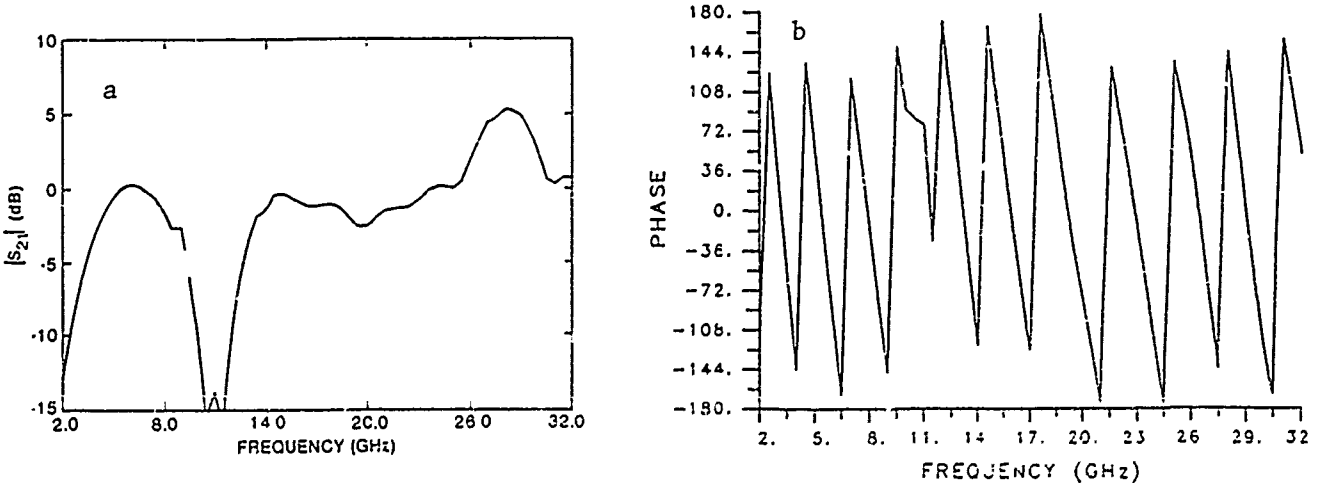

Figure 3: Transfer function calculated from photoconductive sampling data: (a) magnitude, (b) phase.

NOTES

THURSDAY, MARCH 9, 1989

SALON G

8:30 AM–10:00 AM

ThA1–3

TRANSISTORS

J. Murphy, Defense Advanced Research Projects Agency, *Presider*

Silicon FETs at 0.1μm Gate-Length

G. A. Sai-Halasz*

IBM Research Division, T. J. Watson Research Center, Yorktown Heights, N.Y. 10598

An investigation has recently been undertaken regarding the feasibility of FETs in the 0.1μm gate-length regime[1,2] . This paper summarizes the work, starting with the design aspects and ending with ring oscillator performance.

Because of non-scalable parameters and noise margins, operating voltage cannot be indefinitely decreased with dimensions, and one is forced to work with higher voltage levels than dictated by ideal scaling. This becomes most detrimental once performance saturates at less than the operating voltage, due to velocity saturation type characteristics. In such an environment the measure of a good design lies in achieving operation at the lowest feasible voltage. This naturally leads to a low temperature (LT), 77K, design as primary approach. Other advantages to LT operation are: improved performance, better punch through behavior, and the possibility of counteracting the junction potential by forward bias. The lowest practical threshold, even at 77K, was deemed not to be below 150mV. This choice then leads to a ~0.6-0.8V bias for both the drain and the substrate.

As a first feasibility study the work was directed toward NMOS. In the fabrication, tight linewidth and overlay tolerances have been achieved by direct-write electron-beam lithography on all levels[3] . Most test sites have been fabricated in multiple versions with differing gate lengths from 0.27μm down to 0.07μm. A semi-recessed oxide isolation was employed, which allowed horizontal dimensions at the diffusion level to be shrunk only to the extent which would have been consistent with a 0.25μm gate length. Gate oxide thickness was 4.5nm.

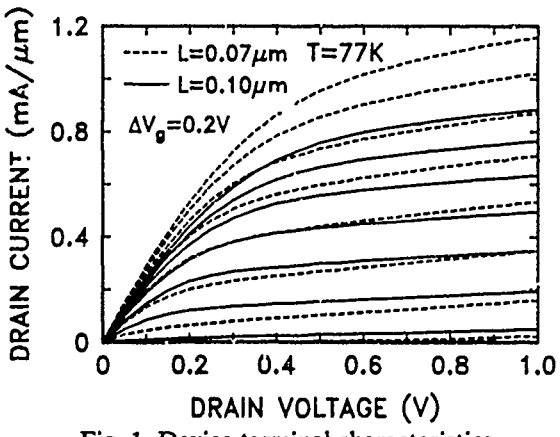

Fig. 1. Device terminal characteristics

Device characteristics strongly depended on processing details. The most important parameter in determining transconductance, g_m , was the source/drain (S/D) resistance. The common feature of the highest performance devices was an abrupt S/D resulting from the use of antimony[4] . The device and circuit results to be presented are all from the same wafer, thus eliminating variations arising from processing differences.

Fig. 1 shows the terminal characteristics of 0.1μm and 0.07μm gate-length devices at LT with 0.6V substrate bias. At V_{DS} = 1V the 0.07μm device has a maximum g_m of over 940μS/μm and the 0.1μm one 770μS/μm. The room temperature g_m of these devices with 0V substrate bias is 590 and 505 μS/μm respectively. The g_m 's of these devices are the highest measured in FETs to date.

Fig. 2 gives g_m as function of gate-length and clearly manifests the effect of velocity overshoot. The plot was made for V_{DS} =0.8V, 0V substrate bias, and for each gate-length at that V_G where g_m peaked. This typically occurred at (V_G -V_T) ~0.6V. The evidence for velocity overshoot is twofold. First, the size of g_m in the shortest devices. If carriers were not capable of exceeding v_{sat} then there would exist an unattainable upper limit for the intrinsic g_{m_i} : $v_{sat} \cdot C_{ox}$. This limit is marked on Fig. 2, and as can be seen, even the measured g_m exceeds the limit set for the intrinsic value. The second manifestation of velocity overshoot is in the trend of g_m with gate-length. The solid line in Fig. 2 is g_m obtained by a conventional two-dimensional simulator (FIELDAY). The curve thus shows how g_m would have behaved in the absence of velocity overshoot. The deviation of the data from the steady state transport curve is a clear sign of velocity overshoot. Detailed self-

consistent Monte Carlo modeling[5] shows that the electron velocities in the shortest devices reach a velocity of $3x10^7$ cm/sec.

To measure switching delay times, 21 stage unloaded ring oscillators and open ended inverter chains have been fabricated. An enhancement mode device with its gate tied to an independent power supply served as the load element, in effect acting as a resistor. The width of the active devices was 5μm, that of the load devices 1.25μm. The fastest per-stage switching delays measured[6] at selected gate lengths, always on the same wafer, were as follows: 19.5ps at 0.20μm, 17.8ps at 0.16μm, 16ps at 0.13μm, and 13.1ps at 0.10μm. For the 0.1μm gate length ring oscillators the room temperature delay was found to be 17.7ps at V_{dd} =1.3V with 0.12mW power per μm of gate width. The values for the 0.1μm circuits are the fastest switching times ever obtained for silicon devices.

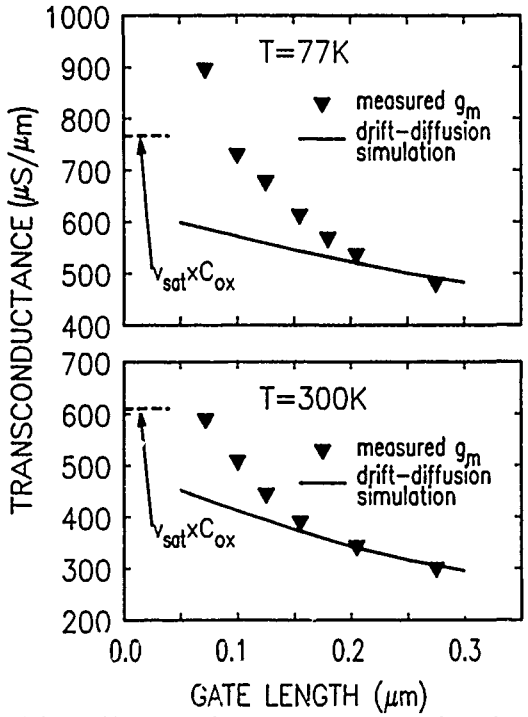

Fig. 2. Transconductance versus gate length

Since the program was exploratory the dose and energy of the threshold adjust implant was varied on different wafers. This particular wafer had a higher threshold, 0.3V with 0.6V bias on the substrate, than our nominal design called for[1]. For this reason the ring oscillators performed best at relatively high voltage levels. Fig. 3 shows delay per stage versus power for the 0.1μm circuits. At each applied power-supply voltage the load current was adjusted to obtain the highest speed. As can be seen, the curve is quite flat. This is expected since the devices exhibit transconductance saturation[1,2] in most of their operational range.

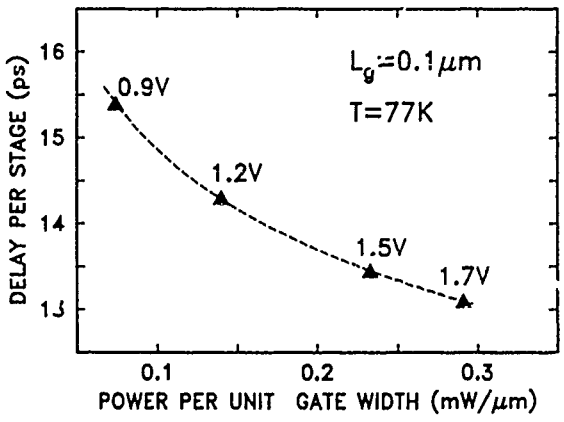

Fig. 3. Delay versus power

Had the threshold of these devices been 0.15V, which is the nominal design value[1], then at the optimal V_{dd} level of 0.6-0.8V one would have already obtained maximum performance. Measurements on the inverter chains gave consistent values with the ring oscillators. The basic message is that delay times are improving with decreasing gate lengths even down to the length of 0.1μm.

Detailed circuit simulations (ASTAP), in which the measured device characteristics[7] were used as input, have also been performed. These showed that the measured delay times were longer than what they should have been based on device performance. The discrepancy was caused by a particular processing problem of this run. the titanium-silicide, which covers both the S/D and the polysilicon gate in a self-aligned manner, had too high sheet resistivity. The excess resistance of the long, thin gates resulted in a 6ps per stage additional RC delay. Accordingly, without this spurious effect the 0.1μm gate length ring oscillators should have reached 7ps delay per stage. In a fully-scaled version of the 0.1μm gate length circuits, with decreased junction capacitance, per stage delays can be below 5ps even with the use of such a relatively thick gate oxide as was done in the present work.

The work presented in this article was an effort of many people in our laboratory. My closest collaborators were M. R. Wordeman, D. P. Kern. S. A. Rishton, E. Ganin, T. H. P. Chang and R.

H. Dennard. Special thanks goes to members of the Silicon Facility in our laboratory for their contributions in processing.

* Present address: IBM, General Technology Division, East Fishkill, Hopewell Junction, NY 12533

REFERENCES

1 G. A. Sai-Halasz, et. al. IEEE Electron Device Lett. EDL-8, 463 (1987).
2 G. A. Sai-Halasz, M. R. Wordeman, D. P. Kern, S. Rishton, and E. Ganin, IEEE Electron Device Lett. EDL-9, 464 (1988).
3 S. A. Rishton, et. al. J. Vac. Sci. Technol. B6, 140 (1988).
4 G. A. Sai-Halasz and H. B. Harrison, IEEE Electron Device Lett. EDL-7, 534 (1986).
5 S. E. Laux and M. V. Fischetti, IEEE Electron Device Lett. EDL-9, 467 (1988).
6 G. A. Sai-Halasz, et. al. IEEE Electron Device Lett. EDL-9, Dec. (1988).

Millimeter Wave AlInAs-GaInAs HEMTs

U.K. Mishra
ECE Department, Box 7911
North Carolina State University
Raleigh, NC 27695-7911
(919) 737-7354

Summary

This paper reports the work done at the Hughes Research Labs in the area of mm-wave AlInAs-GaInAs HEMTS.

Heterostructure FETs based on both GaAs and InP have demonstrated excellent performance in a variety of analog and digital applications. The advantages that heterostructure FETs offer are:

i) The high electron mobility in modulation doped structures reduces parasitic resistances

ii) The inherent high aspect ratio in a HEMT structure enables the design of high performance sub-micron devices with good sub-threshold characteristics.

iii) The probability of velocity overshoot in undoped channels is much higher than in doped channels which leads to higher transconductance and mm-wave gain.

AlInAs-GaInAs HEMTs on InP have several advantages over the GaAs based HEMTs. The mobility at room temperature in GaInAs is much higher than in GaAs (13000 cm^2/V-sec vs. 8000 cm^2/V-sec). The peak velocity is also substantially higher (v_p - $2.7x10^7$ vs. $2x10^7$ cm/sec). The sheet charge density attainable in the AlInAs-GaInAs system is - $4x10^{12}$ cm^{-2} compared to - $2x10^{12}$ cm^{-2} in the GaAs based system. This high charge density coupled with the high mobility leads to an extremely high conductivity of the two dimensional electron gas which decreases the

parasitic resistances in the device. The electronic properties of the material can be improved further by increasing the Indium composition in the channel. These pseudomorphic structures exhibit both higher mobilities and higher sheet charge densities.

Devices with 0.2 micron and 0.1 micron gate length have been fabricated on lattice-matched and pseudomorphic modulation doped structures. The sheet charge density and mobility in these structures were - 3.5×10^{12} cm^{-2} and - 9500 cm^2/V-sec respectively. The lattice matched devices demonstrated a transconductance of 800 mS/mm for the 0.2 micron HEMT and a g_m of 1080 mS/mm for the 0.1 micron HEMT. The f_T of the devices were 140 GHz and 170 GHz respectively. 0.1 micron gate length pseudomorphic HEMTs exhibited an f_T of 205 GHz. This is the first demonstration of a transistor with an f_T of > 200 GHz. The f_{max} of the transistor was - 300 GHz. The minimum noise figure of single stage amplifiers built with these devices ranged between 0.8 dB and 1.4 dB at 63.5 GHz. These are the best results for low noise amplifiers at V-Band. Ring oscillators built with 0.2 micron gate length HEMTs have demonstrated a minimum propagation delay of 6 pS with a fan-out sensitivity of 2.6 pS per gate at room temperature which is a record for HEMTs. Static frequency dividers have worked at a record frequency of 26.7 GHz. This performance is attributable to the high f_T and drive capability of AlInAs-GaInAs HEMTs.

Future work in AlInAs-GaInAs HEMTs will address epitaxial layer design optimization for mm-wave power applications and integrated circuit designs for mm-wave digital and analog applications.

The Permeable Base Transistor: An Update*

Carl O. Bozler

Lincoln Laboratory, Massachusetts Institute of Technology
Lexington, Massachusetts 02173

The PBT was conceived in 1979 as a device capable of amplifying and generating power in the EHF range. The PBT is a GaAs vertical three-terminal device, in which the emitter and collector regions are separated by a submicrometer-periodicity tungsten grating that forms the base of the transistor. Numerous advantages are combined in the PBT structure. A short control region is easily obtained in a PBT because the length of the region is determined by the thickness of the tungsten base grating and the electron concentration in the GaAs, rather than by lithography. This is important, because the unity-current-gain frequency f_T varies inversely with the control length. In addition, the base resistance of a PBT can be comparatively low, because it is determined by the resistivity of a metal. Because the PBT is a vertical device in which many channels are adjacent to one another, it does not suffer from problems analogous to the substrate- and surface-leakage problems of planar high-electron-mobility transistors (HEMTs) and field-effect transistors (FETs). As a result, the PBT has a higher output impedance than either device. The PBT is also a very compact device. Because of its vertical geometry, large effective gatewidths can be achieved in small areas in a PBT. For example, an 8-by-40-μm PBT contains 2 mm of gate periphery. This means that large currents can be controlled with a PBT without the gate voltage distribution problems of a conventional planar FET or HEMT.

Our work over the past two years has concentrated on the optimization and characterization of PBTs for EHF power applications. A number of PBTs have been fabricated, many of which incorporate new refinements in the device design. Measurements of the small-signal and power capabilities of these devices have resulted in several new performance records. A small-signal hybrid amplifier using a PBT fabricated on a semi-insulating GaAs substrate has demonstrated 11.2 dB of device gain at 40 GHz, which is a new record for gain shown by a PBT at this frequency. A small PBT fabricated on a SI GaAs substrate has demonstrated 30 mW of output power with 3 dB of gain at 40 GHz in Class A operation

in an active load-pull measurement. This is a new record for power output from a PBT at this frequency. PBTs having a grating periodicity of 240 nm (reduced from the standard period of 320 nm) have shown a small-signal power gain of 20.1 dB at 26.5 GHz, which extrapolates to a maximum frequency of oscillation f_{max} of 265 GHz. This is the highest small-signal gain reported for any transistor at this frequency. PBT hybrid power amplifiers have demonstrated power-added efficiencies as high as 45% and power output as high as 0.5 W at 22 GHz in Class AB operation. This performance is better than or comparable to that reported for all other transistors in this frequency range. A hybrid amplifier using a PBT of the new power design has shown a power output of 1 W with a PAE of 35% and a gain of 19 dB in Class A operation at 1.3 GHz. This is the highest gain that has been reported for any transistor at this power level and frequency. Extensive analysis has enabled improvements to be made in picosecond electro-optic sampling measurements of transistor performance. There is a current effort to obtain small signal gain and power at 94 GHz and if possible some results will be reported.

* This work was sponsored by the Defense Advanced Research Projects Agency, and the Department of the Air Force. The views expressed are those of the author and do not reflect the official policy or position of the U.S. government.

THURSDAY, MARCH 9, 1989

SALON G

10:30 AM–12:00 M

ThB1–4

LIGHTWAVE TECHNOLOGY

L. A. Coldren, University of California, Santa Barbara, *Presider*

High-Speed Lightwave Systems

Alan H. Gnauck

AT&T Bell Laboratories
Crawford Hill Laboratory
Holmdel, New Jersey 07733

In the past several years lightwave systems have been demonstrated at increasingly higher bit rates. An electrically-time-division-multiplexed (ETDM) system has reached 10 Gbit/s over 80 km [1], while an optical-time-division-multiplexed (OTDM) systems has been operated at 16 Gbit/s over 8 km [2]. A wavelength-division-multiplexed (WDM) system using ten 2 Gbit/s channels has spanned 68 km [3]. ETDM systems place the most severe demands on electronic and opto-electronic components, but the simplicity and economy of such systems continues to make them attractive. In addition, the ETDM system is a building block for WDM and OTDM systems.

An ETDM system is diagrammed in Figure 1. At the transmitter, after electrical multiplexing, either direct or external modulation may be used to perform the electrical-to-optical conversion. Single-frequency lasers are desired for multigigabit systems to reduce fiber dispersion penalties. However, even a single-frequency laser suffers "chirp" when modulated, broadening its spectrum. Additionally, the laser may not be able to be turned completely off (due to spectral or speed considerations) resulting in an extinction-ratio penalty at the receiver. External modulation allows an information-bandwidth-limited spectrum and good extinction ratio, but adds insertion loss and additional complexity to the system. Direct modulation has been demonstrated at 16 Gbit/s [4], while external modulation using a $TiLiNbO_3$ switch has reached 8 Gbit/s [5]. Small-signal bandwidths of ~20 GHz have been reported for both lasers and switches [6,7].

High-quality single-mode fiber has a loss of ~0.4 dB/km at 1.3-μm wavelength and ~0.25 dB/km at 1.55-μm wavelength. Conventional fiber having zero first-order dispersion at 1.3 μm has dispersion of 15-20 psec/km · nm at 1.55 μm. Dispersion-shifted (DS) fiber translates the dispersion zero to the low-loss region at 1.55 μm. Figure 2 shows transmission limits for single-mode fiber due to loss (assuming 1 mW launched power and 500 photons/bit receiver sensitivity) and dispersion. Laboratory results are included for comparison. Transmission limits can be reduced by polarization dispersion and non-linear effects such as stimulated Brillouin scattering and stimulated Raman scattering.

Benchmark values for high-speed APD receiver sensitivities now stand at ~500 photons/bit in the 1.3- to 1.55-μm wavelength region [8]. This is still 17 dB away from the quantum limit of 10 photons/bit for direct detection. Optical pre-amplifiers hold the promise of increasing receiver sensitivity in practice, although the quantum-limited value is estimated to be ~40 photons/bit [9]. Optical preamplifiers used with PIN receivers have already shown improvements over APD receivers at bit rates as high as 8 Gbit/s [10].

Adequate electronic bandwidth and gain flatness become increasingly difficult to obtain as bit rate is increased. Hybrid amplifiers utilizing GaAs FET's have exhibited 10-20 GHz bandwidths. It is likely that, with present technology, WDM and OTDM will be necessary to obtain system bit rates above 20 Gbit/s.

REFERENCES

[1] S. Fujita, et. al., postdeadline paper PD16, OFC '88, New Orleans, LA, 1988.
[2] R. S. Tucker, et. al., J. Lightwave Tech., Vol. 6, No. 11, 1737 (1988).

[3] N. A. Olsson, et. al., paper WB6, OFC '85, San Diego, CA, 1985.
[4] A. H. Gnauck and J. E. Bowers, Electron. Lett., Vol. 23, No. 15, 801 (1987).
[5] S. K. Korotky, et. al., J. Lightwave Tech., Vol. LT-5, No. 10, 1505 (1987).
[6] R. Olshansky, et. al., Electron. Lett., Vol. 23, 839 (1987).
[7] S. K. Korotky, et. al., App. Phys. Lett., Vol. 50, 1631 (1987).
[8] B. L. Kasper and J. C. Campbell, J. Lightwave Tech., Vol. LT-5, No. 10, 1351 (1987).
[9] P. S. Henry, submitted to OFC '89, Houston, TX, 1989.
[10] A. H. Gnauck, et. al., submitted to OFC '89, Houston, TX, 1989.

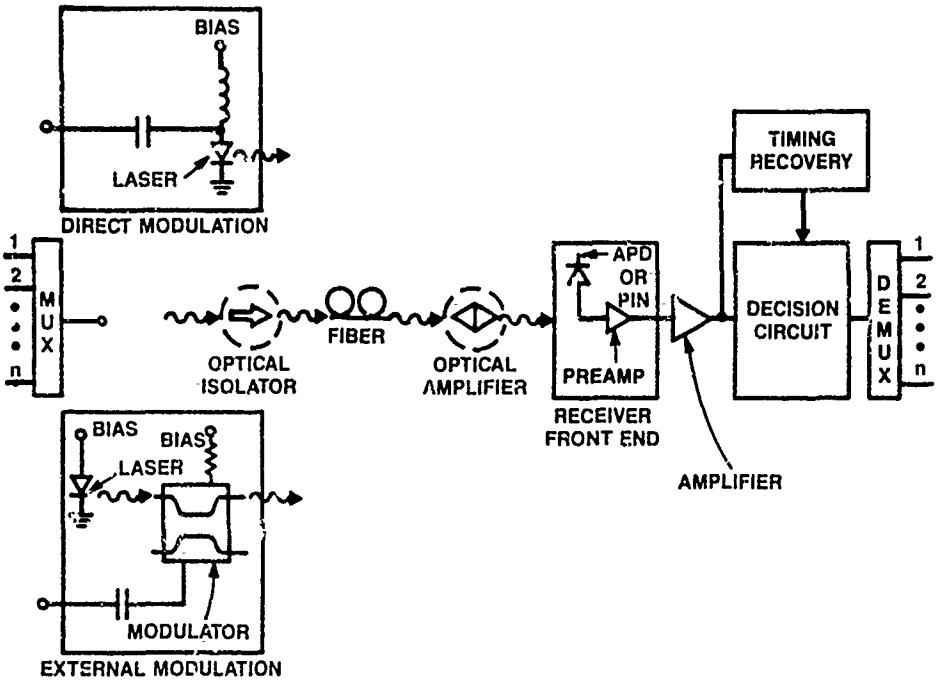

Fig. 1: An electrical time-division-multiplexed lightwave system.

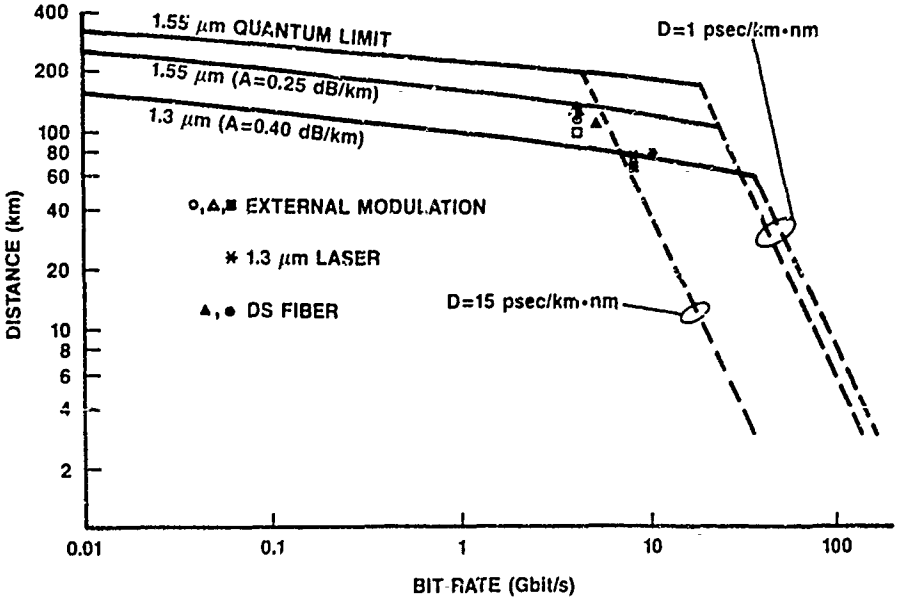

Fig. 2: Transmission limits due to loss (solid lines) and dispersion (dashed lines). Laboratory results are shown for comparison.

Picosecond Lasing Dynamics in Quantum Well Lasers and Its Dependence on the Number of Quantum Wells

Y. Arakawa, T. Sogawa, M. Tanaka, and H. Sakaki
Research Center for Advanced Science and Technology, University of Tokyo
4-6-1 Komaba, Meguro-ku, Tokyo, 153 Japan

Investigation of physics of ultra-fast phenomena in semiconductor lasers is important for high-speed modulation and short pulse generation. It has been recently demonstrated that quantum well (QW) lasers have the advantage to generate shorter light pulses, since the differential gain is ennanced by a factor of four compared to conventional double-hetero structure lasers [1]. In fact, an extremely narrow light pulse (<1.3psec) was successfully observed in a quantum well laser [2]. This is the shortest pulse so far achieved in the semiconductor lasers without external cavity. However, effects of QW structure-parameters, such as thickness and the number of QWs, on the picosecond pulse dynamics have not been discussed sufficiently. In this paper, we investigate short pulse generation in QW lasers with emphasis on dependence of pulse form on the QW structures. The results demonstrate that the pulse duration strongly depends on the QW structures: The QW laser having a smaller number of QWs generates broader light pulses, which results from in both reduced differential gain and higher quasi-Fermi-energy level of electrons E_{Fc}.

In our experiment, we prepared two GaAs/AlGaAs multi-quantum well (MQW) lasers which consist of 50Å GaAs QWs separated by 50Å AlGaAs barriers: One has 16 QWs and the other has 4 QWs, as illustrated in Figures 1 (a) (b). The short pulse generation in the QW lasers was achieved by the gain switching method at room temperature using optical pumping pulses from a dye laser (20psec, 7000Å) excited by a Nd^{+}-YAG laser. The optical pumping method makes the experiment free from the electrical RC constant problem. As shown in Figure 1, the photon energy of the dye laser pulse (1.77eV) is a little higher than $Al_{0.17}Ga_{0.83}As$ optical confinement layer (1.64eV). Since the total thickness of the optical confinement layer and the QW active layer is the same (~ 2000Å) for both lasers, the total number of carriers excited in those layers is the same. As a result, the carrier density (or E_{Fc}) in the QW laser with 4 QWs (QWL4) is much higher than the carrier density in the QW laser with 16 QWs (QWL16), because all excited carriers are relaxed into QWs.

Short pulse generation in those QW lasers were measured by a *single-shot* streak camera. Figures 2 and 3 show measured light pulses from QWL16 and QWL4, respectively. Figure 2 indicates that the estimated pulse duration is less than 2 psec, if the time-resolution of the streak camera is considered. On the other hand, the pulse form of QWL4 is much broader than that of QWL16, as shown in Figure 3. These results demonstrate that the number of QWs has strong

influence on the pulse duration. Since higher carrier density in QWL4 results in energy broadening of carrier distribution, the total relaxation time of carriers into lasing modes is longer. This leads to tailed structures in the pulse form. In addition, under those high carrier density (i.e., high E_{Fc}) condition, the differential gain is also reduced due to the gain flattening effect. Those carrier dynamics were also evidenced by the temporal measurement of spectra through a single shot streak camera with a monochromator. The observed spectra of QWL4 were much broader than that of QWL16.

[References]
[1] Y.Arakawa, T.Sogawa, M.Nishioka, M.Tanaka, and H.Sakaki, Appl. Phys. Lett. 52, 1295 (1987)
[2] T.Sogawa, Y.Arakawa, M.Tanaka, and H.Sakaki, Appl. Phys. Lett., October Issue (1988)

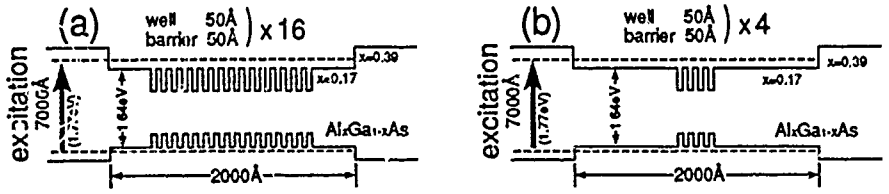

Figure 1: Band diagram for the multi-quantum well (MQW) lasers with (a)16 QWs and (b) 4 QWs

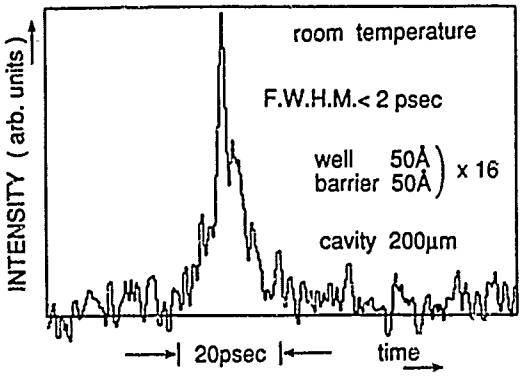

Figure 2: Measured pulse form by a single shot streak camera from the MQW laser with 16 QWs

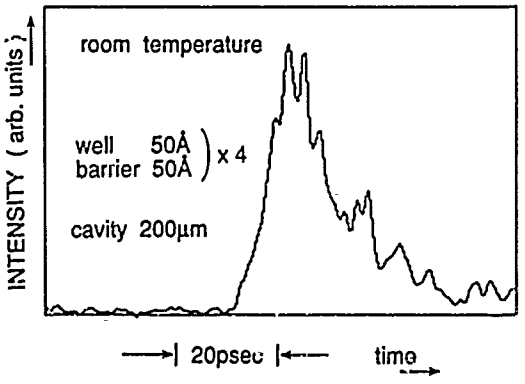

Figure 3: Measured pulse form by a single shot streak camera from the MQW laser with 4 QWs

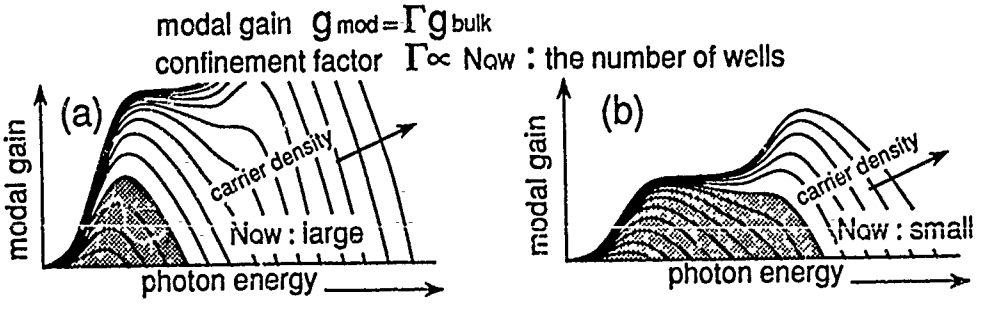

Figure 4: (a) Illustration of the modal gain profile for the MQW laser with 16 QWs; (b) the modal gain profile for the MQW lasers with 4 QWs. Since the total number of carriers excited in the active region is the same, the gain profile of the MQW lasers with 4 QWs is much broader due to the gain flattening effect.

Subpicosecond Multiple Pulse Formation in Actively Mode Locked Semiconductor Lasers

P. A. Morton, A. Mar, D.J. Derickson, S.W. Corzine and J. E. Bowers

Department of Electrical and Computer Engineering, University of California, Santa Barbara, CA 93106.

Mode locked semiconductor laser diodes provide compact sources of stable, ultra short optical pulses. Subpicosecond pulses have been obtained using passive [1,2] and active [3] mode locking with the shortest pulses to date of 0.58 ps being obtained using active mode locking [3]. Pulse widths of this order cannot be described by previous theory [4] which make the approximations of small signal current modulation and constant densities along the cavity length. We describe a new theoretical model using a traveling wave approach to include a spatial variation of electron and photon densities within the laser diode, together with a non-zero reflectivity for the anti-reflection coated facet. This model is shown to agree well with experimental observations of subpicosecond pulses, multiple pulses and pulse powers under all operating conditions, and is used to explain the operation of these devices. The theory is used to explore ways of producing even shorter pulse widths with a single output pulse.

The theoretical model uses a traveling wave approach with the following rate equations for electron density N(x,t), and forward and backward photon fluxes $S^+(x,t)$, $S^-(x,t)$:

$$\frac{\partial N}{\partial t} = \frac{J(t)}{ed} - \frac{N}{\tau_n} - g(N - N_t)(S^+ + S^-) \tag{1}$$

$$\frac{\partial S^\pm}{\partial t} \pm v_g \frac{\partial S^\pm}{\partial x} = \Gamma g (N - N_t) S^\pm - \alpha_i S^\pm + \Gamma \beta M \frac{N}{\tau_n} \tag{2}$$

where J(t) is the applied current density waveform, e the electronic charge, d the active layer thickness, τ_n the electron lifetime, g the differential gain coefficient, N_t the electron transparency density, v_g the group velocity, Γ the confinement factor, α_i the internal loss, β the spontaneous emission into each external cavity mode and M the number of external cavity modes oscillating.These rate equations are integrated numerically using finite difference approximations, with boundary conditions at the facet (x=0,L) of:

$$S^+(0,t) = R_1 S^-(0,t) \tag{3}$$

$$S^-(L,t) = AR\, S^+(L,t) + R_2 C^2 S^+(L,t-\tau_{ext}) \tag{4}$$

where R_1 and R_2 are the power reflectivities of the left and right mirrors, AR is the power reflectivity of the anti-reflection coated facet, C is the coupling loss from laser to external cavity, and τ_{ext} is the external cavity round trip time.The applied current density waveform J(t) is the most important variable, made up of a d.c. bias plus a large signal sinusoidal component. High frequency modulation and large r.f. power are essential to produce subpicosecond pulses [3].

Fig. 1 shows typical experimental autocorrelation traces for three values of r.f. current. For low r.f. values a broad pulse is seen, with a coherence spike at zero time delay. As the

r.f. level is increased, subpicosecond pulses occur, with the autocorrelation traces as in Fig. 1b. This trace represents the autocorrelation of an initial mode locked pulse, followed by pulses at the round trip time of the laser diode cavity. For further increases in r.f. power the trace in Fig. 1c is found, with extra pulses being seen.

Theoretical autocorrelation traces are shown in Fig. 2 for r.f. currents (peak to peak) of (a) 4 mA, (b) 80 mA, and (c) 160 mA. These three cases agree well with the practical observations in Fig. 1, and therefore support the choice of theoretical model. The theoretical model also provides the actual output optical waveform. In the case of Fig. 2b, this shows an initial pulse followed by pulses at the round trip time of the laser diode cavity. In Fig. 2c, a second set of pulses separated by the laser diode cavity round trip time is also seen, with the time separation of the two sets of pulses being arbitrary.

The goal of this research is to produce single mode locked pulses close to the theoretical minimum for semiconductor lasers of around 60 fs. The use of different cavity geometries and modulation schemes will be addressed practically and theoretically, as well as a hybrid approach using both active and passive mode locking techniques. In this short pulse regime, dispersion and the carrier dependent index are important. The inclusion of gain saturation terms in the theoretical analysis due to transient carrier heating [5] and spectral hole burning leads to a better simulation, and their relative importance and merits will be discussed.

References

[1] J. P. van der Ziel, J. Appl. Phys. **52**, 4435-4446 (1981).
[2] Y. Silberberg, P. W. Smith, IEEE J. Quantum Electron. **QE-22**, 759-761 (1986).
[3] S. W. Corzine et al. Appl. Phys. Lett. **52**, 348 (1988).
[4] For example, H. A. Haus, IEEE J. Quantum Electron. **QE-11**, 323-330 (1975).
[5] M. P. Kesler, E. P. Ippen, Appl. Phys. Lett. **51**, 1765 (1987)

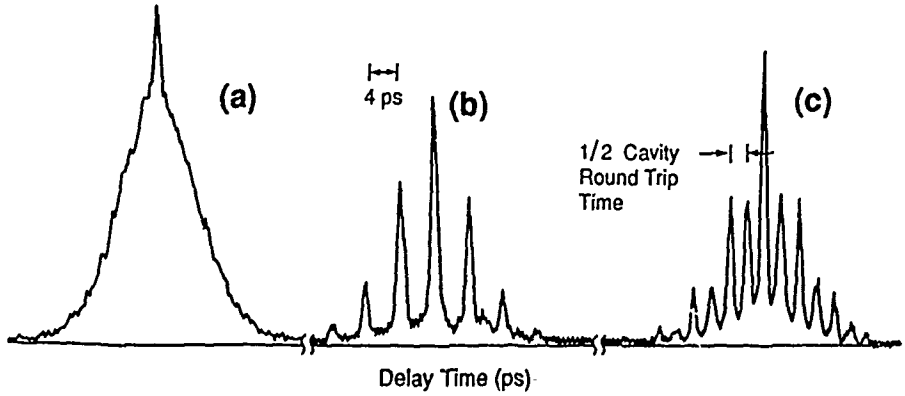

Fig. 1 Experimental autocorrelation traces for 3 values of r.f power.

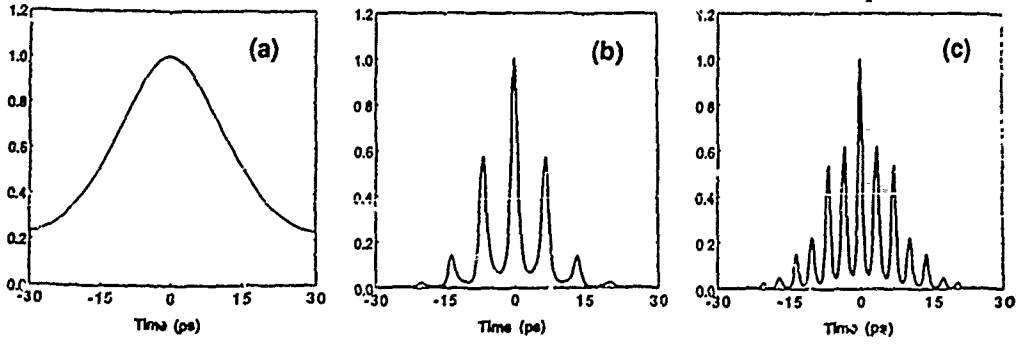

Fig. 2 Theoretical autocorrelation traces for 3 r.f. current levels.

Ultrafast All-Optical Multi/Demultiplexing Techniques for Future Optical Communications

Masatoshi SARUWATARI

NTT Transmission Systems Laboratories

Take 1-2356, Yokosuka-shi, Kanagawa 238-03, Japan

1. Introduction

All-optical switching techniques based on the third optical nonlinearities are expected to be applied to future ultrahigh-speed optical communication systems. In particular, the optical Kerr switching using transparent materials, originating from non-resonant electronic processes, are promising for such applications as optical time-division multi/demultiplexing, photonic switching, etc. , due to its ultrahigh-speed response time of less than 1ps. This could overcome the limitations on transmission capacity and switching speed set by the conventional electronic/optoelectronic devices.

In this paper we will review the principles of several all-optical switching techniques based on the Kerr effect in optical waveguides. Demonstration of time-division multi/demultiplexing of high-speed optical signals[1,2] and its prospect will be also shown.

2. Principle of Optical Kerr Effect

Any Kerr effect device utilizes an instantaneous refractive index change $\Delta n(t)$ or a phase shift $\Delta\phi(t)$ induced by an intense optical pulse given by $\Delta\phi(t) = (2\pi/\lambda)\Delta n(t)L$, where L is interaction length and $\Delta n(t) = n_2 I(t)$. I(t) is pump pulse intensity and n_2 is Kerr coefficient. The optical Kerr devices are roughly classified into two categories; one is interferometric type, the other directional coupler type. In each case, it is essential to reduce required pump power. Aside from the Kerr coefficient value n_2, waveguide structure is preferable because it can focus the transmitting light into a small area over a long distance, resulting in large I(t) and L values. When using long fibers as the Kerr medium, however, walk-off between pump and probe pulses due to chromatic and polarization dispersions must be taken into account[1]. Also, diagonal and nondiagonal components of n_2 [3] must be considered to estimate the net phase shift in each case.

3. All-Optical Switching Devices

(1) Interferometric type: Polarization switching and Mach-Zehnder (M-Z) interferometer devices belong to this category, in which transmittance is sinusoidal with respect to the phase shift. The polarization switching devices operate through the interference between orthogonal polarization components of signal pulse. When polarization directions of pump and signal pulses are set at 45 degrees, the relative phase shift in orthogonal components is introduced by the difference between diagonal and nondiagonal components of n_2 [3]. Ultrafast time division demultiplexing[1,3] and optical sampling (gating) [4,5] have been demonstrated using long fibers. On the other hand, optical M-Z devices operate essentially like electrooptic M-Z modulators. Here, optically induced phase shift is caused by either n_2 component depending on the pump polarization direction.

Some proposals and experiments have been made using various materials[6-10]. Except for fiber types[9-10], intense pump pulses are required for 100% switching due to the short interaction length.

(2) Directional coupler type: This utilizes a directional coupler having two adjacent waveguides coupled into each other. Switching operation, based on the coupling coefficient change induced by $\Delta n(t)$, is characterized by critical input power above which abrupt switching occurs[11]. Several switching experiments have been reported using dual core fibers[12-14] and GaAs waveguides[15]. To reduce the crosstalk originating from edges of the pump pulse, another intriguing approach using optical soliton pulses has recently been proposed[16].

3. Demonstration of All-Optical Multi/Demultiplexing

Time-division demultiplexing of an optical pulse train has been demonstrated using Kerr switching in two polarization-maintaining single-mode fibers spliced with each fast axis crossed[1-2]. Through this birefringence-compensation technique, an original 2-GHz 30ps pulse stream from a gain-switched DFB-LD has been completely demultiplexed into two streams[1-2] using mode-locked YAG laser as a pump. Required peak pump power has been reduced to 3W using 150m long spliced fibers. This was achieved by minimizing the walk-off between pump and probe pulses due to chromatic/polarization dispersion. The required pump power could be reduced further using GeO2-doped fibers with extremely small core-diameter as proposed in Ref.(17). The present Kerr-switching response is limited to around 100 ps mainly due to the pump pulse width or the group delay difference between pump and probe pulses. Less than 1 ps operation can be expected if much shorter control pulses are appliedon the no-group-delay difference condition.

4. Conclusion

Various all-optical switching techniques utilizing the Kerr effect have been reviewed as potential applications to high-speed optical communication systems. Although these techniques are not fully mature to be actually used, they are expected to enhance new conceptual technologies, such as all-optical signal processing, photonic switching, optical computer, and others.

Reference

(1)T.Morioka and M.Saruwatari, IEEE J. Select Area Com., 6, (1988)1186.
(2)T.Morioka, M.Saruwatari and A.Takada, Electron.Lett., 23(1987)454.
(3)T.Morioka and M.Saruwatari, Electron.Lett., 23(1987)1330.
(4)K.Kitayama et al, Appl.Phys. Lett. 46(1985)623.
(5)N.J.Halas et al, Appl.Phys. Lett. 50(1987)886.
(6)H.Kawaguchi, Opt.Lett., 10(1985)411.
(7)L.Thylen, et al, Appl. Phys. Lett., 51(1987)1304.
(8)A.Lattes et al, IEEE J. Quantum Electron., QE-19(1983)1718.
(9)M.J.LaGasse et al, IQEC'88, paper WG-4.
(10)Shirasaki et al, CLEO'87, paper ThO-1.
(11)S.M.Jensen, IEEE J.Quantum Electron., QE-18, (1982)1580.
(12)S.R.Friberg et al, Appl.Phys. Lett., 51(1987)1135.
(13)A.M.Weiner et al, ICUP'88, paper FB2, and CLEO'88, paper ThD3.
(14)Y.Silberberg, IQEC'88, paper WG-5. Y.Silberberg and B.G.Sfez, CLEO'88, paper ThW5.
(15)L.K.P.Wa et al, GaAs Elect. Lett., 21(1985)26.
(16)S.Trillo and S.Wabnitz, IQEC'88, paper WA-4.
(17)I.H.White et al, Electron.Lett., 24(1988)340.

NOTES

THURSDAY, MARCH 9, 1989

SALON G

7:00 PM–8:30 PM

ThC1–5

HIGH SPEED MEASUREMENT TECHNIQUES

G. A. Mourou, University of Michigan, *Presider*

Picosecond Pulse Generation and Sampling with GaAs Monolithic Integrated Circuits

R.A. Marsland, C.J. Madden, V. Valdivia, M.J.W. Rodwell†, D.M. Bloom
Edward L. Ginzton Laboratory, Stanford University, Stanford, Ca 94305.

Diode sampling circuits, which form the heart of most microwave network analysis and time-waveform instrumentation, are limited to ~30 GHz bandwidth primarily by slow pulse generators used for diode gating as well as circuit layout and device parasitics. We have generated 6 V amplitude shock-wave signals with as low as 1.6 ps falltime on a GaAs Nonlinear Transmission Line (NLTL) [1]. We have also fabricated a monolithic diode sampling circuit using an NLTL as the strobe pulse generator to attain a bandwidth of 130 GHz. This is a factor of 5 better than previous room-temperature electrical sampling circuits and comparable with recent Josephson-Junction sampling circuits [2] which require cryogenic cooling.

The 1.6 ps falltime signal was generated on an NLTL with graded, or hyperabrupt, doping in the diodes giving a nonlinear capacitance change that is more than twice that of uniform doped diodes. This allows for shorter length lines that have a fraction of the attenuation of uniform-doped NLTLs.

The sampling bridge is integrated with two uniform-doped NLTLs [3]. One line provides a 3.5 ps strobe pulse which turns on the diodes while the other generates a test signal to be sampled. The input to the NLTL is an 8 V peak to peak sine wave between 3 and 10 GHz. The NLTL turns the sine wave into a 2 V sawtooth wave which has a 4 ps falltime. The derivative of the sawtooth wave is applied to the sampling diodes with a novel, monolithic, differentiating balun which uses both the even and odd modes of coplanar waveguide (CPW). The sawtooth wave comes in from the left of Figure 1, while a test waveform comes from either a 50:1 attenuated NLTL output at the bottom of the figure or from a coplanar probe pad off the top of the figure. The sampled signal is output through two 1kΩ resistors.

The sampling circuit is a simple two diode bridge shown in Figure 2. The 2x5 μm diodes are in parallel with the even CPW mode which is terminated in an airbridge short circuit. The round-trip time of the even CPW mode determines the width of the strobe pulse. The Schottky diodes were fabricated on GaAs MBE material with a 0.6 μm N^- active layer ($3 \times 10^{16}/cm^3$ doping). A buried 0.8 μm N^+ active layer ($3 \times 10^{18}/cm^3$ doping) provided the diode cathode connection. Ti/Pt/Au was used for Schottky contacts and first level interconnections. 1000 Å of PECVD Si_3N_4 was used for the 500 fF MIM sample capacitors. Plated airbridges provided second level interconnections.

With the strobe NLTL driven at 5 GHz and the test signal NLTL driven at 5 GHz + 100 Hz, the test signal repeats at 100 Hz in equivalent-time. The output of the sampler measuring the 4 ps falltime of the test NLTL is shown in Figure 3. A 180 mV, 95 GHz sine wave output from a 5x multiplier on a coplanar probe [4] was also sampled, and harmonic content to 128 GHz has been measured. The sampler is within 0.5% of linearity from 0 to 0.4 V. The minimum detectible voltage is 90 $nV/\sqrt{Hz}$.

This sampling head IC, when packaged in a coplanar probe will allow on-wafer measurements in excess of 100 GHz.

---

† Now at the Department of Electrical and Computer Engineering, University of California at Santa Barbara, Santa Barbara, CA 93106.

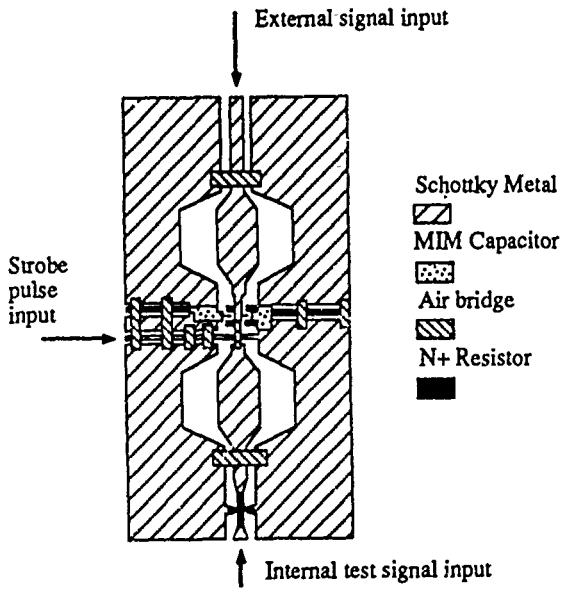

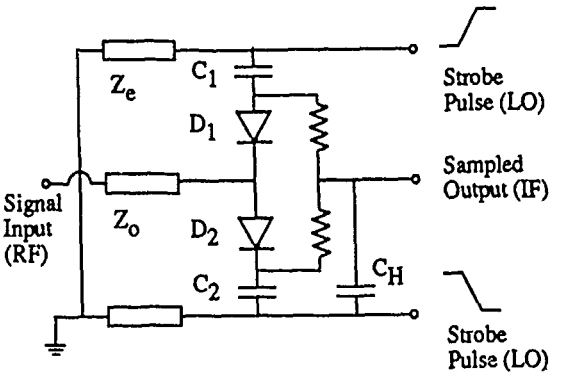

Figure 1. Sampling head layout (left).
Figure 2. Sampling head schematic diagram (above).

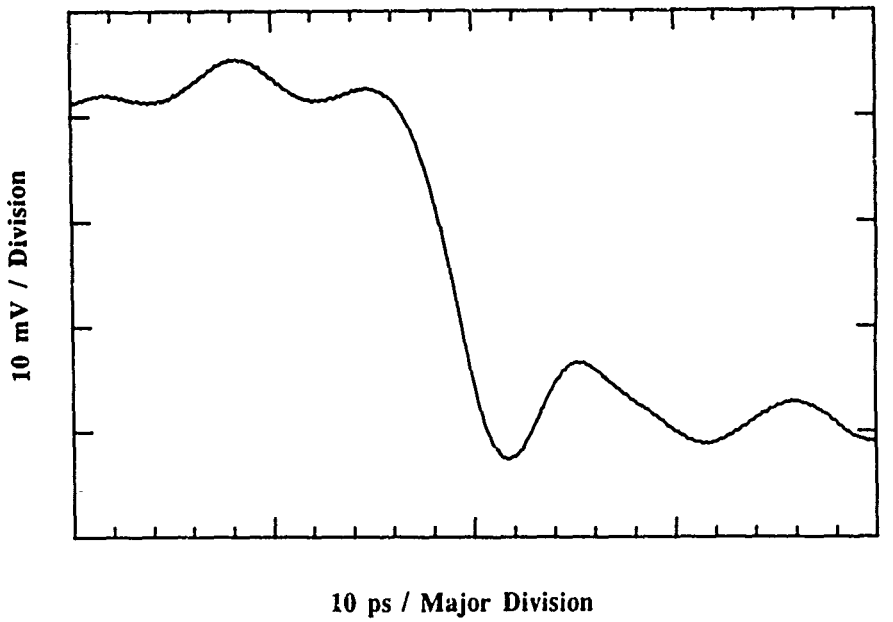

Figure 3. 4ps fall-time of the 50:1 attenuated NLTL measured with the sampling head.

[1] C.J. Madden, R.A. Marsland, M.J.W. Rodwell, D.M. Bloom, Y.C. Pao, to be published in Applied Physics Letters, **54**, No. 11 (1989)

[2] P. Wolf, in *Picosecond Optics and Optoelectronics*, edited by G.A. Mourou, D.M. Bloom, and C.-H. Lee (Springer-Verlag, Berlin, 1985), p. 236

[3] C.J. Madden, M.J.W. Rodwell, R.A. Marsland, D.M. Bloom, Y.C. Pao, IEEE Electron Device Letters, **EDL-9**, No. 6, 303 (1988).

[4] R. Majidi-Ahy, D.M. Bloom, Electronics Letters, **25**, No. 1 (1989).

This work supported by Office of Naval Research (ONR) contract N00014-85-K-0381.
R.A. Marsland acknowledges an ONR fellowship.

ULTRA-HIGH BANDWIDTH DETACHABLE OPTOELECTRONIC PROBES

M. Scheuermann, R. Sprik[1]
J-M. Halbout, P. A. Moskowitz, and M. B. Ketchen
IBM Research Division, T. J. Watson Research Center
Box 218, Yorktown Heights, NY 10598

Picosecond electrical pulses are routinely produced and detected using photoconducting switches activated by short laser pulses.[2-4] Because these switches have such high bandwidths, it is difficult to make reproducible and calibrated connections to a device under test. A probe which can repeatedly and nondestructively contact and detach from the pads of a test site is needed. In this paper the design, fabrication and characterization of such probes is discussed.

A schematic of the probe is shown in Fig. 1a. The photoconducting layer and the metalization defining transmission lines are on the bottom side of the probe. Photoconducting switches are illuminated from the top by focusing the optical pulses through the transparent silicon on sapphire substrate. Contacts from the probe to the device under test are made through gold contacts located at the end of the transmission lines. The geometry of the bottom metalization is shown in Fig. 1b. A balanced co-planer transmission line is used to carry the signals to/from the contacts to photoconducting detector/generator sites. Tapers at the end of the transmission lines are used to match the pad configuration of the device. The transmission line is approximately 2 cm long so that reflections from the far end of the lines will not interfere with the waveform being generated or detected for several hundred picoseconds. Pads at the far end of the lines are used to bias the lines and detect the sampled output.

To characterize the probe, a pulse was generated on the probe, propagated through the taper and contacts and then detected on a chip with a matching taper and transmission line. The resulting waveform shown in Fig. 2a had a FWHM of approximately 3.5 picoseconds. No significant ringing due to the contacts was observed. The probes were also tested in a dual probe configuration. A signal was launched on one probe, propagated through 1 mm of transmission line and the contacts, then 1 mm of transmission line on a wafer and finally through the contacts on a second probe, 2 mm of transmission line and sampled using side gap detection. The detected waveform shown in Fig. 2b has a FWHM of 5.7 picoseconds.

The gold contacts survive well over a hundred hits if used carefully. Care must be taken to insure both contacts hit simultaneously. Approximately two mils of horizontal skating is required to insure good electrical contact. No probe has failed due to the contacts.

The response of a GaAs photodetector was measured to demonstrate the capabilities of the probe. A reverse bias was applied across the photodetector by applying a voltage between the two transmission lines. Figure 3a-b show results obtained by varying the power of the pulses illuminating the photodetector. In both cases a rise time of approximately 10 picoseconds was observed. Increasing the power by a factor of 32 resulted in an increase of 25 in the maximun amplitude of the pulse. At higher power the falltime of the detector was nearly twice as long due to carrier saturation effects.

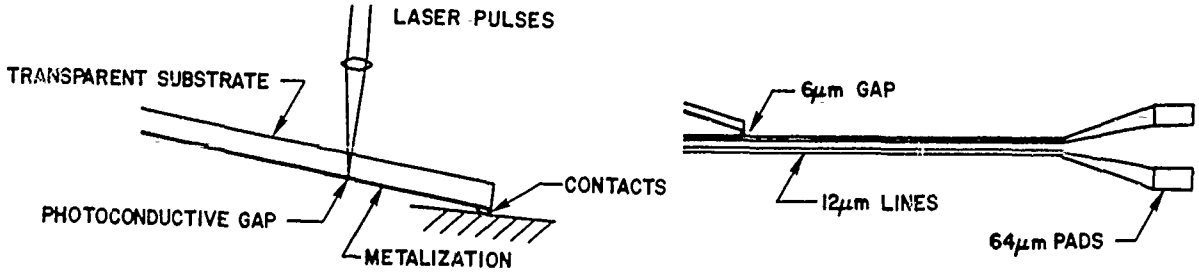

Figure 1 a) Cross-section of the probe. Optical pulses are focused thru the probe onto a photoconducting switch. The electrical pulse propagates to or from the device under test across the contacts at the end of the probe. b) Metalization on the bottom of the probe. The length of the line is 1.8 cm long. The third line is used to provide electrical contact for the side gap. Gold contacts are bonded to the end of the tapers.

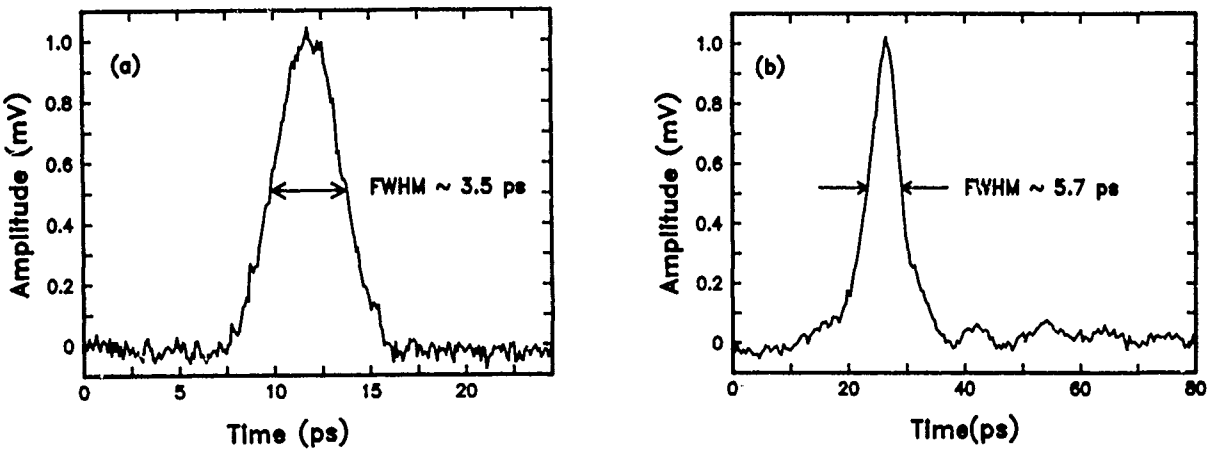

Figure 2 a) Pulse detected after propagation thru contact and 1 mm of transmission line. b) Pulse detected after propagation thru two contacts and a total of 4 mm of transmission line.

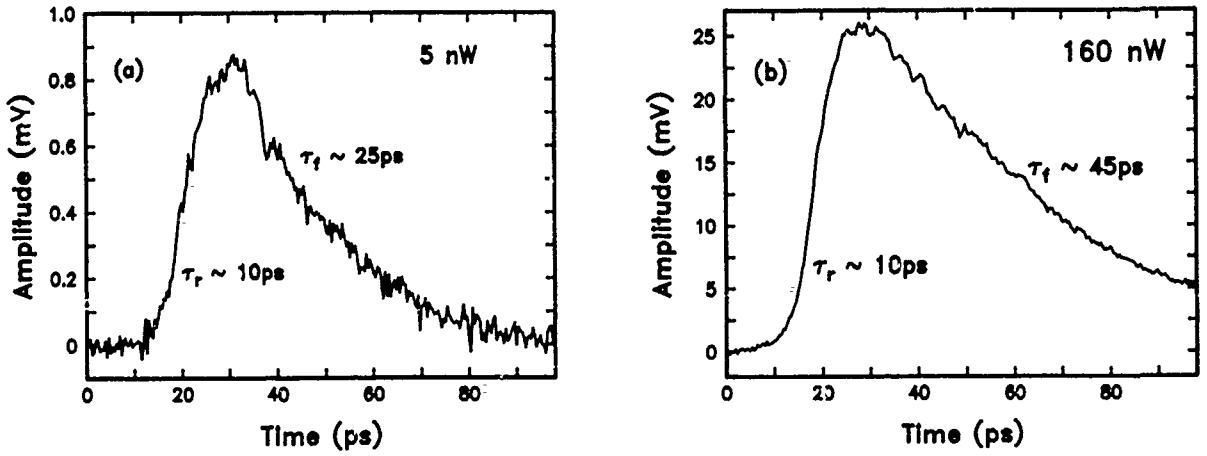

Figure 3. Power dependence of GaAs photodectors a) 5 nW, b) 160 nW.

In conclusion ultra-high speed detachable sampling probes have been fabricated and characterized. Contact to the device under test is controlled, reproducible, and nondestructive. This probe has been used to characterize high speed devices and transmission lines.

We thank R. McIntosh for help in fabrication, D. Grischkowsky for generous use of his laser facilities and D. Rogers for the GaAs photoconductors.

References

1. present address, Natuurkuudig Laboratorium, Valckenierstraat 65,1018 XE, Amsterdam Netherlands, 20-5255661.
2. D. H. Auston, in **Picosecond Optoelectronics** , edited by C. H. Lee (Academic Press, London 1984), p 73.
3. D. R. Dykar, T. Y. Hsiang and G. A. Mourou, in **Picosecond Electronics and Optoelectronics** , edited by G. A. Mourou, D. M. Bloom and C. H. Lee (Springer Verlag, 1985), p 249.
4. P. G. May, G. P. Li, J-M. Halbout, M. B. Ketchen, C. C. Chi, M. Scheuermann, I. N. Duling III, D. R. Grischkowsky and M. Smyth, **Picosecond Electrical Pulses in Microelectronics,** proceedings of the conference on **Ultrafast Phenomena,** June 1986, Snowmass Colorado.

Measurement of Gigahertz Waveforms and Propagation Delays in an InGaAs/InAlAs MODFET using Phase-Space Absorption Quenching

J. M. Wiesenfeld, M. S. Heutmaker, I. Bar-Joseph, D. S. Chemla,
J. M. Kuo, T. Y. Chang, and C. A. Burrus

AT&T Bell Laboratories
P. O. Box 400
Holmdel, N. J. 07733
(201) 888-7247

In this work we report the application of phase-space absorption quenching (PAQ) to the measurement of gigahertz frequency waveforms in an InGaAs/InAlAs modulation-doped quantum well FET (MODFET). We combine the PAQ sampling technique, which is charge-sensitive, with electro-optic sampling, which is voltage-sensitive, to study device operation.

PAQ is based on the significant modification of the absorption spectrum of a quantum well caused by introduction of free carriers. Transitions into the states occupied by the free carriers are inhibited by the Pauli exclusion principle and the absorption at the corresponding wavelengths is therefore quenched. [1,2] PAQ is thus the two-dimensional analogue of the Burstein-Moss effect. The carriers in the quantum well channel of a MODFET therefore bleach the absorption when MODFET is in logic state ON. The absorption is recovered when the channel is pinched-off. For a carrier density in the quantum well of 10^{12} cm^{-2}, the width of the quenched spectral region can be ~60 meV. An optical probe beam with a wavelength within this range can sense the difference in transmission and therefore the *charge* in the channel. Thus, temporal variation of the carrier density in the channel and therefore, the logic state of the device, can be monitored by the optical probe beam. [3]

The device studied is a depletion mode InGaAs/InAlAs MODFET made by molecular beam epitaxy on an InP substrate. [1] A schematic of the experimental arrangement for measuring gigahertz waveforms using the PAQ effect is shown in Fig. 1. Three frequency synthesizers are phase-locked together. Synthesizer #1 drives a modelocked, external cavity semiconductor laser, which produces pulses of 10 - 15 ps duration over the wavelength range from 1.52 - 1.56 μm, at repetition rate f_1. The gate of the MODFET is driven at frequency f_2 by synthesizer #2. Pulses from the laser are incident on the MODFET from the rear, and pass through the quantum well channel under the gate, reflect off the gate contact, and are reflected by a beamsplitter into a receiver. f_2 is slightly larger than f_1, so the pulse train from the laser sweeps through the current waveform at the rate $\Delta f = f_2 - f_1$. Synthesizer #3 is set to Δf and triggers the data acquisition electronics, which records changes in probe beam transmission. A measured waveform at 2 GHz is shown in Fig. 2.

The PAQ sampling of the MODFET can be combined with the technique of direct electro-optic sampling [4,5] to measure propagation delays in the FET. While PAQ sampling is sensitive to charge, electro-optic sampling is sensitive to longitudinal electric fields in the InP substrate of the MODFET and converts electric field (i.e. voltage differences) across the substrate into birefringence along the optical path of the probe beam. Thus, the voltage present at the position of the probe beam is detected as a change in state of polarization of the probe beam. The electro-optic sampling measurement is implemented using the quarter-wave plate (QWP) and analyzer shown by dashed lines in Fig. 1. Propagation delays are measured by a phase-shift technique. Signals measured by electro-optic sampling at the gate and drain pads and by PAQ sampling under the gate electrode are detected using a lockin amplifier, tuned to Δf, for the data acquisition electronics. The phase of the signals measured under the gate electrode and under the drain pad are shown as a function of operating frequency, f_2, in Fig. 3. The propagation delays, relative to input at the gate pad, are determined by the slopes of the data in Fig. 3; i.e. $\Delta t = \Delta\phi/360f_2$, where $\Delta\phi$ is the measured phase shift in degrees.

For the data of Fig. 3, the delay for appearance of the PAQ signal is 14±4 ps and the propagation delay to the drain electrode is 21±6 ps. Because the PAQ signal is sensitive to carriers, the 14 ps delay in its appearance is due to the dynamics of the carriers in charging the gate channel. The combination of PAQ and electro-optic sampling, as demonstrated by the data above, will be a powerful method to study detailed properties of high-speed MODFETs.

REFERENCES

1. I. Bar-Joseph, J. M. Kuo, C. Klingshern, G. Livescu, T. Y. Chang, D. A. B. Miller, and D. S. Chemla, Phys. Rev. Lett., **59**, 1357 (1987).
2. D. S. Chemla, I. Bar-Joseph, J. M. Kuo, T. Y. Chang, C. Klingshern, G. Livescu, and D. A. B. Miller, IEEE J. Quantum Electron., **QE-24**, 1664 (1988).
3. D. S. Chemla, I. Bar-Joseph, C. Klingshern, D. A. B. Miller, J. M. Kuo, and T. Y. Chang, Appl. Phys. Lett., **50**, 585 (1987).
4. B. H. Kolner and D. M. Bloom, IEEE J. Quantum Electron., **QE-22**, 79 (1986).
5. J. M. Wiesenfeld, R. S. Tucker, A. Antreasyan, C. A. Burrus, A. J. Taylor, V. D. Mattera, and P. A. Garbinski, Appl. Phys. Lett., **50**, 1310 (1987).

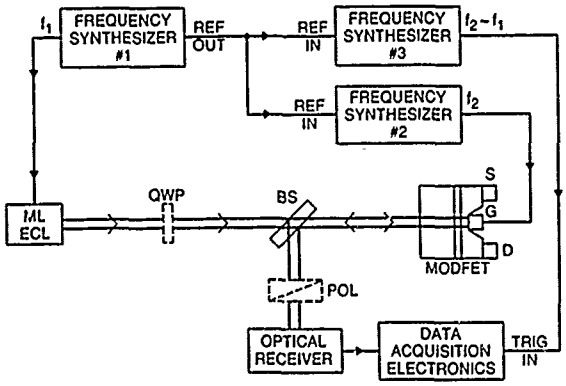

Figure 1: Experimental schematic. ML ECL = modelocked external cavity semiconductor laser.

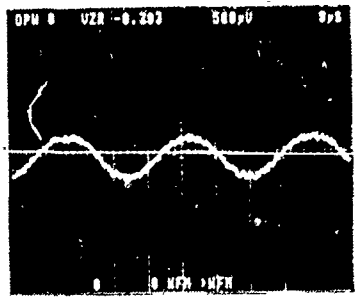

Figure 2: Waveform measured by PAQ sampling. Horizontal axis is 137 ps/division.

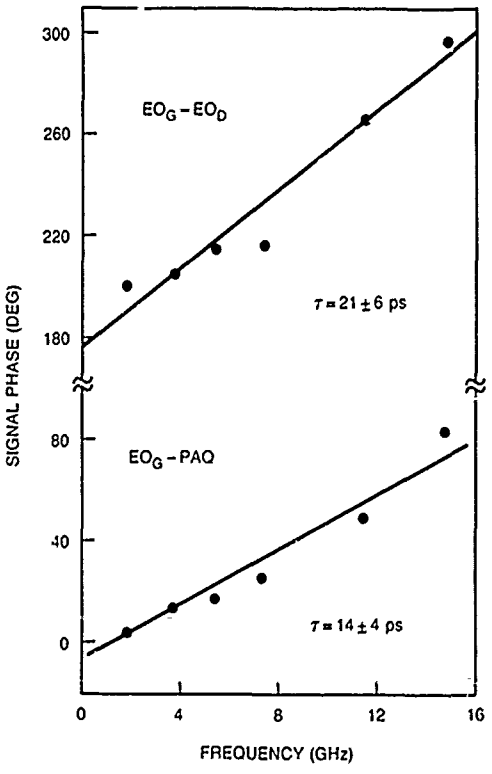

Figure 3: Phase shift as a function of frequency, f_2. EO_G, PAQ, and EO_D are signals measured under the gate pad, gate channel, and drain pad, respectively.

120 GHz Active Wafer Probes for Picosecond Device Measurement

R. Majidi-Ahy, D.M. Bloom
Edward L. Ginzton Laboratory, Stanford University
Stanford, CA 94305.

On-wafer frequency domain measurements of high speed devices are presently limited to 40 GHz. Accurate characterization and understanding of millimeter-wave devices however, requires their measurements at higher frequencies. We have developed active wafer probes for 80-120 GHz measurements of ultrafast devices. An active probe frequency-multiplier [1] generates the stimulus signal and supplies it to the device under test. An active probe harmonic mixer detects the output signal from the device under test. Both probes have coplanar waveguide tips which contact the device pads on wafer. The probes are interfaced with external instrumentation via their coaxial connectors.

The circuits were fabricated on 5 mil thick alumina substrates, with Ti-Au metallization and 1 micron Au plating. Beam-lead GaAs anti-parallel Schottky diode pairs were used as the nonlinear elements in both circuits.

The frequency-multiplier circuit consists of an input low-pass filter and matching network, an anti-parallel diode pair in shunt, and an output bandpass filter and matching network. A 16-25 GHz input signal is multiplied by five to 80-120 GHz by this circuit. The input filtering and matching is performed by a direct-coupled coplanar waveguide circuit. Output filtering and matching is implemented by a coupled-line coplanar waveguide circuit. The quintupler bandwidth, shown in Figure 1, was from 80 to 125 GHz, with a maximum output power of -11 dBm. The average conversion loss was 38 dB. The time-waveform of a 95 GHz signal generated by the active probe frequency multiplier, and measured by a recently reported electrical sampler [2] is shown in Figure 2.

The harmonic mixer circuit consists of a diplexer, a LO/IF low-pass filter and matching network, an anti-parallel diode pair in series, and an RF high-pass filter and matching network. A 4-6 GHz LO signal drives the nonlinear element, where its 20th harmonic is mixed with the 80-120 GHz RF signal to obtain a down-converted 20 MHz IF signal. The input and output filtering and matching were implemented by direct-coupled coplanar waveguide circuits. The harmonic mixer bandwidth, shown in Figure 1, was from 80 to 120 GHz with an average conversion loss of 48 dB.

The active probes were used in conjunction with an HP 8510 network analyzer, to measure frequency response of a 20 dB coplanar waveguide attenuator. The calibration was performed by using the frequency response of the active probes, shown in Figure 3, via a 50 ohm coplanar waveguide as the reference. The measured insertion loss of the 20 dB attenuator is also shown in Figure 3.

Integration of the quintupler, harmonic mixers and directional devices into one active probe, will allow on-wafer S-parameter measurements of ultrafast devices to 120 GHz.

[1] R. Majidi-Ahy, D.M. Bloom, submitted to IEE Electronic Letters for publication.

[2] R.A. Marsland, V. Valdivia, C.J. Madden, M.J.W. Rodwell, D.M. Bloom, unpublished.

[3] R. Matreci, Hewlett-Packard Journal, November 1986, pp 22-26.

This work was supported by Air Force Office of Scientific Research (AFOSR) contract F49620-85K-0016. R. Majidi-Ahy acknowledges a Rockwell/Stanford CIS Fellowship.

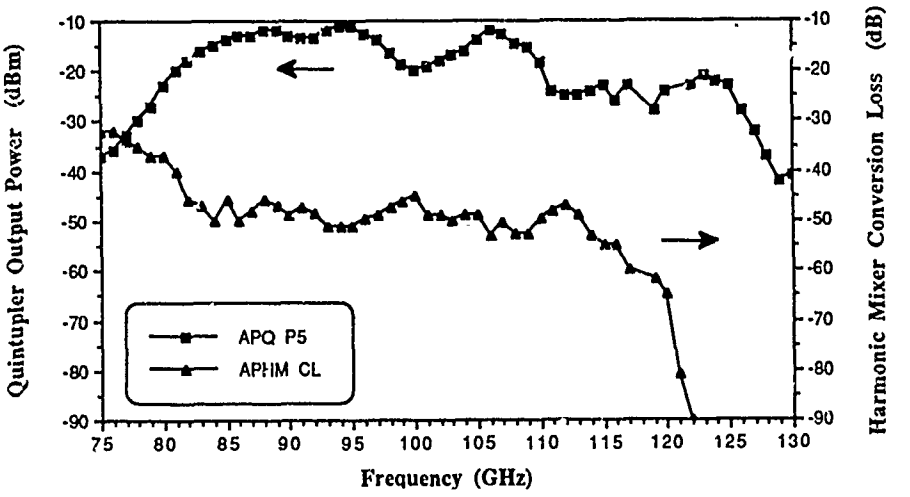

Figure 1: Output Power of the quintupler and conversion loss of the harmonic mixer active probes.

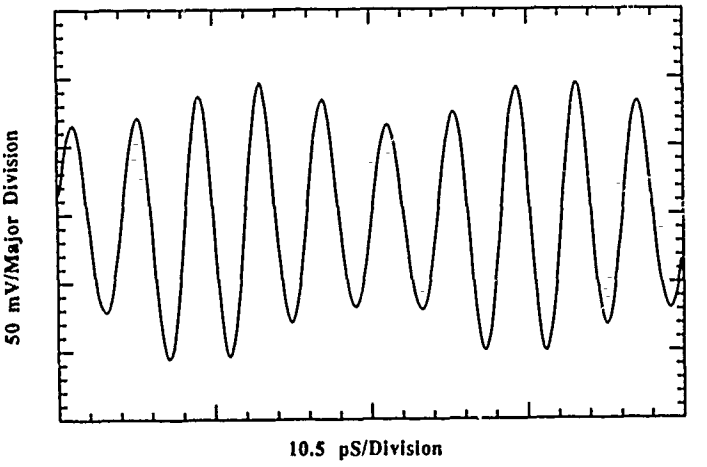

Figure 2: Time-waveform of the quintupler's 95 GHz output signal.

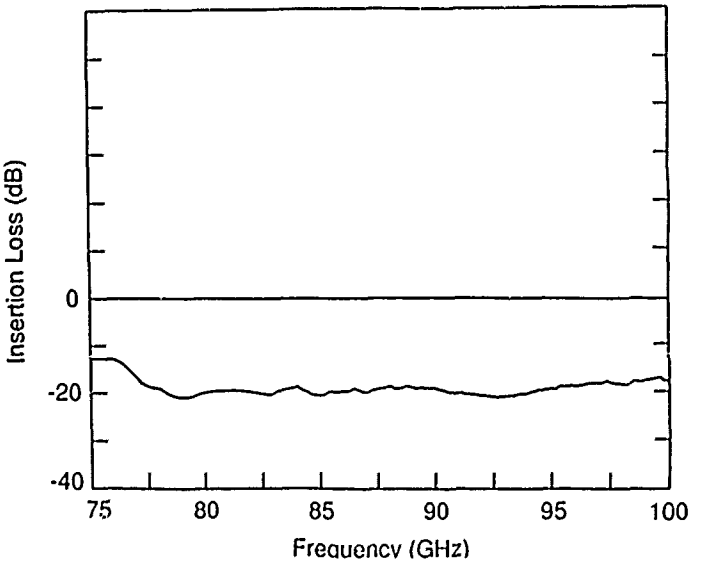

Figure 3: Measured insertion loss of a 20 dB attenuator by the acitve probes.

Femtosecond Excitonic Electroabsorption Sampling

W.H. Knox, J.E. Henry, B. Tell, K.D. Li,
D.A.B. Miller and D.S. Chemla

AT&T Bell Laboratories
Holmdel, NJ 07733

Optoelectronic sampling based on the Pockels' effect[1] has become an important technique for the measurement of electrical signals with the highest time resolution, currently at 300 fs. We present first results obtained using a new technique for femtosecond electrical pulse measurement: excitonic electroabsorption sampling (EES). We have previously shown that excitons exhibit a femtosecond electroabsorption response, however the device which was used did not facilitate propagation studies over macroscopic distances[2]. In our new embodiment, a coplanar stripline is fabricated on a GaAs multiple quantum well mesa ridge structure (Fig. 1). We thus obtain optical modulation by parallel-field electroabsorption, which is due to lifetime broadening by field ionization of the excitons[3]. The detection sensitivity is about 1%/volt in a 10 micron structure. We etch the GaAs substrate down to a 1 micron AlGaAs stop-etch layer in a 1x2 mm area and leave the stripline free-standing on the 1 micron thick film, thus obtaining an extremely low dispersion structure to test the EES concept. We use an infrared dye laser which produces femtosecond pulses at a wavelength of 805 nm[4] at 82 MHZ repetition rate. The exciton energy is temperature-tuned to the laser with a Peletier device, in this case operating at about 5 degrees above ambient temperature. At 300 fs pulsewidth the laser spectrum is already comparable to the exciton linewidth, and we expect that shorter pulses will provide reduced sensitivity relative to the DC response. We expect that time resolution of 100 fs or less may be possible with this technique. We note that electroabsorption is a purely electronic phenomenon, with no ionic lattice contribution such as that of $LiTaO_3$.

Figure 2 shows the first results, obtained with a generated signal of a few hundred mV at 40 v bias. The signal is detected after about 1 mm of propagation by passing a weak probe beam through the stripline. The pump beam is chopped at a frequency of 1 kHz and the transmitted probe beam is detected with a lock-in amplifier. The 10-90% risetime is 500 fs, which appears to be limited by the 300 fs laser pulsewidth. This signal, accumulated over ten consecutive forward-backward scans appears to show a feature which may be due to a reflection from a small gap in the line at about 2 ps time delay. Further studies of dispersion in this thin film structure and results at higher time resolution are in progress.

.....

[1] J.A. Valdmanis, G.Mourou and C.W. Gabel, IEEE JQE QE-19, 664 (1983).
[2] W.H. Knox, D.A.B. Miller, T.C. Damen, D.S. Chemla, C.V. Shank and A.C. Gossard, Appl. Phys. Lett. 48, 864 (1986).
[3] D.A.B. Miller, D.S. Chemla, T.C. Damen, A.C. Gossard, W. Wiegmann, T.H. Wood and C.A. Burrus, Phys. Rev. B32, 1043 (1985).
[4] W.H. Knox, JOSA B4, 1771 (1987).

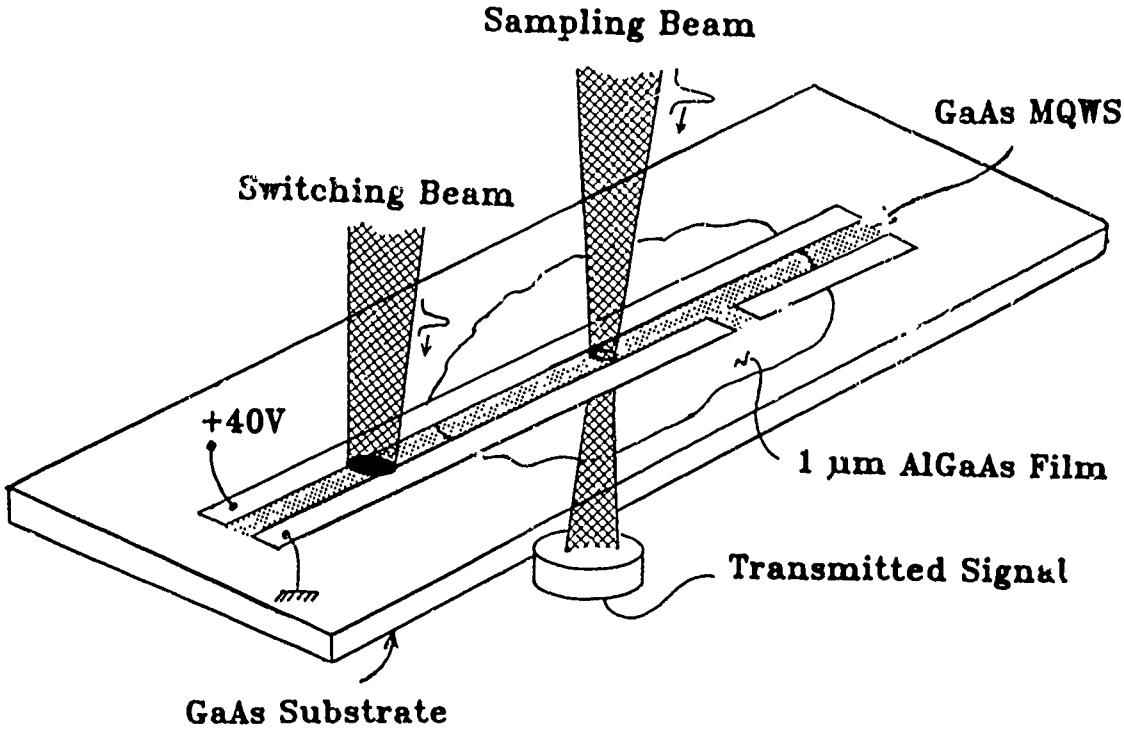

Figure 1. Sample structure showing generation and probing beams.

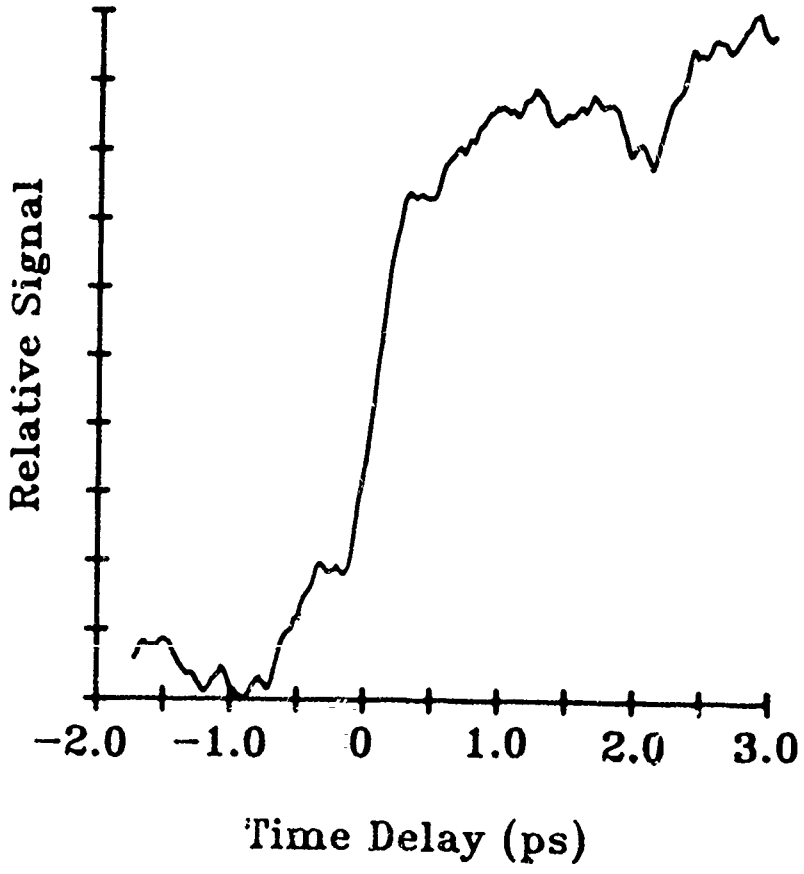

Figure 2. Signal detected after about 1 mm propagation shows 500 fs risetime.

NOTES

FRIDAY, MARCH 10, 1989

SALON G

8:30 AM–10:00 AM

FA1–4

TRANSISTORS AND TRANSPORT

P. Asbeck, Rockwell International Science Center,
Presider

GaAs MESFET and HBT Technology in Picosecond Electronics

Kazuyoshi Asai and Tadao Ishibashi

NTT LSI Laboratories
3-1, Morinosato Wakamiya, Atsugi-Shi,
Kanagawa Pref., 243-01 Japan

Ultra-high speed signal processing with a bit rate of over 10 Gb/s will be soon available in GaAs MESFET and HBT integrated circuits. Propagation delay times of inverters have been reduced to below 10 ps/gate, and maximum toggle frequencies of flip-flop circuits have exceeded 20 GHz. Wide-band amplifiers with a band width of about 10 GHz have also been obtained. This paper reviews recent progress in the high-speed performance of these devices.

Improvement in cutoff frequency is necessary for faster transistor circuit switching speed. The short channel effect is a problem in ion-implanted MESFET. To a scale down the FET structure (Fig. 1(a)) suppressing the short channel effect, a thin and highly doped active channel layer is essential. A new WSiN metal cap annealing technique can enhance carrier concentration to suppress GaAs surface degradation due to As out-diffusion[1]. A 96 GHz cutoff frequency has been achieved for 0.2 μm gate MESFET. Low power characteristics of a 0.3 μm gate DCFL ring oscillator have been reported, namely a t_{pd} of 6.7 ps/gate with 16 mW/gate power consumption (Fig. 2). The 0.3 μm gate MESFET has a 60 GHz cutoff and exhibits 31.4 GHz toggling by a 1/4 static frequency divider with an LSCFL circuit, as shown in Fig. 3. The dissipated power is as low as 150 mW/T-FF. Application to DC wide-band amplifiers demonstrates up to 10.1 GHz range with 19.8 dB gain.

AlGaAs/GaAs HBT design and fabrication technique have made rapid progress in the last few years[2]. Graded base and near-ballistic collection structures (Fig. 1(b)) have successfully increased the cutoff frequency to about 100 GHz. A t_{pd} value of 1.9 ps/gate with a power consumption of 44 mW/gate has been observed in an ECL ring oscillator (Fig. 2). A maximum toggle frequency of 22.15 GHz has been reported for a 1/4 static frequency divider. HBT is very suitable for wide-band amplifiers because of it's high open-loop gain. Two-stage differential amplifiers yielded gains of 20 dB and 11 dB with bandwidths of 9 GHz and 15 GHz.

These two devices' fundamental features and characteristics are listed in Table 1. The merits of MESFET are simple process, low power and low noise and those for HBT are high speed and high gain. Taking these merits into account, high frequency applications will expand from 10 to 20 Gb/s signal processing, for example, wide band amplifiers, MUX/DMUX, LD drivers and decision circuits, for optical links and fiber communications.

REFFERENCES:
(1)M.Tokumitsu et al, 46th Device Research Conference, VA-2 (1988)
(2)T.Ishibashi et al, 45th Device Research Conference, IVA-6 (1987)

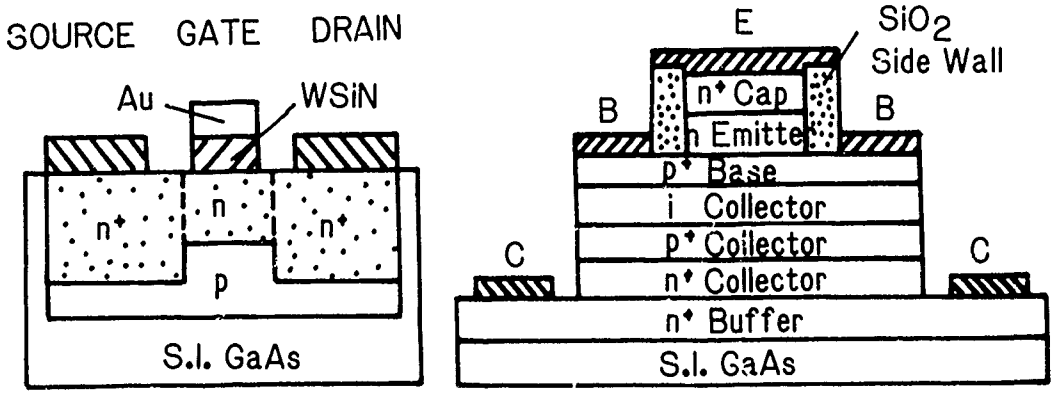

Fig. 1. MESFET (a) and HBT (b) basic structures.

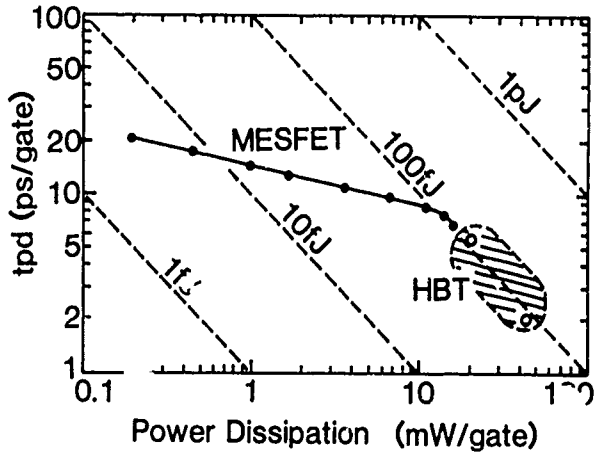

Fig. 2. Ring oscillator comparison.

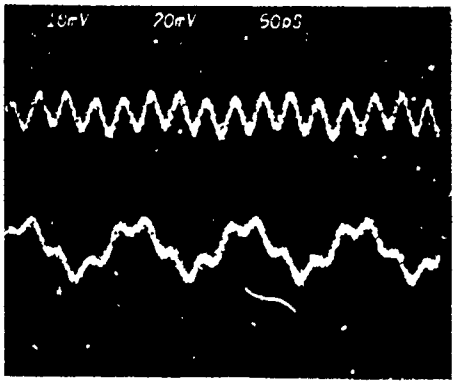

Fig. 3. Waveform of 31.4 GHz MESFET static frequency devider.

Device		MESFET	HBT
Technology		ion implantation n^+ self-align WSiN metal cap anneal buried p-layer	MBE base electrode self-align non-alloy emitter cap graded base near ballistic collector
Size		0.2 μm gate	2 μm x 5 μm emitter
Performance	gm	630 mS/mm	
	f_T	96 GHz	105 GHz
	f_{max}	100 GHz	80 GHz

Table 1. Device features and characteristics.

High Speed Heterostructure Bipolar Transistors

R.N. Nottenburg, Y.K. Chen, A.F.J. Levi, M.B. Panish, R.A. Hamm and D.A. Humphrey

AT&T Bell Laboratories, 600 Mountain Avenue, Murray Hill New Jersey 07974

ABSTRACT

Heterostructure bipolar transistors (HBT's) have attracted considerable attention because of ultra high speed digital and microwave applications. Due to a relatively mature technology AlGaAs/GaAs has been used most extensively for realizing HBT's, and impressive results have been obtained [1,2]. However, interest in InP based HBT's has increased because of the intrinsically superior transport properties of InGaAs and compatibility with long-wavelength 1.3-1.55μm photonic devices. InP/InGaAs transistors can be scaled to very small lateral dimensions while maintaining high current gain [3], and microwave results show that both the AlInAs/InGaAs and InP/InGaAs devices are promising for ultra-high speed applications [4,5]. Molecular beam epitaxy permits doping beyond the solubility limit and reduction in transistor vertical dimensions to a few hundred angstroms. Experimental results highlighting the importance of non-equilibrium electron transport will be presented. This paper will review the field and discuss scaling of typical III-V semiconductor heterostructure bipolar transistors .

References

[1] P.M. Asbeck, M.F. Chang, K.-C. Wang, D.L. Miller, G.J. Sullivan, N.H. Sheng, E. Sovero and J.A. Higgins, IEEE Trans. Electron Devices, vol. ED-34, pp.2571-2585, 1987.

[2] T. Ishibashi, Y. Yamauchi, O. Nakajima, K. Nagata, and H. Ito, IEEE Electron Device Lett., vol. EDL-8, pp.194-196, 1987

[3] R.N. Nottenburg, Y.K. Chen, M.B. Panish, R. Hamm, and D.A. Humphrey, IEEE Electron Dev. Lett., vol. EDL-9, pp.524-526, 1988

[4] H. Fukano, Y. Kawamura, and Y. Takanashi, IEEE Electron Dev Lett., vol. EDL-9, pp.312-314, 1988

[5] R.N. Nottenburg, Y.K. Chen, M.B. Panish, D.A. Humphrey, and R. Hamm, IEEE Electron Device Lett., vol. 10, pp.30-32, 1989

Electron-Hole Effects on the Velocity Overshoot in Photoconductive Switches

R. Joshi, S. Chamoun and R. O. Grondin

Center for Solid State Electronics Research

Arizona State University, Tempe, AZ 85287-6206.

It has recently been demonstrated that ultrafast photoconductive transients can be obtained by using subpicosecond laser pulses and the electrical waveforms measured by elaborate electro-optic sampling techniques [1-3] with subpicosecond resolution. In the above experiments, the optical intensity of the laser pulses has tended to be relatively high. Given the high density plasma that is actually created, it is natural to expect strong carrier-carrier effects which need to be appropriately included in any theoretical treatment of the transient transport. We shall, therefore, examine this aspect using a Monte Carlo simulation and show that its inclusion yields a more pronounced velocity overshoot than predicted previously [4,5].

A second important feature seen in the photoconductive experiments is the bias dependent delay in the initial rise of the velocity following short wavelength excitations. Such delays are associated with the intervalley transfer mechanism and is dominated by the negative velocity electrons left behind in the gamma valley. The physical mechanism is similar to the one noted in certain Gunn diode transients and would not show up in large bandgap materials like AlGaAs.

The computations for the ultrafast dynamics were performed by using the Ensemble Monte Carlo approach. The initial optical generation of carriers included the heavy hole, the light hole and the split-off bands allowing for an anisotropic distribution of the electron momentum in the gamma valley. Carrier degeneracy was suitably included through a rejection technique [6]. Electron-hole, electron-phonon and hole-phonon interactions were used based on a time dependent static screening model. A rejection scheme, originally proposed by Brunetti et al. [7] was used to adjust for the time varying carrier scattering rates.

The results for the transient velocity at 300 K are shown in Fig. 1. The curve at the higher excitation density shows a much greater overshoot. The electron-hole interaction reduces the final steady state velocity because of the two following reasons. First, the excitation energy is above the intervalley transfer threshold leading to a substantial build up of the L valley population. Owing to the higher L valley density of states and the smaller mismatch between the L valley and hole effective masses, a greater exchange of energy and momentum is made possible. Secondly, the value of the electric field is sufficiently high to maintain a substantial difference between the velocities of the L valley electrons and the holes. The electron-hole effects would be reduced at either smaller electric fields or for lower energy excitations. The electron-hole effect would remain dominant at lower temperatures despite the hot phonon effects. Finally, the initial delay seen in the rise time of these curves is a Jones-Rees type effect which has been discussed elsewhere [8].

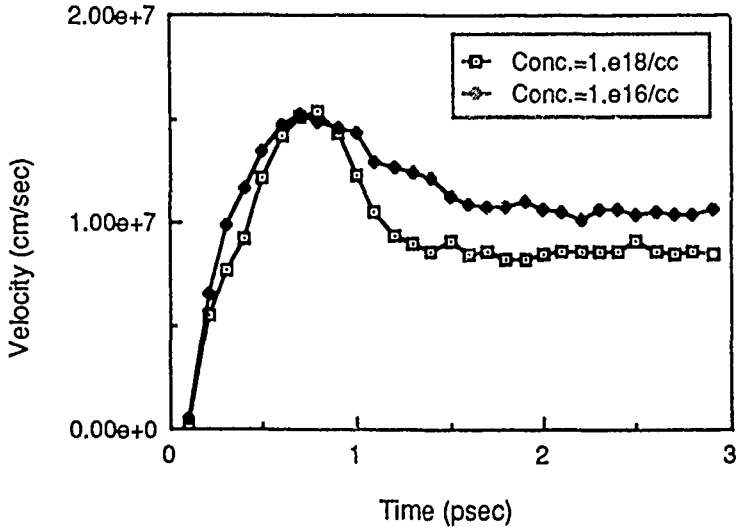

Fig. 1. The transient electron velocities for GaAs at 300K for carrier concentrations of 1E16 and 1E18 /cc. The simulations were for an applied field of 10 KV/cm, laser energy of 2eV and a pulse width of 20fs FWHM.

---

1. D. H. Auston, IEEE J. Quantum Electron. 19, 639 (1983).
2. J. A. Valdmanis, G. A. Mourou, and C. W. Gabel, IEEE J. Quantum Electron. QE-19, 664 (1983).
3. G. A. Mourou, K, Meyer, J. Whitaker, M. Pessot, R. Grondin, and C. Caruso in Picosecond Electronics and Optoelectronics II, Springer Series in Electronics and Photonics 24, 40 (1987).
4. M. Osman and H. Grubin, Solid State Elec. 31, 471 (1988).
5. A. Evan Iverson, G. M. Wysin, D. L. Smith, and Antonio Redondo, Appl. Phys. Lett. 52, 2148 (1988).
6. P. Lugli and D. K. Ferry, IEEE Trans. Elec. Devices ED-32, 431 (1985).
7. R. Brunetti, C. Jacoboni, A. Matulionis, and V. Dienys, Physica 134B, 369 (1985).
8. R. O. Grondin and M. J. Kann, Solid State Elec. 31, 567 (1988).

The Role of Electron-Electron Scattering on the Ultrafast Relaxation of Hot Photoexcited Carriers in GaAs*

M.-J. Kann and D. K. Ferry
Center for Solid State Electronics Research
Arizona State University, Tempe, AZ 85287-6206

The advances in ultrashort laser pulse techniques have led to the generation of laser pulses as short as 6 fs, which have made it possible to experimentally measure the polarization dephasing rate [1], and the initial exponential decay time constant for carriers in the excitation volume (in phase space) in semiconductors [1-5]. As the dimensions of electronic devices reach the submicron region, the energy and momentum losses due to carrier-carrier interactions play a crucial role in device performance [6].

Investigations of hot photoexcited carrier relaxation in semiconductors have shown that a quasi-equilibrium energy distribution is developed in less than 1 ps. However, the initial stages of carrier relaxation occurs through an interplay of both carrier-carrier and carrier-phonon scattering, so that the understanding of the initial rapid cooling observed experimentally requires the knowledge of how this thermalization is established on the femtosecond time scale. For this purpose, careful ensemble Monte Carlo (EMC) calculations are required.

It is known that these EMC calculations are appropriate techniques for studying the transient femtosecond dynamics. We have shown previously that, in the absence of carrier-carrier scattering, the decay of electrons from the initial excitation volume in phase space occurs no faster than about 75-80 fs [7]. Experiments in which faster decay rates are observed must entail another process, such as carrier-carrier scattering. However, most analytical approaches with carrier-carrier scattering do not fully incorporate the energy scattering inherent in this process, and are complicated by approximations to detailed time-dependent screening. In this paper, we utilize a novel molecular dynamics (MD) approach to calculate the inter-carrier Coulomb forces [8] directly. In these calculations, each particle (2000 are used here) interacts simultaneously with all other particles in the ensemble through a real space Coulomb potential. The details of the structure of the process is similar to that reported previously for Si [8], in which two basic boxes are used in real space. One box is of a size determined by the number of particles and the simulated electron density, while the second is a moving box centered on each particle and in which the MD forces are evaluated. This latter box ensures that we evaluate the net force by summing through the shortest set of equivalent particles in the Ewald sum [9]. By utilizing the MD approach, we thus can treat the inter-carrier potentials exactly and avoid any assumptions on the dielectric function which is used in the screening process.

In the studies reported here, we report initial results treating just the dynamics of the electrons at 300 K. In Fig. 1, we show the population of electrons in the central

valley that remain in the initial excitation volume after being excited from the heavy hole band. The scattering out of this initial optically excited state is basically dominated by a single exponential decay at short times (we use a 20 fs excitation pulse). In Fig. 2, this single exponential time determined from such curves is plotted as a function of the density of excited electrons. The values shown in this latter figure agree well with those inferred from the dephasing experiments of Becker *et al.* [1] and also give good agreement with the values cited by Tang *et al.* [3] for the various time constants. This time is almost totally dominated by the electron-electron scattering process as suggested by the former authors. Only at the lower values of electron density does the decay rate slow sufficiently that the intervalley scattering process becomes a significant part of the total rate.

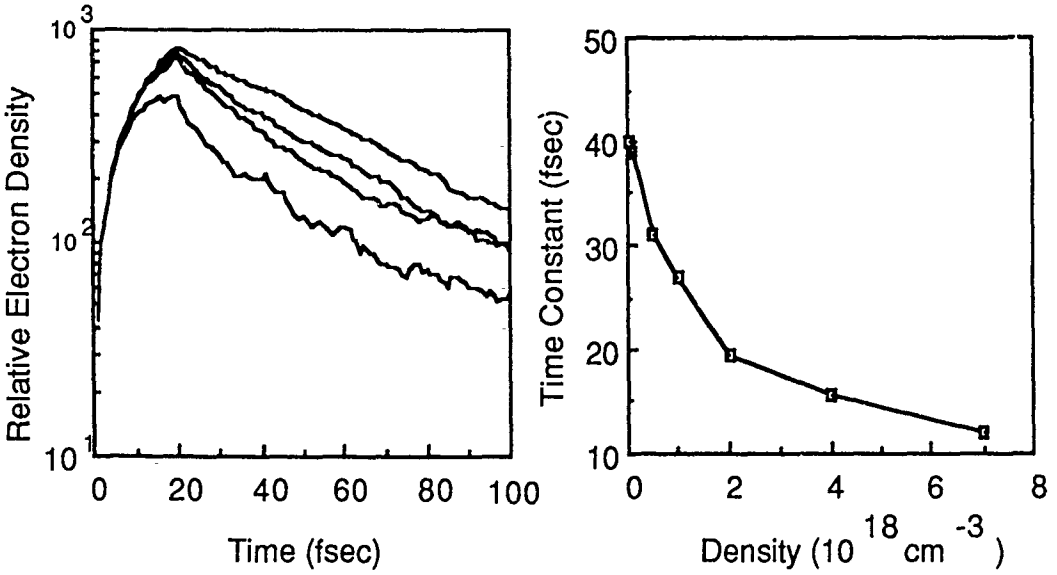

Fig. 1 (Left) The increase and decrease of population in the excitation volume in phase space for 0.05, 0.5, 1.0, 7.0x10^{18} cm^{-3} (decreasing in the figure). **Fig. 2** (Right) Values of the decay times for a single exponential fit to the curves of Fig. 1.

* This work supported by the Office of Naval Research

1. P. Becker, H. Fragnito, C. Brito Cruz, R. Fork, J. Cunningham, J. Henry, and C. Shank, Phys. Rev. Letters **61**, 1647 (1988).
2. M. J. Rosker, F. W. Wise, and C. L. Tang, Appl. Phys. Letters **49**, 1726 (1986).
3. F. W. Wise, I. A. Walmsley, and C. L. Tang, Appl. Phys. Letters **51**, 605 (1987).
4. R. W. Schoenlein, W. Z. Lin, E. P. Ippen, and J. G. Fujimoto, Appl. Phys. Letters **51**, 1441 (1987).
5. W. Z. Lin, J. G. Fujimoto, E. P. Ippen, and R. A. Logan, Appl. Phys. Letters **51**, 161 (1987).
6. M. A. Osman and D. K. Ferry, Phys. Rev. B **36**, 6018 (1987).
7. D. K. Ferry, R. P. Joshi, and M. J. Kann, Proc. SPIE **942**, 2 (1988).
8. P. Lugli and D. K. Ferry, Phys. Rev. Letters **56**, 1295 (1986).
9. D. J. Adams and G. S. Dubey, J. Comp. Phys. **72**, 156 (1987).

NOTES

FRIDAY, MARCH 10, 1989

SALON G

10:30 AM–12:00 M

FB1–5

PHOTOCONDUCTIVE SWITCHES AND APPLICATIONS

D. H. Auston, AT&T Bell Laboratories, *Presider*

FB1-1

Picosecond GaAs-based Photoconductive Optoelectronic Detectors

F. W. Smith*, S. Gupta†, H. Q. Le*, M. Frankel†, V. Diadiuk*,
M. A. Hollis*, D. R. Dykaar†, G. A. Mourou†, T. Y. Hsiang†, and A. R. Calawa*

*Lincoln Laboratory, Massachusetts Institute of Technology
Lexington, Massachusetts 02173

†Laboratory for Laser Energetics, University of Rochester
Rochester, New York 14623

High-speed photoconductive optoelectronic detectors have been the subject of intense research for the past decade owing to their use as picosecond optoelectronic switches and sampling gates, high-speed detectors for fiber-optic communication and optical-computing systems, and signal-processing devices.[1] Picosecond photoconductive detectors based on InP, amorphous silicon and silicon-on-sapphire (SOS) have been reported.[1] Many of these devices, however, suffer from serious limitations, such as instability over time, poor sensitivity, and the inability to easily integrate the switch with high-speed GaAs-based devices and circuits. We report here the development of a GaAs-based high-speed photoconductive detector that overcomes these limitations. The measured speed of the current device is approximately 1.6 ps (full width at half-maximum, FWHM) and the response is of the order of a volt using a bias of 10 V and an 80-fs laser pulse of 90-pJ energy. The material appears to be stable for indefinite periods of time and can be easily integrated with GaAs discrete devices and circuits. In fact, the material that is used for this device also offers substantial performance improvements for GaAs devices and circuits.[2]

The photoconductive detector is fabricated on a layer deposited by molecular beam epitaxy (MBE) using Ga and As_4 beam fluxes at a substrate temperature of 200°C. These films of low-temperature (LT) GaAs have both electrical and optical properties that are markedly different from GaAs grown at the conventional growth temperature of 580°C.[2] Although the LT GaAs is crystalline, as demonstrated by x-ray diffraction measurements and high resolution transmission electron miscroscopy, it has a resistivity that is substantially greater than that of semi-insulating GaAs ($\rho_{LT\ GaAs} > 10^7\ \Omega$-cm).[3] The abnormally high resistivity has so far precluded measurements of carrier mobility. Further, the LT GaAs exhibits virtually no photoluminescence.[2] The properties of LT GaAs appear to be associated with a deviation from stoichiometry to highly arsenic-rich conditions (~ 1 at.%).[2]

The picosecond speed of a LT-GaAs photoconductive-gap switch was measured using the technique of electro-optic sampling.[4] A schematic cross section of the LT-GaAs sample and a schematic top view of the switch used in this study are shown in Fig. 1 (a) and (b), respectively. The electrodes are indium metal and a 10-V square-wave signal at 3.7 MHz was applied across the input side of the transmission line. A probe beam consisting of ~ 80-fs laser pulses at a 100-MHz repitition rate with a wavelength of 620 nm and an average power of ~ 9 mW (90 pJ/pulse) was focused onto the 20-μm gap. The electrical pulse generated by this optical pulse was sampled at two points, labeled as A and B in Fig. 1(b), on the output side of the transmission line using a second 80-fs time-delayed optical pulse. The results are shown in Fig. 2. The FWHM of the pulse at both points is approximately 1.6 ps, corresponding to a 3-dB bandwidth of 220 GHz. The measured maximum voltage of the impulse is ~ 0.4 V, for a laser pulse energy of 90 pJ. The 1.6-ps result is comparable with the highest speeds ever reported for a photoconductive switch and the measured sensitivity is over an order of magnitude greater than that which we have measured for switches based on damaged materials or oxygen-implanted SOS.

By optimizing this device, it may be possible to achieve even greater speeds and/or sensitivity. Since LT GaAs is compatible with GaAs device and IC technologies, this photoconductive switch could find extensive use in high-speed-device and circuit testing.

The Lincoln Laboratory portion of this work was supported in part by the Department of the Air Force. The Laboratory for Laser Energetics is supported in part by the United States Air Force Office of Scientific Research under contract to the Ultrafast Science Center, and by the National Science Foundation. Additional

support was provided by the sponsors of the Laser Fusion Feasibility Project at the Laboratory for Laser Energetics: Empire State Electric Corporation, New York State Energy Research and Development Authority, Ontario Hydro, and the University of Rochester.

REFERENCES

[1]D. H. Auston, in *Picosecond Optoelectronic Devices*, edited by C. H. Lee (Academic, Orlando, 1984), pp. 73-117.
[2]F. W. Smith, C. L. Chen, G. W. Turner, M. C. Finn, L. J. Mahoney, M. J. Manfra, and A. R. Calawa, to be presented at the IEEE International Electron Devices Meeting, San Francisco, CA, Dec. 11-14, 1988.
[3]M. Kaminska, Z. Liliental-Weber, E. R. Weber, T. George, J. B. Kortright, F. W. Smith, B-Y. Tsaur, and A. R. Calawa (unpublished).
[4]J. A. Valdmanis and G. Mourou, IEEE J. Quantum Electron. QE-22, 69 (1986).

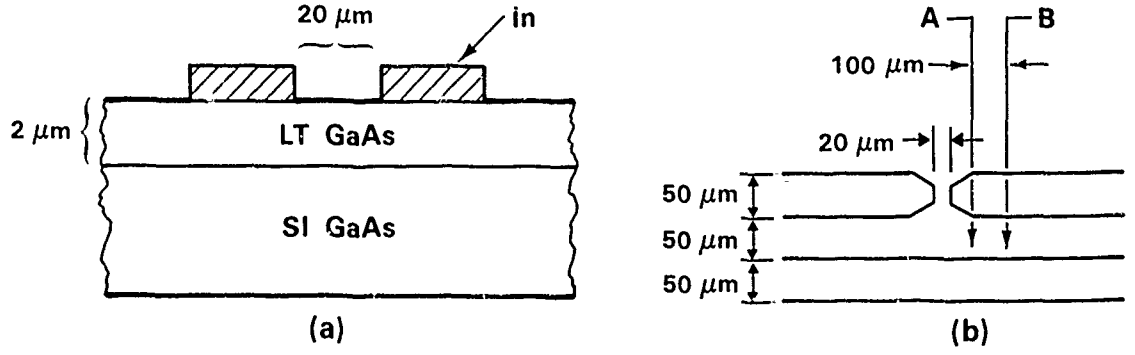

Fig. 1. LT GaAs photoconductive-gap switch used for the electro-optic sampling measurement: (a) schematic cross section, and (b) schematic top view. Also shown in (b) are two points on the transmission line labeled as A and B. The electrical impulse is sampled by the probe beam at both points.

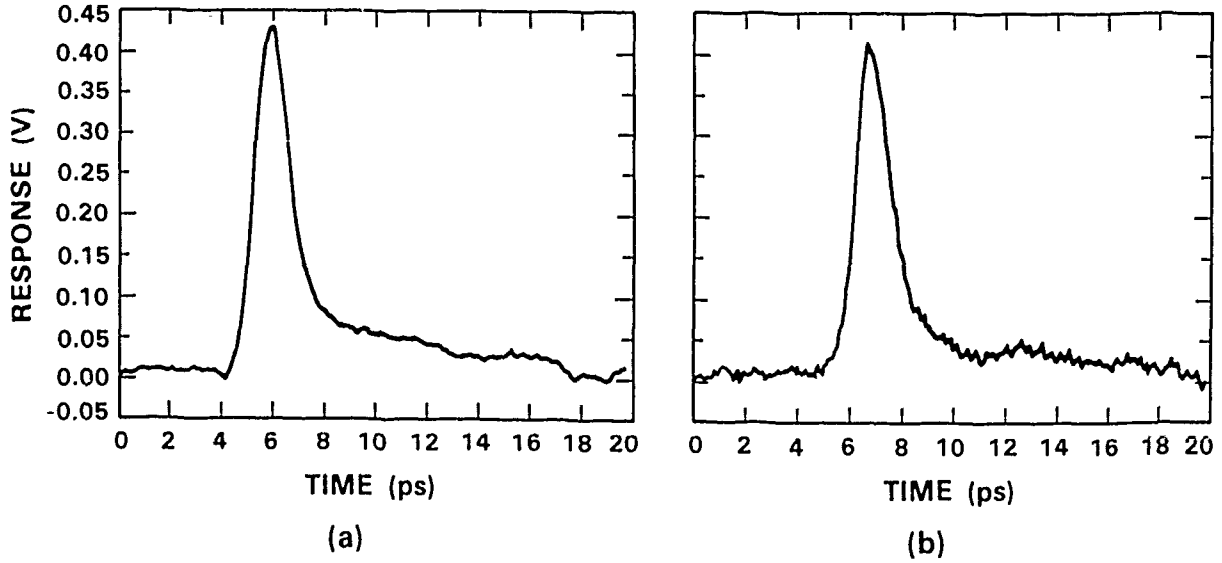

Fig. 2. Electrical impulse generated by a 70-fs laser pulse as measured by electro-optic sampling: (a) measured at point A [see Fig. 1(a)], and (b) measured at point B [see Fig. 1(a)].

MOBILITY AND LIFETIME MEASUREMENTS ON PECVD AND TYPE IIa DIAMOND *

D. R. Kania and O. L. Landen
M. S. 473
P. O. Box 5508
Lawrence Livermore National Laboratory
Livermore, CA 94550

L. Pan and P. Pianetta
Stanford University
Stanford Synchrotron Radiation Laboratory
Bin 99, P. O. Box 4349
Stanford, CA 94309

K. V. Ravi
Crystallume, Inc.
125 Constitution Dr.
Menlo Park, CA 94025

Insulating diamond has many exciting properties that make it a very attractive electronic material. Diamond has a large resistivity and thermal conductivity, high dielectric breakdown strength, and large carrier mobilities. These and other properties of diamond show great promise for applications in high speed and high power devices.[1] We have fabricated photoconductive devices from natural type IIa and CVD diamond films. With these devices the carrier mobility and lifetimes were measured using picosecond UV laser light excitation.

The thin film diamond samples were produced using plasma enhanced chemical vapor deposition (PECVD) on silicon. The films were one micron thick and scanning electron micrographs show the films are polycrystaline with a crystalite size of one micron. Stimulated Raman scattering measurements have demonstrated that sp^3 or diamond bonds dominate the films. Photoconductors were fabricated on these films and the silicon substrate was etched away from the back of the active region. This prevented free charge carriers produced in the silicon

[1] P. Das and D. K. Ferry, Sol. State Elec., **19**, 851.

*This work was performed under the auspices of the U.S. Department of Energy by the Lawrence Livermore National Laboratory under contract No. W-7405-ENG-48.

from contributing to the measured photoresponse. The natural diamonds were 1 x 1 x 1 mm cubes of material. Ohmic contacts were applied to the samples and they were mounted in 50 Ohm transmission lines.

UV photons are required for intrinsic excitation of diamond which has a band gap of 5.5 eV. Two different lasers were used to generate short pulses of UV photons by frequency upconversion in beta-$BaBO_4$. Fifty picosecond pulses of 213 nm (5.82 eV) radiation were generated by mixing the second and third harmonic of a Nd:YAG laser in beta-$BaBO_4$. These pulses contained up to 2 mJ of energy. The second method involved frequency tripling the output of a sync-pumped dye laser. This technique produced 2 ps pulses of 6.2 eV radiation with 2 μJ per pulse.

The output pulses of the photodetectors was recorded on a high speed oscilloscope. From this data, the carrier lifetime and mobility could be measured. The carrier lifetime in the natural samples varied form 100 to 500 ps and the mobilities varied from 2000 to 3000 cm^2/V-s. This variability is attributed to uncontrolled differences in the natural samples where the lifetime is controlled by impurity trapping. The thin film samples had a lifetime of 500 ps and a mobility of 0.4 cm^2/V-s. These samples are very pure, therefore, we do not expect that the lifetime is determined by impurities. The low mobility can be explained by the polycrystaline structure of film. If we assume that the carrier mobility in a crystalite is comparable to the natural samples, 1000 cm^2/V-s, and that all of the carriers trap out on the crystalite boundaries which have a characteristic dimension of 1 μm, the measured mobility would be signiticantly less than that of the crystalite material and the lifetime would be determined by the carrier transit time across a crystalite. A simple calculation using this model is consistent with our measured lifetime and mobility for the thin film sample.

In conclusion, we have measured the photoconductive response of natural and PECVD produced thin film diamond. impurities determine the response of the natural samples and the polycrystaline structure of the thin films controls the characteristics of the thin films.

Picosecond Optoelectronic Integrated Antennas for Broadband Dielectric Measurements

Y. Pastol, G. Arjavalingam, J.-M. Halbout, and G.V. Kopcsay

IBM Research Division, T.J. Watson Research Center
P. O. Box 218, Yorktown Heights, NY 10598

High speed electronic devices now operate in the 10-100 GHz region. For accurate design and modelling of such devices, a detailed knowledge of the dielectric properties of the materials used to fabricate them is required. Unfortunately, little information is yet available on these materials with wide frequency coverage because most dielectric measurements are carried out at discrete frequencies where sources and related hardware (e.g. waveguides) are available. Moreover, traditional waveguide methods have some fundamental limitations which are difficult to overcome at millimeter waves, especially in the case of low loss samples. We present a coherent microwave transient spectroscopy (COMITS) technique which, in a single experiment, permits the measurement of the complex dielectric constants of materials over a wide frequency range. COMITS is performed using the picosecond transient radiation from optoelectronically pulsed broadband integrated antennas. The apparatus consists of one transmitting and one receiving antenna, with the sample to be characterized located between them.

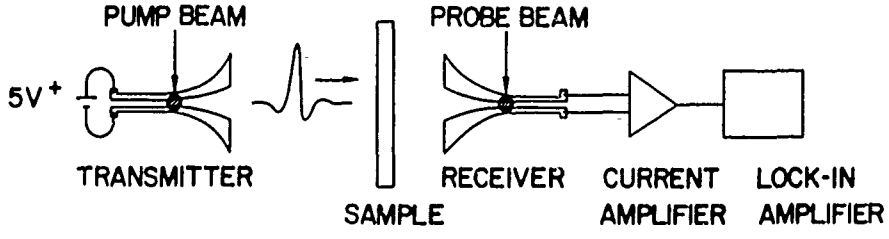

Figure 1. Schematic of the COMITS experimental setup.

The antennas consist of exponentially tapered coplanar transmission lines fabricated on silicon on sapphire substrates by lithographic techniques. The full characterization of their radiation properties has been presented elsewhere [1,2]. A standard picosecond optical pump-probe arrangement is used to excite the transmitter and to photoconductively sample the received signal (see Fig.1). A typical received waveform, recorded with no sample between the two antennas, is shown in Fig.2 along with its amplitude spectrum. The spectroscopy apparatus was first characterized using microwave filters of well-known and predictable behavior. Among others, a Fabry-Pérot interferometer, built with two titanium coated glass slides, was used as a sample. The transmission function (amplitude and phase) for a Fabry-Pérot interferometer with the two metallized faces 4 mm apart is shown in Fig.3. The maxima in the amplitude spectrum, and the corresponding variations in the phase follow the expected behavior for the electric field transmission function. The dielectric properties of several materials were also investigated. The results of these measurements will be presented. For instance, we measured the microwave refractive index of fused silica to be 1.94 $\pm$1% from 10 to 125 GHz. This is consistent with earlier data. The experimental set-up is particularly useful for measuring the dielectric properties of low loss materials, many of which are of interest for the fabrication of high-speed circuits. We also investigated the use of lenses to collimate the radiation diverging from the transmitter and to refocus it onto the receiver. This increases the signal to noise ratio while permitting transmission over substantially longer distances. Results of these experiments will also be presented.

REFERENCES

1. A.P. De Fonzo and C. Lutz, Appl. Phys. Lett. 51, 212 (1987).
2. Y. Pastol, G. Arjavalingam, J.-M. Halbout and G.V. Kopcsay, to be published in Electronics Letters.

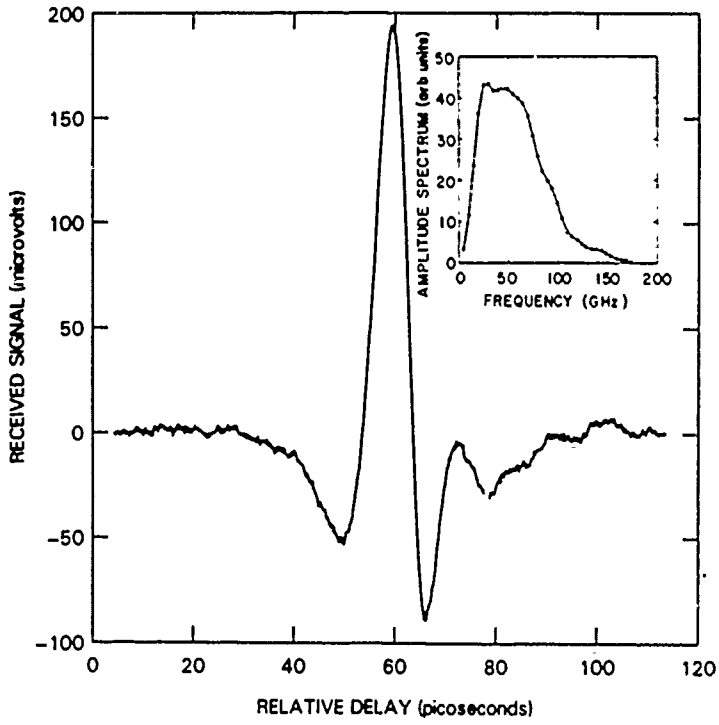

Figure 2.

Received waveform with no sample between the transmitter and the receiver. The corresponding amplitude spectrum is shown in inset.

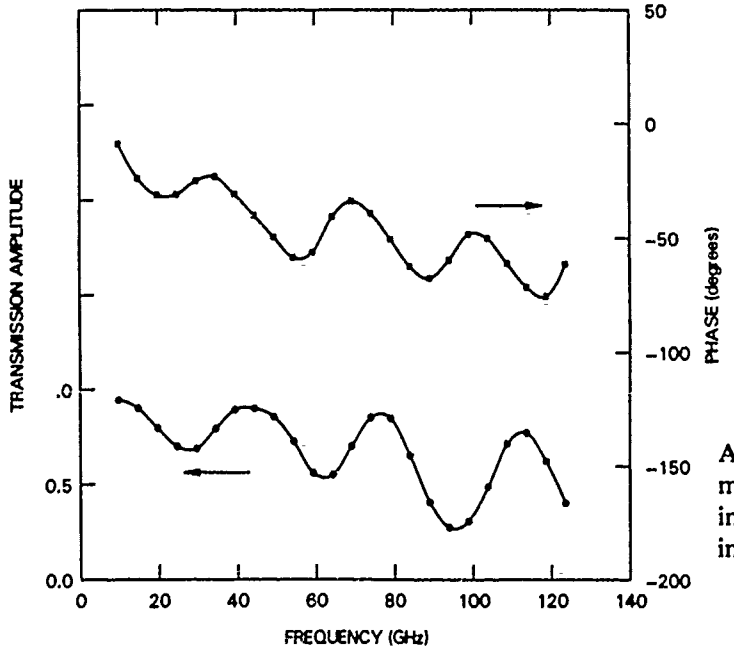

Figure 3.

Amplitude and phase of the transmission function of a Fabry-Pérot interferometer with the two reflecting surfaces 4 mm apart.

Beams of teraHz Electromagnetic Pulses

Ch. Fattinger and D. Grischkowsky

IBM Watson Research Center, P.O. Box 218, Yorktown Heights, NY 10598

In this paper we report the application of a new optical technique (1) to the generation of diffraction limited teraHz beams with a relatively large source size, by locating an ultrafast dipole source at the focal point of a collimating lens. This technique allowed us to produce, for the first time, diffraction limited beams of single cycle 0.5 teraHz pulses from a 5 mm diameter coherent source (with time dependence much faster than the transit time across the source). Because of their relatively low divergence the single-cycle pulses were easily measured after a propagation distance of 100 cm.

For the teraHz radiation source, the 20 micron sized subpsec electric dipoles were created by photoconductive shorting a charged coplanar transmission line with 70 fsec pulses from a colliding-pulse, mode-locked dye laser. The transmission line consisted of two parallel 5 micron wide, 1 micron thick aluminum lines separated from each other by 15 microns. The line was fabricated on an undoped silicon-on-sapphire wafer, which was heavily implanted to ensure the required short carrier lifetime. The teraHz radiation detector was a photoconductive gap of 5 microns spacing with a width of 25 microns fabricated on a separate SOS chip. During operation the gap is biased by the incoming teraHz radiation pulse polarized across the gap. One side of the gap is grounded, and a current amplifier is connected across the gap. The measurement was made by shorting the gap via the 70 fsec ultrashort optical pulses in the detection beam and measuring the collected charge (current) vs the time delay between the excitation and detection pulses.

The teraHz optics illustrated in Fig.1a consisted of two 9.5 mm dia, crystalline sapphire, spherical lenses contacted to the backside (sapphire side) of the SOS chips. For the radiation source the Hertzian dipole was located at the focus of the lens, while for the detector the photoconductive gap was at the focus. Because of the relatively high dielectric constant of sapphire (approximately 10), most of the radiation emitted from the transient electric dipole is contained in a 40 degree full angle cone normal to the surface of the SOS chip and directed into the sapphire. This situation gives exceptionally good collection and collimation of the teraHz radiation; the central portion of the spherical lens captures essentially all of the emitted radiation. After collimation we obtained a 5 mm diameter beam with diffraction limited divergence.

Figures 1b and 1c display the detected teraHz radiation pulses after propagation distances in air of 10 cm and 100 cm, respectively. As can be seen, the signal strength dropped by about 20 times as the propagation distance was increased from 10 cm to 100 cm, indicating a full angle beam divergence of about 100 mrad. This is an average value with respect to the frequency content of the pulse, because the diffraction angle and the divergence are proportional to the wavelength. Both, these high signal-to-noise measurements of the freely propagating pulses were made in single 2 minute scans of the relative time delay between the excitation and detection pulses. With the exception of the initial dip in the ob-

served pulseshape, the measured time dependence roughly approximates the time derivative of the transient dipole source. The main component of the signal is seen to be independent of propagation distance for distances greater than 10 cm, corresponding to the far-field of the 5 mm dia source. However, the oscillations on the trailing edge (dne to absorption by water vapor) increased with propagation distance.

The amplitude spectrum of the pulse of Fig. 1b peaks at approximately 0.4 THz and extends from low frequencies up to above 1 THz. Consequently, these beams are immediately useful for transmission spectroscopy, where by Fourier analysis of the input and transmitted pulses the absorption and disperison of the investigated materials can be obtained. Finally, the wide bandwith of these beams shows their enormous capacity as a potential communication channel.

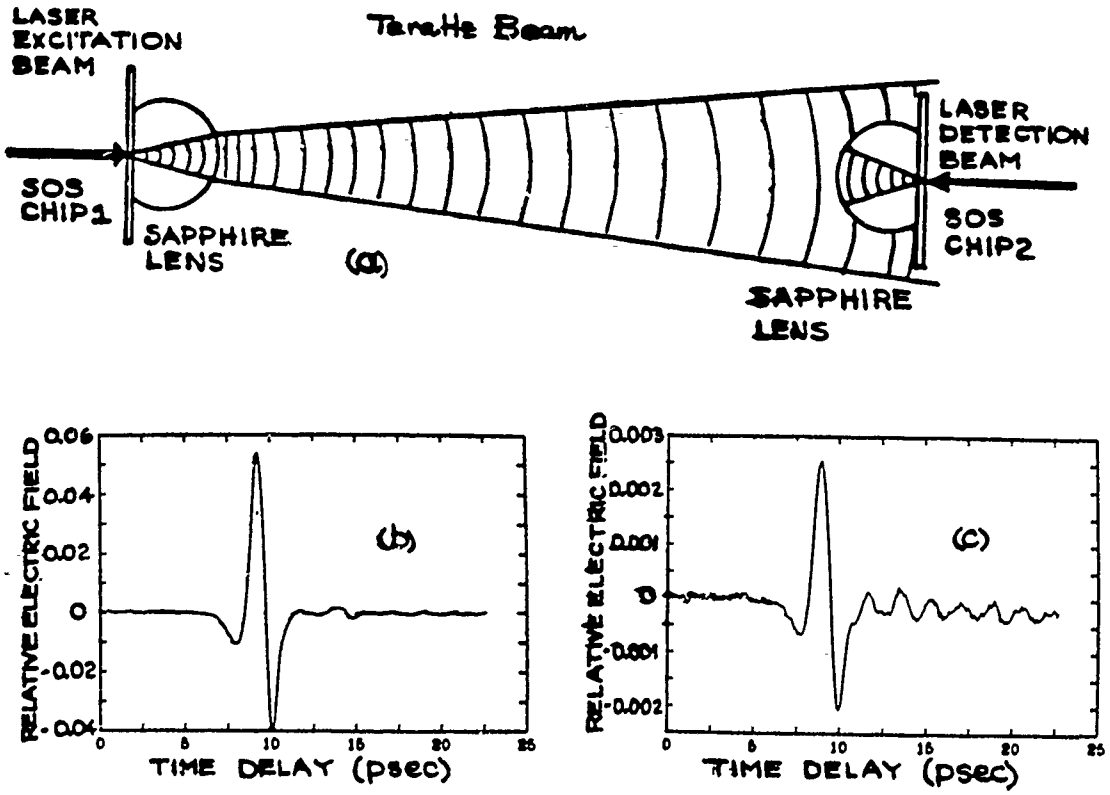

Figure 1. (a) Schematic diagram of the collimating and focusing teraHz optics. (b) Measured electrical pulse of the freely propagating teraHz beam with the detector located 10 cm from the source. (c) Measured pulse with the detector 100 cm from the source.

This research was partially supported by the U.S. Office of Naval Research.

References

1. Ch. Fattinger and D. Grischkowsky, Appl. Phys. Lett., Vol. 53, 1480 (1988).

Photoconductive Characterization of Integrated Optoelectronic MM-Wave Antennas

Charles R. Lutz and Alfred P. DeFonzo
Department of Electrical and Computer Engineering
University of Massachusetts, Amherst, Ma 01003

Photoconductive and electro-optic sampling techniques have proven to be versatile and effective approaches for measuring and characterizing the performance of high speed electronic devices [1-5]. These methods offer distinct advantages over conventional microwave sources and measurement techniques which do not possess sufficient resolution or rise time to observe electrical signals on picosecond or sub-picosecond time scales. In addition, optoelectronic measurement techniques can characterize device properties over a wide range of frequencies simultaneously, permitting easy analysis of frequency dependent phenomena. Researchers have begun to realize the importance of radiative effects in devices operating within the picosecond and femtosecond regime[1,4]. A better understanding of these effects will require the development of new measurement and analysis techniques.

In this paper we present the preliminary results of recent experiments in which photoconductive sampling was used to characterize picosecond pulse propagation on integrated coplanar stripline antenna elements capable of generating and directing short coherent pulses of electromagnetic radiation within the millimeter-wave region [4]. We demonstrate how photoconductive sampling can be used to directly perform reflectometry measurements on these devices, aiding in the analysis and characterization of impedance discontinuities and parasitic effects within the device. We will also describe a novel method for measuring the far-field radiation patterns by sampling the electric field radiated from these broadband structures.

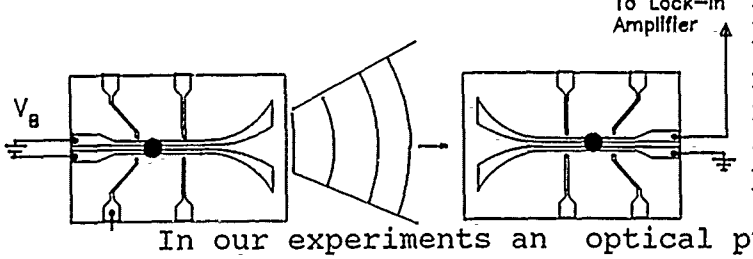

FIGURE 1. A schematic diagram of the experiment. One antenna radiates a short burst of radiation which is received by a second device and photoconductively sampled.

In our experiments an optical pump/probe arrangement is used to coherently generate and sample ultrashort electrical pulses propagating and radiating from millimeter wave integrated antennas. A schematic of the devices used in this investigation is depicted in Figure 1. Two laser beams, derived from a sync-pumped dye laser, were coupled into single mode optical fibers; the beam exiting the pump fiber was focussed to a 20 um spot which illuminated the biased gap in the coplanar transmission line, creating a photoconductive transient which traveled along the structure. The beam from the second fiber could be used to sample the current pulse on the transmitting antenna by illuminating one of the sampling gaps located along the device or sample the radiated electric field by illuminating a second receiving antenna. The structures were fabricated by photolithographically processing a 0.5 um aluminum film deposited on silicion-on-sapphire which was subsequently ion implanted.

In Figure 2 a series of correlation traces, obtained for several different positions of the excitation laser pulse along the feedline, are displayed. This data shows that the signal propagating on the structure consists of an initial short transient followed by several secondary pulses of increasing duration and decreasing amplitude. The reflection sources associated with these features can be easily identified by analyzing the time shifts between reflection peaks and the initial pulse as a function of the pump position. In addition to locating and identifying discontinuities within the structure, this information can be used to determine relative magnitudes of impedance changes along the device as well as analyze the effects of device packaging and transition parasitics.

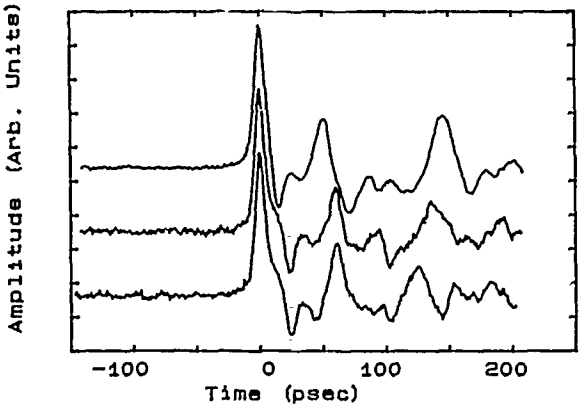

FIGURE 2. Measured signal propagating on the device for different positions of the pump pulse.

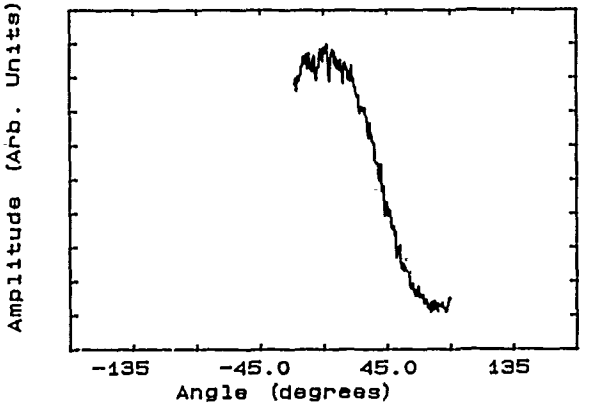

FIGURE 3. Sampled electric field as a function of angle.

Figure 3 shows the dependence of the electric field amplitude, in the E-plane, as a function of rotation angle. This data was obtained by scanning the transmitting antenna through approximately 110 degrees while maintaining a constant antenna separation of 36 mm. The pattern exhibits a broad gaussian-like central lobe with a half-power beamwidth of approximately 32 degrees.

In summary, we have presented a novel method for measuring far-field radiation patterns using coherent photoconductive sampling. This approach allows both the temporal and spatial characteristics of transient radiation to be studied in the far-field and should prove to be a useful technique for investigating radiative effects from a variety of picosecond electronic devices. Current experiments are underway to further characterize and model the radiation and propagation properties of these broadband antennas. We are presently redesigning the antenna mounting structure to allow measurements of radiation patterns at angles further from the endfire position as well as far-field measurements of the H-plane radiation patterns.

[1] P.R. Smith, D.H. Auston, and M.C. Nuss,JQE 2,255, (1988)
[2] J.F. Whitaker, R. Sobolewski,D.R. Dykaar, T.Y.Hsiang, and G.A. Mourou,MTT 36,277,(1988)
[3] D.R. Grischkowsky, M.B. Ketchen, C.-C. Chi, I.N. Duling, N.J. Halas,J.-M.Halbout,and P.G.May,JQE,24,221,(1988)
[4] A.P. DeFonzo and C.R. Lutz, APL, 51, 212, (1987)
[5] J.A. Valdmanis Electron Letts.,23,1308,(1987)

NOTES

FRIDAY, MARCH 10, 1989

SALON G

1:30 PM–3:00 PM

FC1–4

OPTICAL DETECTORS AND SWITCHES

C. H. Lee, University of Maryland, *Presider*

High Speed Metal-Semiconductor-Metal Detectors

D. L. Rogers

IBM T.J. Watson Research Center
P.O. Box 218
Yorktown Heights, NY 10598

Introduction

The Interdigitated-Metal-Semiconductor-Metal (IMSM) photodiode as originally proposed in 1980 by Sugeta at NTT [1] offered the promise of a high performace photodiode that could be easily fabricated on insulating GaAs substrates along with additional circuitry. In the years that followed the detector had been shown by several workers to definitely be capable of high speed response but suffered from an anomolous low frequency gain, low responsivities and large dark currents. Recently, however, using techniques to prevent surface trapping [2] and WSi contacts that minimize the dark current [3] very good devices have been obtained. The result has been easily fabricated detectors with the combination low capacitance, high responsivity, sub-nanoamp dark currents, and bandwidths as high as 105 GHz [4].

Using a simple form of this detector with WSi contacts and a implanted layer near the surface to limit surface trapping, complete compatibility with a high performance, self-aligned, refractory gate, LSI MESFET process has been realized. Being able to use such a standard MESFET process has made possible for the first time complex, high performance OEICs. Optoelectronic preamplifiers with bandwidths as large as 5.2 GHz [5] and 1200 gate optoelectronic clock-recovery/multiplexor circuits operating at 1 Gb/sec [6] have been demonstrated.

These detectors have also increased the potential for high sensitivity optoelectronic receivers due to the low dark current and low parasitic capacitances possible. This was recently demonstrated in an opto-electronic preamplifier for fiber optic systems operating at a sensitivity of -39.5 dBm with a data rate of 250 Mb/s. This sensitivity is comparable to that achieved with state of the art hybrid circuits [7].

In addition to IMSM detectors fabricated on GaAs there is also recent interest in this type of detector fabricated on InGaAs layers which absorb light in the longer wavelengths of particular interest in fiber optics. In these detectors

InGaAs epitaxial layers are grown on either GaAs [8] or InP [9] substrates with a graded GaAs/AlGaAs layer at the surface to allow good schottky contacts and inhibit surface trapping. Using these techiniques detectors with bandwidths greater than 8 GHz and internal quantum efficiencies near 100 percent have been demonstrated. Dark currents as low as 1 microamp have been recently observed.

References

1. T. Sugeta, T. Urisu, S. Sakata and Y. Mizushima, "Metal-Semiconductor Metal Photodetector for High-Speed Optoelectronic Circuits", Jap. Jour. Appl. Phys., V19, Suppl 19-1, 1980, p459-464.

2. D.L. Rogers, "MESFET Compatible IMSM Detectors", Proc. Picosecond Electronics and Optoelectronics Conf., p116, January 1987.

3. M. Ito and O. Wada, "Low Dark Current GaAs Metal-Semiconductor-Metal (MSM) Photodiodes Using WSi Contacts", J. Quan. Elect., v. QE-22, no. 7, July 1986.

4. B.J. Van Zeghbroeck, et. al., "105-GHz Bandwidth Metal-Semiconductor-Metal Photodiode", Electr. Dev. Lett., EDL-9, pp527-529, 1988.

5. C.S. Harder, et. al.,"5.2 GHz Bandwidth Monolithic GaAs Optoelectronic Receiver", Elect. Dev. Lett., v. 9, n. 4, p171, 1988.

6. J.F Ewen, et. al. "Gb/s Fiber Optic LInk Adapter Chip Set", Proc. GaAs IC Symp., Nov. 1988

7. R.J. Bates, D.L. Rogers, "A Fully Integrated High Sensitivity PIN/FE Optical Receiver at 250 MBaud", Proc. Opt. Fiber. Comm. Conf., 1988.

8. D.L. Rogers, et. al.,"High Speed 1.3 micron GaInAs Detectors Fabricated on GaAs Substrates", Elect. Dev. Lett., v. 9, n. 10, 1988.

9. H. Schumacher, et. al.,"An Investigation of the Optoelectronic Response of GaAs/InGaAs MSM Photodetectors", Elect. Dev. Lett., v. 9, n. 11, 1988.

Coplanar vacuum photodiode for measurement of short-wavelength picosecond pulses

J. Bokor, A. M. Johnson, W. M. Simpson, and R. H. Storz
AT&T Bell Laboratories
Holmdel, NJ 07733

P. R. Smith
AT&T Bell Laboratories
Murray Hill, NJ 07974

A vacuum photodiode is the most elementary photoelectric detector. Such a device is sensitive to photon energies which exceed the photocathode work function in accord with the classical photoelectric effect. For vacuum ultraviolet and soft X-ray radiation, photoelectric quantum yields in excess of 50% can be reached.[1] With a carefully designed external circuit, the response time of such a detector is limited by the diode capacitance. The present state-of-the-art risetime in a commercial biplanar vacuum photodiode[2] is 60 psec.

Recent studies[3] have demonstrated the utility of the coplanar transmission line geometry with lateral dimensions of several micrometers for the generation and propagation of picosecond electrical pulses. We have realized an ultrafast vacuum photodiode detector by taking advantage of a microfabricated coplanar stripline geometry. Two parallel stripline electrodes themselves serve as the photocathode and collection anode. A representation of our initial devices is shown in Figure 1. In the application primarily envisioned for this device, namely the measurement of short soft X-ray pulses radiated by picosecond laser plasma sources, the photodiode is optimized to give high sensitivity for soft X-rays, while a small portion of the pump laser pulse used to create the plasma is also used to trigger a conventional photoconductive sampler in order to read out the photodiode pulse.

The device has been tested using 266 nm ultraviolet (UV) laser pulses of ~500 fsec duration derived from a compressed, mode-locked Nd:YAG laser. The results are shown in Figure 2. With 60 V applied bias, we obtained a 4 psec rise time and a 12 psec fall time.

The performance of the device has been analyzed by calculating the potential distribution and electron trajectories. We find that the photoemitted electrons are primarily accelerated in the normal direction and do not bend around to be collected by the anode strip. The rise and fall times are governed by the transit times of the electrons through the local field in the neighborhood of the strips out to a distance of several times the strip spacing, and are found to scale as $V^{-1/2}$ in agreement with the observations. It was not possible to apply a higher bias voltage to this device due to avalanche breakdown of the silicon between the lines. By eliminating the silicon between the lines, higher bias voltage and hence higher speed should be achievable. It was not possible to apply a higher bias voltage to this device due to avalanche breakdown of the silicon between the lines. By improving the device processing to eliminate the silicon between the striplines, higher bias voltage and hence higher speed

should be obtained.

REFERENCES

1. J. A. R. Samson, *Techniques of Vacuum Ultraviolet Spectroscopy,* (Pied Publications, Lincoln, Nebraska, 1967).

2. e.g. Hamamatsu Corp., Middlesex, NJ. model R1328U.

3. M. B. Ketchen, et al., Appl. Phys. Lett. **48,** 751(1986).

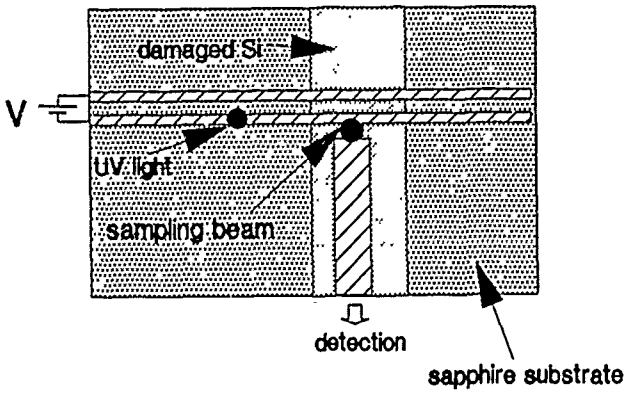

Fig. 1: Coplanar vacuum photodiode and conventional sidegap photoconductive sampler.

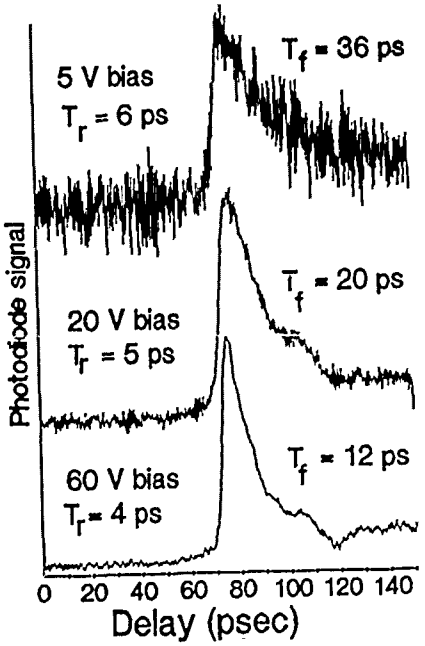

Fig. 2: Response of device to 500 fsec UV laser pulses at various applied bias voltages. The sidegap sampler was independently measured to have 2 psec response time.

20 picosecond resolution single-photon solid-state detector

M.Ghioni, A.Lacaita, S.Cova and G.Ripamonti

Politecnico di Milano, Dipartimento di Elettronica and
Centro di Elettronica Quantistica e Strumentazione Elettronica CNR
Piazza L. da Vinci 32, 20133 Milano,Italy

Single Photon Timing techniques have proven to be of considerable interest in various fields. Remarkable performances have been reported in optical fiber characterization by Optical Time Domain Reflectometry, in laser ranging, in fluorescence and luminescence decays measurements. Single photon sensitivity can be achieved with Photomultiplier Tubes (both discrete-dynode and microchannel plate) but also with avalanche photodiodes. Geiger-mode single-photon detectors have been demonstrated in silicon, germanium and III-V compounds [1].

The purpose of this work has been to develop a Geiger-mode Avalanche Photodiode with the highest timing resolution in single photon detection.

The basic requirements to obtain a proper operation of the device are:

i) the breakdown voltage must be uniform over the entire active area, that is, the occurrence of microplasmas and edge breakdown must be prevented.

ii) the detector dark count rate must be minimized. A dark count rate below 1 kpps is needed when a passive quenching circuit is adopted, due to the long recovery time. The adoption of an active quenching circuit relaxes to 100 kpps the tolerable rate.

Silicon is the material of choice because the more mature technology achieves long minority carriers lifetime and a low trap density in the detector depletion layer.

In previous works, we pointed out that the Full Width at Half Maximum (FWHM) time resolution is function of the maximum electric field in the junction. An empirical formula can be obtained from such results:

$$FWHM = A\,(E-E_b)^{-k}$$

where E_b is the maximum electric field at the breakdown voltage, k is 0.5 in shallow diffused junctions and A is a parameter that was found to increase with increasing thickness of the multiplying region at breakdown. This is physically related to the statistics of the avalanche build-up time as confirmed by computer simulation. We concluded that the best time resolution should be given by using diodes with the lowest possible breakdown voltage. Increased dark count rate is however expected in these

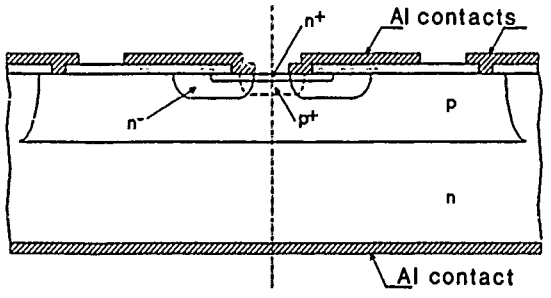

Fig.1 Cross section of the SPAD device.

diodes due to Frenkel-Poole and phonon-assisted tunneling effects. Based on these considerations we designed and fabricated Single Photon Avalanche Diodes (SPADs) having different breakdown voltages in the 10 to 30 Volts range.

The schematic cross section of the devices is shown in Fig.1. The active junction is built in the p epilayer (2.5 Ohmcm resistivity). An implanted phosphorus guard ring prevents the edge breakdown. Moreover a field plate was introduced to increase the breakdown voltage of the guard ring up to 70 V. A boron implantation in the active region was adopted to achieve a careful control of the breakdown voltage. Gettering action is provided by the insulation phosphorus diffusion. In operating conditions the substrate-epilayer junction is zero or reverse biased.

Accurate measurements of the resolution curve FWHM versus the excess bias voltage were carried out with a conventional Time-Correlated Single-Photon Timing set-up. The light source was an Opto-Electronics Inc. gain-switched diode laser emitting at 785 nm. The best time resolution was achieved with the samples having 13 V breakdown voltage, at 6 V excess bias. In such conditions, the dark count rate at room temperature was higher than 100 kpps, therefore the use of an active quenching circuit was imperative. A total FWHM of 43 ps was obtained. As the contributions of the electronic circuit jitter and of the laser pulse width are significant, they must be quadratically subtracted, in order to evaluate the true resolution of the SPAD. A time jitter of 15 ps FWHM is due to electronic noise. It was measured by using a current pulse generator for emulating the SPAD current pulses. The optical pulse width of the 785 nm diode laser was known to be about 28 ps FWHM by autocorrelation measurements. It is thus found that the device resolution at room temperature is better than 30 ps. Fig.2 shows the laser pulse detected with the same detector cooled at -65 C at 6V of excess bias. The total FWHM is 38 ps and the detector time resolution is therefore estimated to be 20 ps. To our knowledge, this is the highest time resolution so far reported in single-photon timing measurements with solid-state devices.

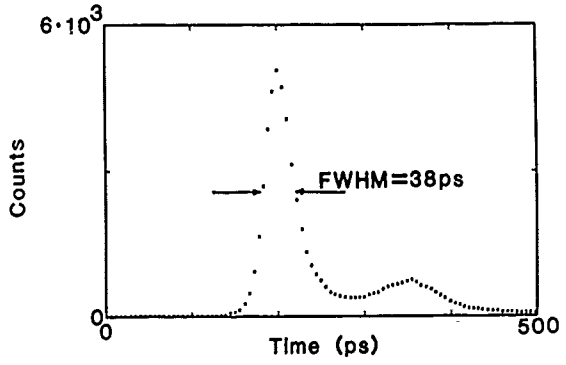

Fig.2 Measurement of the optical pulse of an Opto-Electronics Inc. gain-switched laser diode emitting at 785 nm, performed with the epitaxial SPAD with 6V excess bias voltage above breakdown at -65 C.

[1] S. Cova, G. Ripamonti and A. Lacaita, "Avalanche Semiconductor Detector for Single Optical Photons with a Time Resolution of 60 ps," Nucl. Instrum. Meth., vol. A253, pp. 482-487, 1987 and references herein.

Ultrafast Optical Switching through Virtual Charge Polarization in DC Biased Quantum Well Structures

Masamichi Yamanishi,

Department of Physical Electronics, Hiroshima University,
Saijyocho, Higashihiroshima, 724 Japan.

Field-induced modulation of optical properties of quantum wells (QWs) termed quantum-confined Stark effect[1] has been attracting a great deal of attention on its uses in high speed optical devices. The intrinsic response time of the optical properties for the electric field is expected to be extremely short, less than picosecond, determined by coherence dephasing time (T_2-time) or inverse of detuning frequency ($1/\Delta$). However, in actual cases, the switching time of the devices is limited by modulation speed in the applied field, i.e., by a C•R time constant because the field is controlled by an external voltage. In order to break through the above-mentioned limit on the switching speed, a new modulation scheme based on internal field screening due to virtual pairs excited by an off-resonant light in a DC-biased QW has been proposed and discussed by Yamanishi[2] and by Chemla et al.,[3] independently of each other. The switching time of this modulation scheme is expected to be extremely short, and free from the C•R time constant and from carrier life time. In this talk, we will discuss the extremely fast modulation scheme, named virtual charge-induced optical nonlinearity (VCON)[2] and relevant optical nonlinearities with some comments on the uses of the VCON in ultrahigh speed devices.

In a DC-biased QW structure shown in Fig.1, polarized charges would be induced by virtual excitation caused by an off-resonant pump light with a photon energy $\hbar\omega_p$ far below the fundamental gap of the QW, $E_{1e\text{-}1h}$. The induced positive (virtual holes) and negative (virtual electrons) charges may partially screen the original DC-field E_0, resulting in a decrease in the internal electric field.[2,3] The virtual excitations can last only during the pump light ON period and do not participate in any relaxation process.[4] Also, the field cancellation directly results from the internal charges inside the QW. Therefore, the modulation speed of the internal field is not limited by the recombination life time and C•R time constant. The above-mentioned field screening, i.e., optical rectification is described by a second order nonlinear susceptibility $\chi^{(2)}_{zxx}(0{:}\omega_p, -\omega_p)$ which is estimated to be ~1.7×10^{-4}[esu] for a detuning energy with respect to 1e-1h exciton, ~15meV in a GaAs/AlAs QW with a thickness L_z, 200Å, biased by an electric field, 20kV/cm.[5] Refractive index and absorption coefficient would be changed with the internal field modulation. This is illustrated by a third order nonlinear coefficient $\chi^{(2)}_{x,x,x,x}(\omega_p{:}\omega_p, -\omega_p, \omega_p)$ which is expected to be ~10^{-9}[esu] in a GaAs/AlAs QW with a thickness L_z, 100Å, biased by an electric field, 60kV/cm and pumped by an off-resonant light with a detuning energy, ~10meV.[6] In addition to the ultrafast optical nonlinearity, an extremely short voltage pulse could be generated through virtual charge polarization in the biased multiple QW structure.[3] For instance, the internal voltage modulation could switch quantum interference currents (electro-static Aharonov-Bohm effect[7]) at a low temperature, resulting in a fairly short switching time, ~1psec and, consequently, a small power-delay product, ~50f•J.[4] Many devices stacked on a single chip would be simultaneously driven by a single pump pulse since the virtual process is, in principle, loss free. This is an important advantage of this kind of modulation scheme based on virtual excitations over those based on real ones.

The proposed modulation scheme may open up entirely new opportunities in ultrahigh speed

optoelectronics. However, there has been a quite few experimental results on this modulation scheme.[8] More experimental efforts regarding this class of nonlinearities are crucially important to make our knowledge abundant.

References

1. For a review, see D.A.B.Miller, D.S.Chemla and S.Schmitt-Rink, in Optical Nonlinearities and Instabilities in Semiconductors, ed. by H.Haug (Academic, 1988) Chap. 13.
2. M.Yamanishi, Phys. Rev. Lett., **59**, 1014 (1987).
3. D.S.Chemla, D.A.B.Miller and S.Schmitt-Rink, Phys. Rev. Lett., **59**, 1018 (1987).
4. M.Yamanishi, M.Kurosaki, Y.Osaka and S.Datta, to be published in Proc. Int. Conf. Ultrafast Phenomena, Mt. Hiei, (July, 1988) Springer-Verlag.
5. M.Yamanishi and M.Kurosaki, IEEE J. Quantum Electron. **QE-24**, 325 (1988).
6. T.Hiroshima, E.Hanamura and M.Yamanishi, Phys. Rev. **B-38**, 1241 (1988).
7. S.Datta, M.R.Melloch, S.Bandyopadhyay and M.S.Lundstrom, Appl. Phys. Lett. **48**, 487 (1986).
8. H.Q.Le, J.V.Hryniewicz, W.D.Goodhue and V.A.Mims, Optics Lett. **13** 859 (1988).

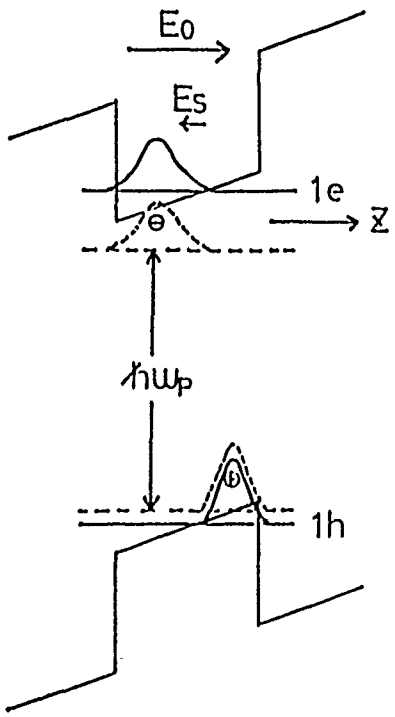

Fig.1 Energy band diagram of QW biased by a DC electric field E_0 and pumped by an off-resonant light, $\hbar\omega_p < E_{1e-1h}$.[2]

NOTES

NOTES

NOTES